AD-A995 297

OPERATION REDWING—PROJECT 6.4
AIRBORNE ANTENNAS AND PHOTOTUBES FOR
DETERMINATION OF NUCLEAR-WEAPON YIELD

A.J. Waters, Project Officer
R.E. Clapp

Advance Industries, Inc.
Cambridge, Massachusetts

May - July 1956

7 August 1959

NOTICE:
This is an extract of WT-1352, Operation REDWING, Project 6.4.

Approved for public release;
distribution is unlimited.

Extracted version prepared for
  Director
  DEFENSE NUCLEAR AGENCY
  Washington, DC 20305-1000

1 April 1985

DTIC
ELECTE
SEP 16 1985
S   D
I

85 09 13 004

Best
Available
Copy

Destroy this report when it is no longer needed. Do not return
to sender.

PLEASE NOTIFY THE DEFENSE NUCLEAR AGENCY,
ATTN: STTI, WASHINGTON, DC 20305-1000, IF YOUR
ADDRESS IS INCORRECT, IF YOU WISH IT DELETED
FROM THE DISTRIBUTION LIST, OR IF THE ADDRESSEE
IS NO LONGER EMPLOYED BY YOUR ORGANIZATION.

REPORT DOCUMENTATION PAGE

Form Approved
OMB No. 0704-0188
Exp. Date: Jun 30, 1986

1a. REPORT SECURITY CLASSIFICATION	1b. RESTRICTIVE MARKINGS
UNCLASSIFIED	

2a. SECURITY CLASSIFICATION AUTHORITY	3. DISTRIBUTION/AVAILABILITY OF REPORT
2b. DECLASSIFICATION/DOWNGRADING SCHEDULE	Approved for public release; distribution is unlimited.

4. PERFORMING ORGANIZATION REPORT NUMBER(S)	5. MONITORING ORGANIZATION REPORT NUMBER(S)
	WT-1352(EX)

6a. NAME OF PERFORMING ORGANIZATION	6b. OFFICE SYMBOL (If applicable)	7a. NAME OF MONITORING ORGANIZATION
Advance Industries, Inc.		Defense Atomic Support Agency

6c. ADDRESS (City, State, and ZIP Code)	7b. ADDRESS (City, State, and ZIP Code)
Cambridge, MA	Washington, DC

8a. NAME OF FUNDING/SPONSORING ORGANIZATION	8b. OFFICE SYMBOL (If applicable)	9. PROCUREMENT INSTRUMENT IDENTIFICATION NUMBER

8c. ADDRESS (City, State, and ZIP Code)	10. SOURCE OF FUNDING NUMBERS			
	PROGRAM ELEMENT NO.	PROJECT NO.	TASK NO.	WORK UNIT ACCESSION NO.

11. TITLE (Include Security Classification)
OPERATION REDWING - PROJECT 6.4, AIRBORNE ANTENNAS AND PHOTOTUBES FOR DETERMINATION OF NUCLEAR-WEAPON YIELD, EXTRACTED VERSION

12. PERSONAL AUTHOR(S)
A.J. Waters and R.E. Clapp

13a. TYPE OF REPORT	13b. TIME COVERED FROM 5605-- TO 5607--	14. DATE OF REPORT (Year, Month, Day) 1959, August 7	15. PAGE COUNT 142

16. SUPPLEMENTARY NOTATION This report has had sensitive military information removed in order to provide an unclassified version for unlimited distribution. The work was performed by the Defense Nuclear Agency in support of the DoD Nuclear Test Personnel Review Program.

17.	COSATI CODES		18. SUBJECT TERMS (Continue on reverse if necessary and identify by block number)
FIELD	GROUP	SUB-GROUP	Redwing, Proj. 6.4 Electromagnetic Detection
18	3		IBDA Thermal Radiation
20	14		Yield Determination Radiation Detection

19. ABSTRACT (Continue on reverse if necessary and identify by block number)
Airborne equipment was designed for determining the location and yield of a nuclear detonation. This equipment for indirect bomb damage assessment determines yield from a measurement of the interval between the time of the burst and the time of the second peak in the thermal radiation intensity curve. Flush-mounted ferrite-core magnetic loop antennas for use in detecting the electromagnetic signal and thus fixing the time of the burst, performed successfully during Operation Redwing. Two kinds of phototubes for detecting the second thermal peak were tested and were found about equally satisfactory. The method selected for yield determination gave results accurate to $\pm$ 16 percent for five shots.

A detailed study of the collected data showed that the electromagnetic signal, consisting of a direct pulse followed by a series of ionosphere-reflected sky waves, could be used in many ways to give information concerning the detonation and the ionosphere. From the time intervals between the ground wave and sky waves it was found possible to compute both the distance between burst and receiver and the height of the reflecting ionosphere layer. From

20. DISTRIBUTION/AVAILABILITY OF ABSTRACT	21. ABSTRACT SECURITY CLASSIFICATION
☒ UNCLASSIFIED/UNLIMITED ☐ SAME AS RPT. ☐ DTIC USERS	UNCLASSIFIED

22a. NAME OF RESPONSIBLE INDIVIDUAL	22b. TELEPHONE (Include Area Code)	22c. OFFICE SYMBOL
Betty L. Fox	202-325-7042	STTI

DD FORM 1473, 84 MAR

83 APR edition may be used until exhausted
All other editions are obsolete.

19. ABSTRACT (Continued)

the oscillatory period of the individual sky waves or ground wave the yield could be estimated. The wave form of a sky wave could be used for an estimate of the height of the receiving equipment. The amplitudes in a sequence of sky waves could be used to give the radian frequency characterizing the ionosphere, and to extrapolate to the amplitudes of other sky waves or the ground wave.

For a number of tests shots, the thermal radiation intensity data was compared with the expected irradiance to give estimates of atmospheric attenuation due to clouds and haze. Measurements of ambient light intensity and of the variability of ambient light were also made, to aid in the evaluation of the IBDA system.

On the sequence photographs the position of the burst could be determined from: (1) the intersection of bright radial lines; (2) the center of symmetry of the condensation dome; (3) the fireball itself; or (4) the stem of the nuclear cloud. When the fireball was visible, its radius could be used as a measure of yield, provided that the picture and the range between burst and camera were known.

FOREWORD

Classified material has been removed in order to make the information available on an unclassified, open publication basis, to any interested parties. The effort to declassify this report has been accomplished specifically to support the Department of Defense Nuclear Test Personnel Review (NTPR) Program. The objective is to facilitate studies of the low levels of radiation received by some individuals during the atmospheric nuclear test program by making as much information as possible available to all interested parties.

The material which has been deleted is either currently classified as Restricted Data or Formerly Restricted Data under the provisions of the Atomic Energy Act of 1954 (as amended), or is National Security Information, or has been determined to be critical military information which could reveal system or equipment vulnerabilities and is, therefore, not appropriate for open publication.

The Defense Nuclear Agency (DNA) believes that though all classified material has been deleted, the report accurately portrays the contents of the original. DNA also believes that the deleted material is of little or no significance to studies into the amounts, or types, of radiation received by any individuals during the atmospheric nuclear test program.

SUMMARY OF SHOT DATA, OPERATION REDWING

Shot Name (Technical/Kind)	Date (1956)	Time (Approximate)	Location	Type	MS Coordinates (Actual Ground Zero)	Geographic
Lacrosse	5 May	0629	Eniwetok Yvonne	Surface Land	124515 E 104685 N	11 33 29 162 21 18
Cherokee	21 May	0551	Bikini Off Charlie	Air Drop (4320x150 ft) Over Water	96200 ± 100 E 145100 ± 500 N	11 43 39 165 18 44
Zuni	28 May	0556	Bikini Tare	Surface Land Water	110009 E 100154 N	11 29 44 165 22 09
Yuma	28 May	0756	Eniwetok Sally	200-ft Tower	112155 E 130604 N	11 37 24 162 19 13
Erie	31 May	0615	Eniwetok Yvonne	300-ft Tower	127390 E 102060 N	11 32 41 162 21 52
Seminole	6 June	1255	Eniwetok Irene	Surface Land	75537 E 149997 N	11 40 35 162 11 08
Flathead	12 June	0626	Bikini Off Dog	Barge Water	115764 E 140054 N	11 40 22 165 20 13
Blackfoot	12 June	0626	Eniwetok Yvonne	200-ft Tower	126000 E 101035 N	11 33 04 162 21 35
Kickapoo	14 June	1126	Eniwetok Sally	300-ft Tower	114018 E 132295 N	11 37 41 162 19 12
Osage	16 June	1314	Eniwetok Yvonne	Air Drop (680x35 ft) Over Land	124647 ± 50 E 102951 ± 50 N	11 32 44 162 21 39
Inca	22 June	0956	Eniwetok Pearl	200-ft Tower	105300 E 133540 N	11 38 02 162 17 40
Dakota	26 June	0606	Bikini Off Dog	Barge Water	116707 E 147097 N	11 41 22 162 21 07
Mohawk	3 July	0606	Eniwetok Ruby	300-ft Tower	109777 E 132565 N	11 37 49 162 17 49
Apache	9 July	0606	Eniwetok Flora	Barge Water	69227 E 83444 N	11 30 17 162 11 08
Navajo	11 July	0556	Bikini Off Dog	Barge Water	116504 E 146097 N	11 40 48 162 21 07
Tewa	21 July	0546	Bikini Charlie-Dog Reef	Barge Water	99776 E 147794 N	11 40 26 165 20 22
Huron	22 July	0616	Eniwetok Flora	Barge Water	70015 E 85067 N	11 30 19 162 12 09

See ITR-1344 for further details.

4
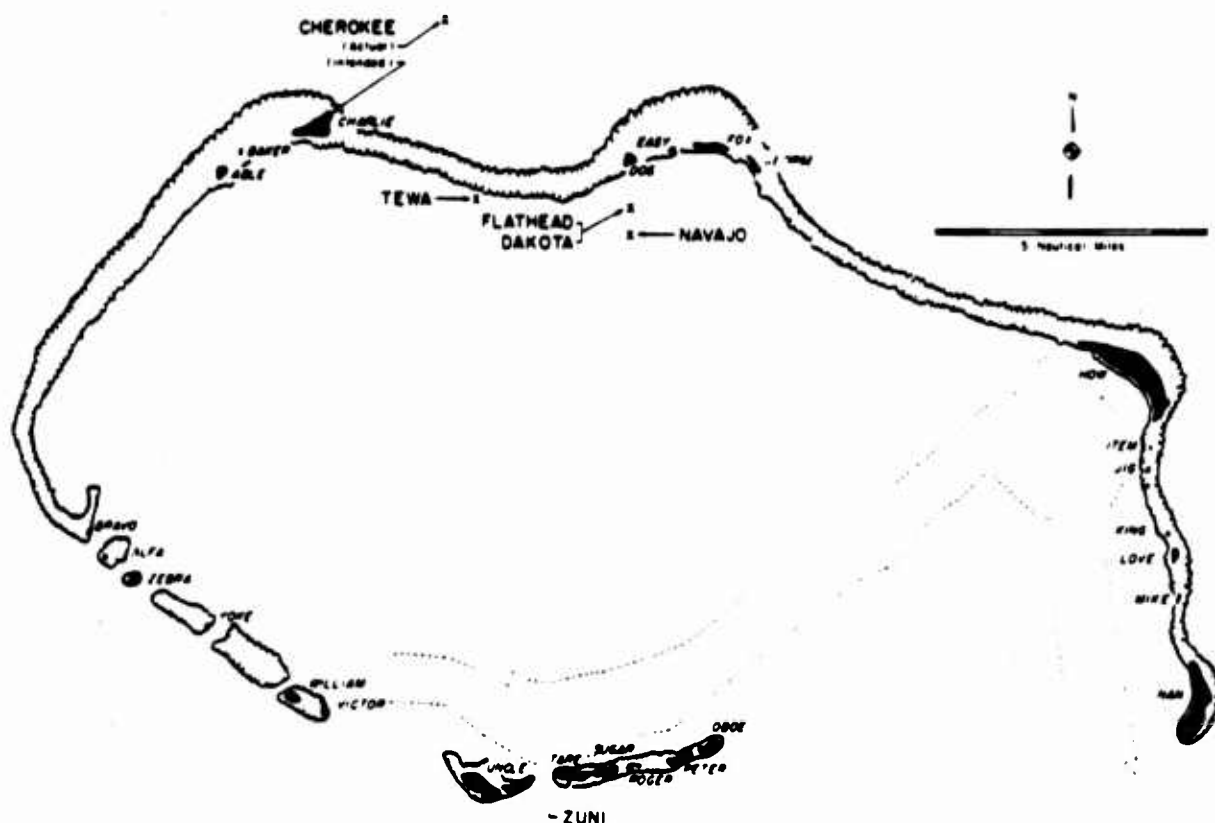
Airukiiji	Oboe	Bokoaetokutoku	Alfa	Enilrikku	Uncle	Rochikarai	Love
Airukiraru	Peter	Bokobyaadaa	Able	Eninman	Tare	Romurikku	Fox
Aomoen	George	Bokonejien	Baker	Enyu	Nan	Rukoji	Victor
Arrikan	Yoke	Bokonfuaaku	Item	Ionchebi	Mike	Uorikku	Easy
Bigiren	Roger	Bokororyuru	Bravo	Namu	Charley	Yomyaran	Jig
Bikini	How	Chieerete	William	Ourukaen	Zebra	Yurochi	Dog
		Eniairo	King	Reere	Sugar		

Bikini Atoll. Locations of test detonations during Operation REDWING
are indicated by large lettering and arrows. Native island names
with corresponding military identifiers are given in the tabulation.

5

Eniwetok Atoll. Locations of test detonations during Operation REDWING are indicated by large lettering and arrows. Native island names with corresponding military identifiers are given in the tabulation.
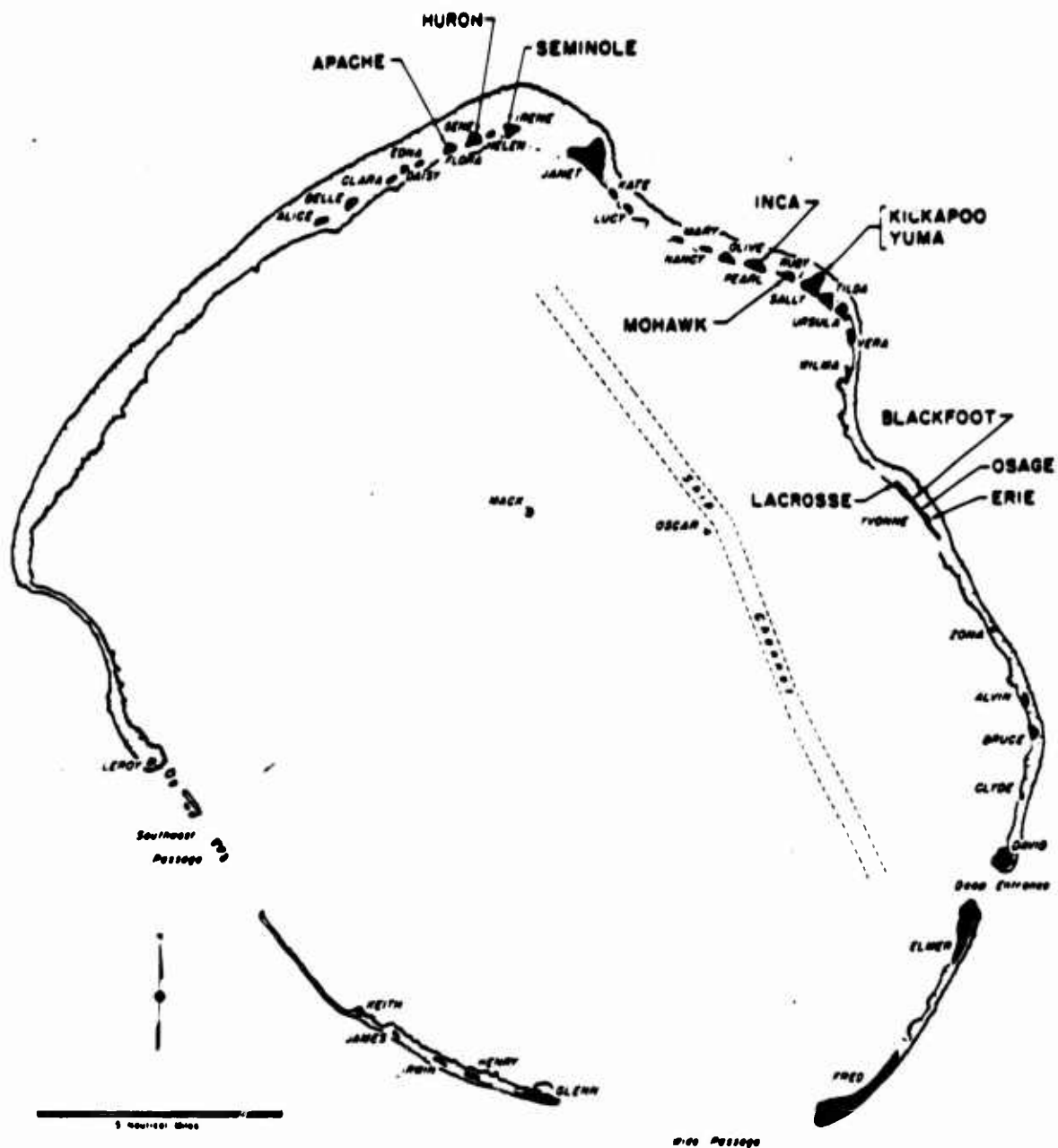
Aaraanbiru	Vera	Chinieero	Alvin	Igurin	Glenn	Ribaion	James
Altau	Olive	Chinimi	Clyde	Japtan	David	Rigili	Leroy
Aniyaanii	Bruce	Cochita	Daisy	Kirinian	Lucy	Rojoa	Ursula
Aomon	Sally	Coral Heads	Mack, Oscar	"M"	Zona	Ruchi	Clara
Biijiri	Tilda	Eberiru	Ruby	Mui	Henry	Rujoru	Pearl
Bogairikk	Helen	Elugelab	Flora	Musin	Kate	Runit	Yvonne
Bogallua	Alice	Engebi	Janet	Parry	Elmer	Sandildefonso	Edna
Bogombogo	Belle	Eniwetok	Fred	Piiraai	Wilma	Teiteiripucchi	Gene
Bogon	Irene	Giriinien	Keith	Pokon	Irwin	Yeiri	Nancy
Bokonaarappu	Mary						

6

ABSTRACT

A nuclear detonation generates three categories of characteristic phenomena which can be measured from a high-speed aircraft: (1) low frequency electromagnetic radiation which can be received by an electric or magnetic antenna; (2) thermal radiation detectable by phototubes; and (3) pictorial characteristics which can be photographed.

Airborne equipment has been designed for determining the location and yield of a nuclear detonation. This equipment for indirect bomb damage assessment (IBDA) determines yield from a measurement of the interval between the time of the burst and the time of the second peak in the thermal radiation intensity curve. Flush-mounted ferrite-core magnetic loop antennas, for use in detecting the electromagnetic signal and thus fixing the time of burst, performed successfully during Operation Redwing. Two kinds of phototubes for detecting the second thermal peak were tested and were found about equally satisfactory. The method selected for yield determination gave results accurate to ± 16 percent for five shots with yields in the range . to 5.0 Mt.

A detailed study of the collected data showed that the electromagnetic signal, consisting of a direct pulse followed by a series of ionosphere-reflected sky waves, could be used in many ways to give information concerning the detonation and the ionosphere. From the time intervals between the ground wave and sky waves it was found possible to compute both the distance between burst and receiver and the height of the reflecting ionosphere layer. From the oscillatory period of the individual sky waves or ground wave the yield could be estimated. The wave form of a sky wave could be used for an estimate of the height of the receiving equipment. The amplitudes in a sequence of sky waves could be used to give the radian frequency, ω_r, characterizing the ionosphere, and to extrapolate to the amplitudes of other sky waves or the ground wave.

For a number of test shots, the thermal radiation intensity data was compared with the expected irradiance to give estimates of atmospheric attenuation due to clouds and haze. Measurements of ambient light intensity and of the variability of ambient light were also made, to aid in the evaluation of the IBDA system.

On the sequence photographs the position of the burst could be determined from: (1) the intersection of bright radial lines; (2) the center of symmetry of the condensation dome (see below); (3) the fireball itself; or (4) the stem of the nuclear cloud. When the fireball was visible, its radius could be used as a measure of yield, provided that the timing of the picture and the range between burst and camera were known. The condensation dome, produced in humid air by the rarefaction phase of the shock wave, appeared in all burst sequences and was found useful in determining a rough value of the range and of the time of the burst relative to the timing of the photographs.

FOREWORD

This report presents the final results of one of the projects participating in the military-effect programs of Operation Redwing. Overall information about this and the other military-effect projects can be obtained from WT-1344, the "Summary Report of the Commander, Task Unit 3." This technical summary includes: (1) tables listing each detonation with its yield, type, environment, meteorological conditions, etc.; (2) maps showing shot locations; (3) discussions of results by programs; (4) summaries of objectives, procedures, results, etc., for all projects; and (5) a listing of project reports for the military-effect programs.

PREFACE

CONTENTS

TABLES

Chapter 1
INTRODUCTION

1.1 OBJECTIVES

There would be great reconnaissance value to the Air Force in a bomb damage assessment system which could provide immediate information on bomb damage and which could be carried on an aircraft delivering the nuclear weapon. Ideally, this system should measure the yield, the position, and the height of the detonation. Of these, the measurement of yield has required the greatest amount of study.

A nuclear detonation produces four characteristic effects which could be used for an airborne estimate of yield: (1) very-low-frequency electromagnetic radiation with a characteristic wave form related to yield; (2) thermal radiation with a characteristic time dependence related to yield; (3) a visible fireball with a yield-dependent rate of growth; and (4) a nuclear cloud with a yield-dependent pattern of development. Preliminary analysis based on earlier experiments indicated that the detection of Item 1 and the detailed measurement of Item 2 could provide a determination of yield with a 20-percent accuracy under favorable meteorological conditions. A more detailed measurement of Item 1 and measurements of Item 3 and Item 4 could provide auxiliary determinations of yield.

For the determination of the height of the detonation and its range from the aircraft the analysis pointed to the use of a radio link with the bomb pod itself, but for angular location in azimuth a camera in the aircraft was necessary. Auxiliary methods could be used for the measurement of range and detonation height. These are discussed later in this report.

Airborne equipment has been developed for obtaining the measurements needed for the assessment system. Project 6.4 was formed as a part of Operation Redwing to test certain portions of this airborne equipment and to accumulate data concerning the phenomena on which its operation was based. Three categories of equipment were used. (1) For the measurement of the very-low-frequency electromagnetic signal a specially designed flush-mounted antenna was utilized, along with associated amplification and presentation equipment. (2) The measurement of the thermal radiation from the detonation was by means of phototubes with their associated electronic and recording equipment. (3) A sequence camera was used to photograph the burst itself with its fireball and to photograph the nuclear cloud.

In addition to the gathering of information concerned directly with the evaluation of the specific equipment under test, an effort was made in each case to extract from Operation Redwing measurements any information which might be of more general value. Particular attention, from the point of view of both the general program and the specific equipment, was paid to the effect of ambient meteorological conditions, especially the variation of ambient light from the sky and from sunlit clouds as it affected the measurement of the burst-produced thermal radiation in the visible and adjacent ultraviolet and infrared portions of the spectrum.

As originally phrased, in order of importance to the test program, the objectives of Project 6.4 were listed as follows: (1) to determine the effectiveness of flush-mounted airborne antennas and phototubes at various ground-to-air ranges in detecting characteristic low frequency electro-

magnetic radiation and visible radiation, respectively; (2) to determine the temporal and amplitude characteristics of the low-frequency electromagnetic radiation at various ground-to-air ranges; (3) to determine the temporal and intensity characteristics of visible radiation at various ground-to-air ranges; and (4) to determine the effects of ambient conditions upon the satisfactory measurement of the parameters specified in Items 1 and 2 above.

1.2 BACKGROUND

In accordance with the need for airborne assessment information, Advance Industries, Inc. (formerly Ultrasonic Corporation), under Purchase Order 221 to the Convair Division of General Dynamics Corporation, Fort Worth, Texas, on Air Force Prime Contract AF33(038)-21250, was made responsible for the development of an indirect-bomb-damage-assessment (IBDA) system for incorporation in the B-58 weapon system. The B-58 weapon system involves a supersonic aircraft capable of velocities up to Mach 2 and capable of delivering an atomic warhead at long ranges in compatability with the Strategic Air Command (SAC) requirements. IBDA enables the B-58 weapon system to collect preliminary and perhaps final reconnaissance data during the primary mission, thus effectively increasing the striking power of the Air Force.

In the design of IBDA equipment which would be applicable to supersonic aircraft, two factors were considered of special importance: (1) All devices should be mounted flush or nearly flush with the skin of the aircraft; and (2) after release of the warhead the aircraft would evacuate the area as rapidly as possible, and the ground-to-air range between burst and aircraft could be as large as 250 naut mi.

Participation in Operation Redwing provided the opportunity for the acquisition of quantitative data on long-range reception by flush-mounted devices, particularly flush-mounted aircraft antennas capable of detecting low-frequency electromagnetic radiation (approximately 15 kc). Prior to Operation Redwing no direct data existed on the problem of airborne reception of the low-frequency electromagnetic signal from a nuclear explosion. Prior to Operation Redwing, also, there had been no long-range airborne measurements of thermal intensities received from the detonation under varying meteorological conditions.

The IBDA system developed by Advance Industries, Inc., has as its core a bhangmeter-type instrument for collecting the characteristic data from which a determination of the yield of the explosion may be made. At the time of Operation Redwing, the IBDA program had reached the equipment-design stage, and bhangmeter prototypes had been constructed. It was this prototype equipment, in addition to standard laboratory instruments and other equipment specially constructed for the tests, that was used in Operation Redwing.

1.3 THEORY

The airborne IBDA system was designed to use the very-low-frequency electromagnetic signal as the fiducial mark fixing the moment of detonation. For the determination of yield, the time interval between the moment of detonation and the second peak in the thermal radiation intensity curve was selected as the most satisfactory yield-dependent parameter that could be measured from the aircraft. The main purpose of the sequence camera in the IBDA system was to give a photographic record from which the azimuth location of the burst could be determined.

The time of the electromagnetic fiducial signal, the time of the second radiation peak, and the angular position of the burst were the three items of information which the IBDA system required for the fulfillment of its operational function. Operation Redwing measurements were undertaken for the primary purpose of obtaining data directly related to the first two of these three items of information. However, the actual measurements contained additional information of more general value concerning the electromagnetic signal, the thermal radiation, and the pic-

torial aspects of the detonations. In this report the intention has been to present in as useful a
form as possible all the information obtained during the tests.

1.3.1 Comparison of Time Scales. Figure 1.1 gives a comparison of the time scales char-
acterizing those nuclear detonation effects which are discussed in this report.

The electromagnetic pulse received by a magnetic core loop antenna, of the type used in the
tests, has a characteristic three-lobe wave form shown in Curve A of Figure 1.1 on a time scale
measured in microseconds. The spikes shown superimposed on the first lobe in Curve A were
not actually received by the Operation Redwing equipment because its band width was too narrow.
In the upper part of Curve B the wave form in Curve A has been compressed into a longer time
scale measured in milliseconds. It appears as the ground wave and is followed by a succession
of sky waves. These are separate versions of the same pulse received after having been reflected
one or more times from the ionosphere and from the ground.

The lower part of Curve B shows the beginning of the thermal radiation intensity curve. The
thermal intensity rises to a first peak which has been shown compressed in Curve C where the
time scale is measured in seconds. The thermal radiation falls to a minimum shown in Curve C
and then rises to a broader second peak after which it falls off gradually.

The growth of the fireball is illustrated in the lower part of Curve C. At about the time of the
first thermal radiation peak the shock wave moves out ahead of the fireball surface and continues
to grow at a faster rate than the fireball. When there is sufficient moisture in the air the rare-
faction following the shock causes a condensation of the moisture into a visible dome known as
the condensation cloud effect. The growth of the fireball and of the condensation dome have been
indicated on a still slower time scale measured in minutes in the upper part of Curve D.

The development of the nuclear cloud has been suggested in the lower part of Curve D. As in
the other parts of Figure 1.1 the sketches are not meant to be more than schematic. Insofar as
they could be considered to apply to a detonation of a given yield, however, the yield would be of
the order of one Mt.

1.3.2 Electromagnetic Signal. The main features of the electromagnetic signal have been
attributed to radiation by electrical currents consisting of Compton electrons ejected from air
molecules by high-energy gamma rays from the nuclear detonation. (See Reference 1 for a de-
tailed discussion and for further references.) The period and field strength of the main oscilla-
tion are related to some extent to the total yield of the detonation.

Function as Fiducial Marker. A measurement of the time from burst to the second
peak of the thermal radiation curve could, in general, use either the electromagnetic signal or
the fast rise to the first thermal peak as the zero-time reference point or fiducial marker. How-
ever, under the operational conditions for which the airborne IBDA equipment was designed, it
was anticipated that the thermal radiation might be so highly attenuated that the first peak would
not be detectable, even though the more intense second peak remained strong enough to be
measured.

The electromagnetic signal was not subject to strong attenuation in the atmosphere. It was,
therefore, considered more reliable under operational conditions and was chosen as the fiducial
marker for the measurement of the time to the second peak.

However, the experimental data on which the choice was based was not very extensive. The
thermal radiation had been studied at relatively short ranges, but no data was available on
thermal irradiance at long ground-to-air ranges, under varied meteorological conditions. The
electromagnetic signal had been studied in ground-to-ground situations, but no attempt had been
made to record its characteristics in an aircraft. Operation Redwing presented an opportunity

17
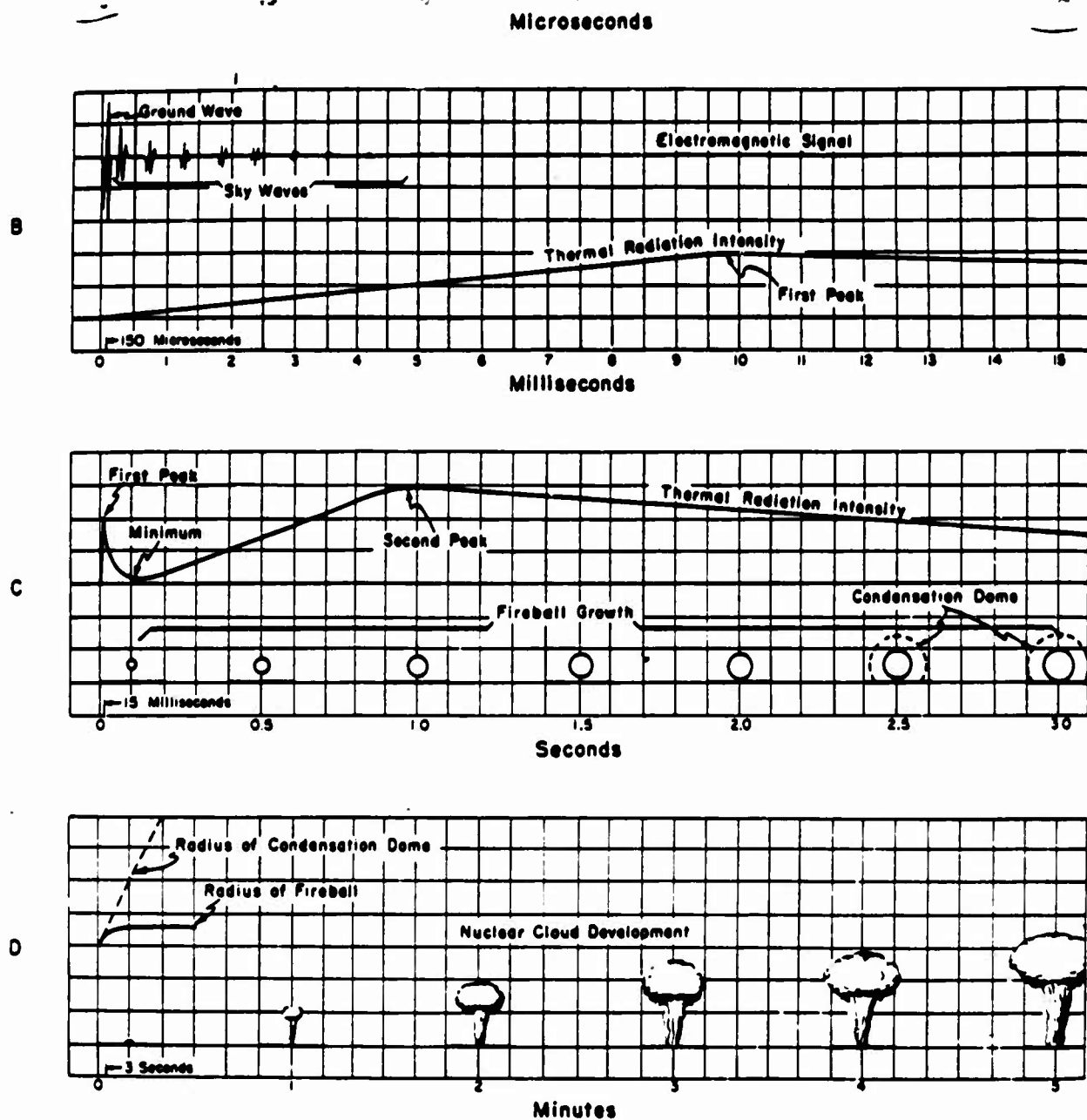
Figure 1.1 Comparison of time scales for effects characteristic of a nuclear detonation, (A) in microseconds, (B) in milliseconds, (C) in seconds, (D) in minutes.

to obtain data which could either tend to reinforce the choice of the electromagnetic signal as the fiducial marker or lead to reconsideration of that choice.

Antenna Design. Detection of the very-low-frequency electromagnetic signal by equipment carried on a supersonic aircraft presented a significant problem. The polarization of the electromagnetic pulse was known from prior tests to be vertical. The wave form was known to be a damped sinusoid with an oscillatory frequency of approximately 15 kc, ranging roughly from 7 to 30 kc as a function of yield. The magnitude of the electric field (at the peak of an oscillation) was known to vary over a considerable range as a function of yield and distance. For most operational conditions it was expected to lie between 0.1 and 50 volts per meter.

Prior tests had been made with ground-mounted vertical wire antennas of high impedance. Antennas of this character were not considered appropriate for supersonic aircraft. Vertical protuberances on such an aircraft result in large aircraft performance penalties. A vertical rod short enough to be aerodynamically acceptable would have to be operated at a very high impedance level. It would then be vulnerable to many kinds of electrical interference picked up locally. A longer vertical antenna would be more satisfactory, but the configuration of a supersonic aircraft is such that there are no vertical dimensions of any appreciable length other than the vertical stabilizer. If a vertical wire were inserted flush in the side of the stabilizer, the resultant efficiency of this antenna would be very low because of the proximity of the remainder of the aircraft relative to the wave length (20,000 meters) associated with the 15-kc oscillations in the electromagnetic signal. If the vertical stabilizer could be isolated electrically from the rest of the aircraft, the stabilizer itself could become an effective antenna, but the mechanical and electrical problem of isolating part or all of the stabilizer (and the equipment carried in it) made such a solution undesirable.

As a consequence, attention was directed toward the magnetic component rather than the electric component of the low-frequency electromagnetic signal. The magnetic field was known to be horizontal, in compatibility with the aircraft configuration, and was free from degradation in positions where the field lay parallel and contiguous to the metallic surface of the aircraft.

Design studies indicated that a loop antenna would be satisfactory. The size of this loop antenna was kept small, in accordance with the low weight and space objectives of supersonic weapon systems, by the use of a ferrite core. The loop was wound on the core as a single-layer solenoid, a coil of maximum magnetic efficiency. The coil was loaded capacitatively to give a tuned circuit resonating at approximately 15 kc, and loaded resistively to produce a circuit Q of unity. The result was that the output of the terminated antenna included the energy in a broad band of frequencies centered at 15 kc.

An incident electromagnetic wave with an electric field strength of one volt per meter has a magnetic field strength of 0.0027 ampere-turns per meter. The antenna was so constructed that, when properly terminated, it gave an output of 10 mv when placed in a 15-kc magnetic field of the above field strength. For a given antenna length, the shape of the antenna cross section could vary over a wide range without greatly changing the effectiveness of the antenna, provided that there was no change in the product of the cross sectional area of the ferrite core and the number of turns in the coil. The antenna could be buried almost any place within the aircraft structure as long as it was not completely shielded from the magnetic component of the incident electromagnetic wave.

Laboratory tests of such an antenna with radiation fields were virtually impossible. Since the wave length was of the order of 20,000 meters, the induction field extended to a considerable distance, well outside the confines of any building of normal size. Preliminary tests were made with a standard magnetic-field test loop used for generating the incident magnetic field. Final verification of the validity and effectiveness of this type of antenna was left until Operation Redwing, during which the actual electromagnetic signal from the test detonations was used as the incident field.

Electromagnetic Wave Form.

representation of the wave form from a smaller detonation (8 kt). Curve A of Figure 1.2 is an actual trace, slightly idealized, received at an Air Force Cambridge Research Center (AFCRC) station about 220 nautical miles from the detonation center. The detonation was Shot Bee of Operation Teapot (see Reference 2 and Figure 1 (d) of Reference 1). The ground wave and the first sky wave (the pulse arriving after one reflection from the ionosphere) are shown as received with a vertical antenna responding to the electric component of the electromagnetic signal.

Curve B of Figure 1.2 has been constructed from Curve A by differentiation. It simulates the output wave form to be expected from a simple, non-resonant loop antenna. The voltage induced in such an antenna is proportional to the rate of change of the incident magnetic field and is, therefore, proportional also to the rate of change of the incident electric field, since the electric and magnetic fields are directly proportional in a traveling electromagnetic wave.

In Operation Redwing tests the antenna used was not a simple non-resonant antenna and its response was somewhat more complicated. However, for frequencies that were not too high, the general wave form shown in Curve B of Figure 1.2 was found to be a valid representation of the electromagnetic signal as received on the type of fiducial antenna used in Operation Redwing tests. It should be noted that the two lobes in the ground wave of the upper trace, Curve A, have become three lobes in the ground wave of the lower trace, Curve B, while the first sky wave in the upper trace, with its three lobes, has become a four-lobed oscillation in the lower trace, after it has been differentiated to simulate reception by a loop antenna. The fourth lobe, however, is considerably weaker in amplitude than the first three lobes.

Period and Yield. It was found in earlier tests that a correlation existed between the yield of the detonation and the period of the main oscillation in the electromagnetic pulse. The correlation is shown in Figure 1.3, which was drawn from the data in Figure 9 of Reference 1.

The curve of Figure 1.3 shows that a wide range of yields is covered by a relatively narrow range of periods. Furthermore, experimental points from previous test detonations showed considerable scatter about the curve. Consequently a yield determination based on the measurement of the period of the electromagnetic pulse was not expected to be accurate, except perhaps for high yields. The upper part of the curve, above 1 Mt shows a much faster variation of period with yield than does the lower part, near 10 kt.

Field Strength. The field strength of the electromagnetic ground wave was measured extensively in earlier tests. There was a large scatter in the data, but a rough correlation between peak field strength and detonation yield was found. The correlation is shown in Figure 1.4, which is taken from Figure 11 of Reference 1. The field strength has been referred to a range of 100 km or 54 naut mi (62 statute miles).

The electromagnetic ground wave is not significantly attenuated by atmospheric absorption. For ranges which are not great enough for the ground wave to be blocked by the curvature of the earth, it is sufficient to consider the field strength to be inversely proportional to range. The ground wave field strength, $E_{(D)}$, at a particular range, D, in nautical miles, can then be obtained from the field strength at 54 miles, $E_{(54)}$, through the use of Equation 1.1.

$$E_{(D)} = \frac{54}{D} \ E_{(54)} \tag{1.1}$$

In Figure 1.4 the field strength has been given as E_{max}, in volts per meter, center to peak. The corresponding magnetic field, H_{max}, in ampere-turns per meter, can be obtained from E_{max} through division by 377 ohms, which is the characteristic impedance of a plane wave in free space.

Sky Waves. The characteristics of sky wave propagation are discussed in considerable mathematical detail in References 3 and 4. Each sky wave has a different total path length and a

20
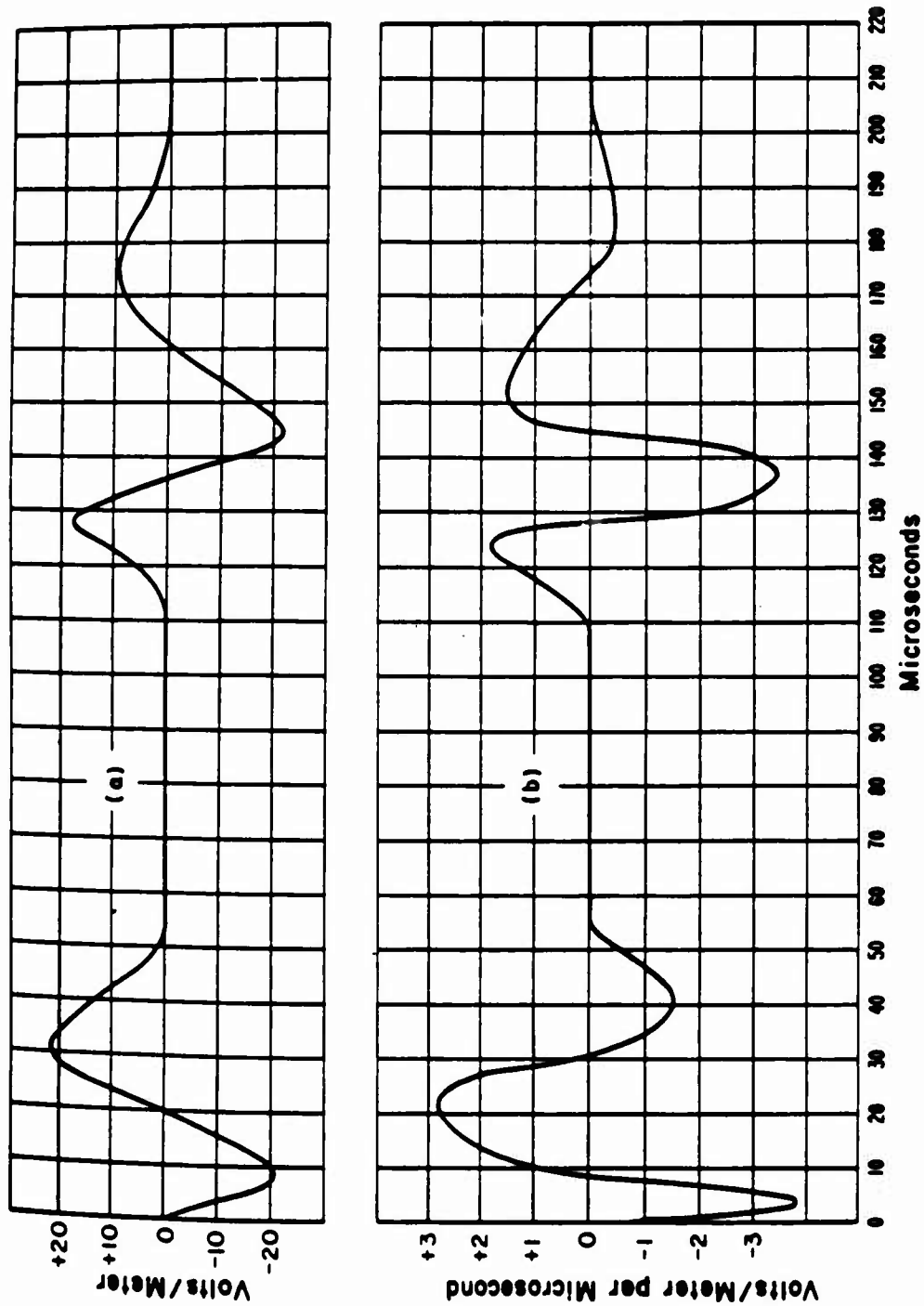
Figure 1.2 Electromagnetic wave form, (A) as received by a vertical whip antenna, and (B) differentiated, to simulate reception by a loop antenna.
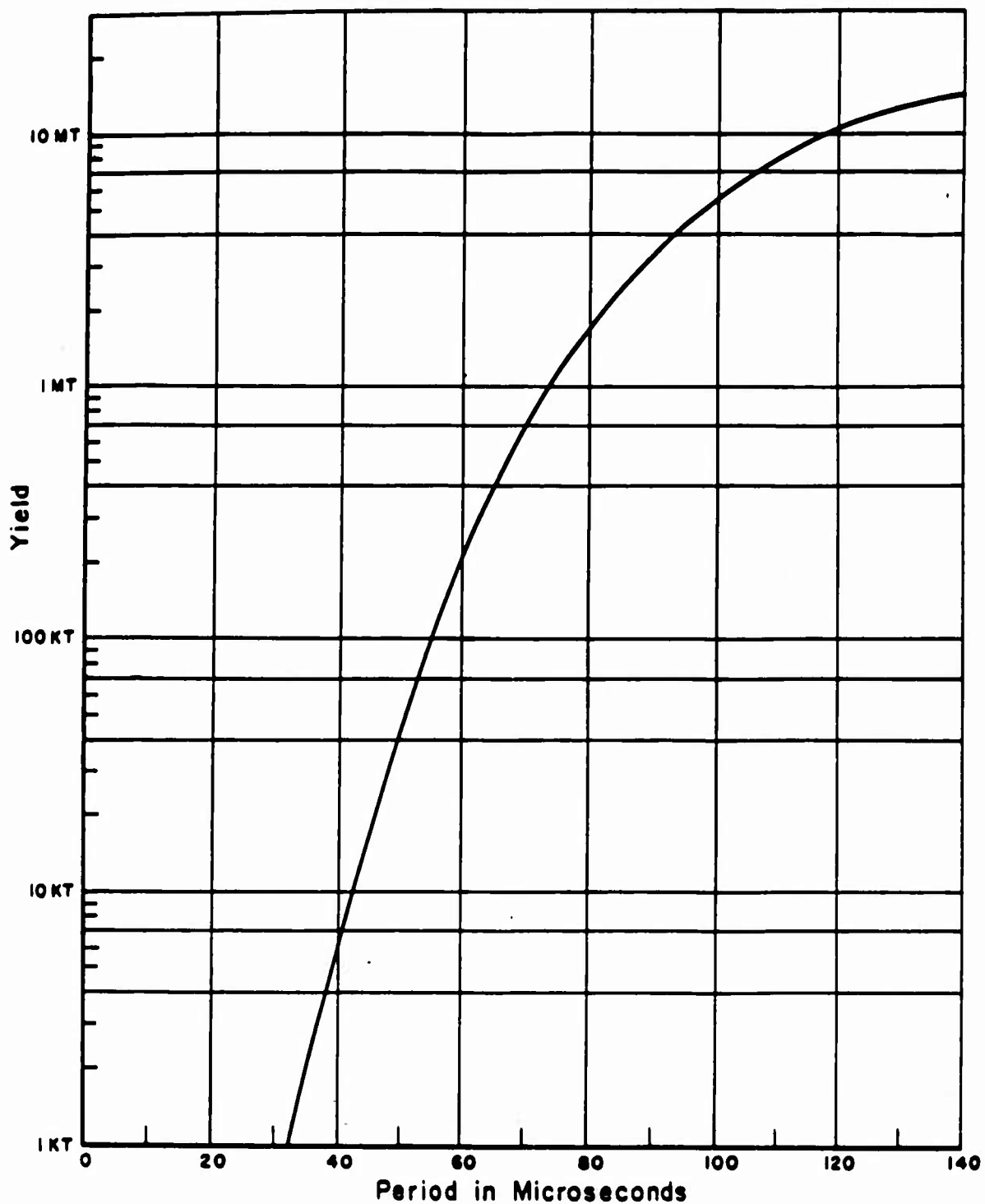
Figure 1.3 Empirical curve relating detonation yield and the period of the electromagnetic pulse.
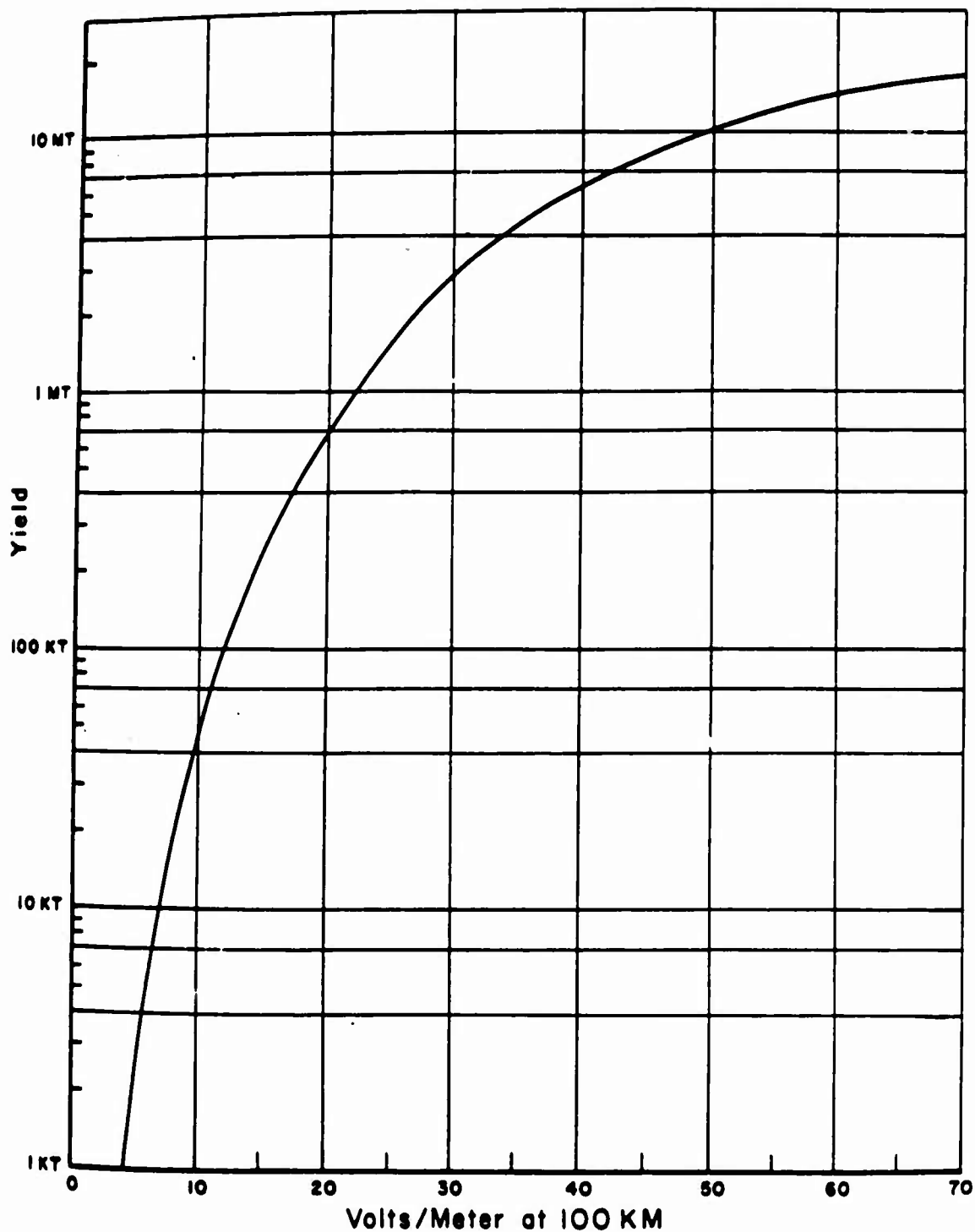
Figure 1.4 Empirical relation between detonation yield and the field strength of the electromagnetic pulse, referred to a range of 100 km (54 naut mi).

different angle of arrival at the receiver. Reference 4 includes a tabulation of sky wave path lengths covering a range of values for the ionosphere height and for the ground distance between source and receiver. Also tabulated are values for the angle of arrival, θ, and for the slightly different angle of reflection at the ionosphere, $\bar{\delta}$

The first sky wave follows a propagation path from the source up to the point of reflection at the ionosphere and then down to the receiver. The path of the second sky wave is up to the ionosphere, down to the ground for a second reflection, up to the ionosphere for a third reflection, and then down to the receiver. When the receiver is itself located in an aircraft at a significant altitude above the ground, each sky wave is split into two waves, the direct sky wave moving down toward the receiver from the ionosphere, and the ground-reflected sky wave moving up toward the receiver after one additional reflection from the part of the ground almost directly below the aircraft. In Operation Redwing, the aircraft was generally at an altitude of 18,000 feet, and the time interval between the reception of the direct sky wave and the reception of its ground-reflected companion was in the range of 20 to 40 μsec.

Timing of Sky Waves. As shown in Curve B (Figure 1.1) the sky waves form a train of pulses that follow the ground wave, on an oscilloscope presentation with a relatively slow sweep covering several milliseconds. The actual time intervals between ground wave and sky waves depend both on the range, D, from source to receiver and on the height, H, of the ionosphere. As indicated in the previous section, the time of reception also depends upon the altitude h, of the aircraft carrying the receiver.

Figure 1.5 shows the time intervals between the ground wave and the first few sky waves as functions of the range, D, for three values of ionosphere height, 90, 80, and 70 km, respectively. During the night the ionosphere is usually at a height near 90 km. When the sun strikes the upper atmosphere just before dawn, the ionosphere starts moving down toward its usual daytime height of about 70 km. Since most of the test detonations occurred just before or just after dawn, the 80-km curves were included to allow for intermediate positions that the ionosphere might assume at the moment of burst.

The curves of Figure 1.5 were drawn so they could be used in practice for a rough determination of the range from burst to receiver whenever a measurement had been made of several of the time intervals between the ground wave and the sky waves. The procedure used is illustrated in "Timing of Sky Waves", Chapter 3.

Numerical information similar to that contained in Figure 1.5 is tabulated in Table I of the first article in Reference 4. In Figure 1.5, as in the referenced table, no allowance was made for the refraction of the electromagnetic wave near the surface of the earth, caused by atmospheric density gradients, or for diffraction effects.

Dashed curves have been included in Figure 1.5 to show the modifications that were required when the receiver was located at an altitude of 18,000 feet, as it was during most of the Operation Redwing measurements. For a particular value of n, the dashed curve refers to the direct sky wave reaching the receiver after n reflections from the ionosphere and n − 1 reflections from the ground. There is also a ground-reflected sky wave reaching the receiver after n ionosphere reflections and n ground reflections. It would be represented by a curve lying just to the right of the solid curve, about as far to the right as the dashed curve is to the left.

Field Strength of Sky Waves. The first sky wave has a longer distance to travel than the ground wave, and each successive sky wave travels a still longer distance. The field strength of the sky waves is reduced because of the longer path, in accordance with Equation 1.1 but in addition there is a further attenuation associated with losses during the reflection processes at the ionosphere and at the earth's surface.

In Operation Redwing tests the reflections from the earth's surface were nearly always reflections from sea water, which is a perfect reflector for frequencies below 20 kc. However,

24
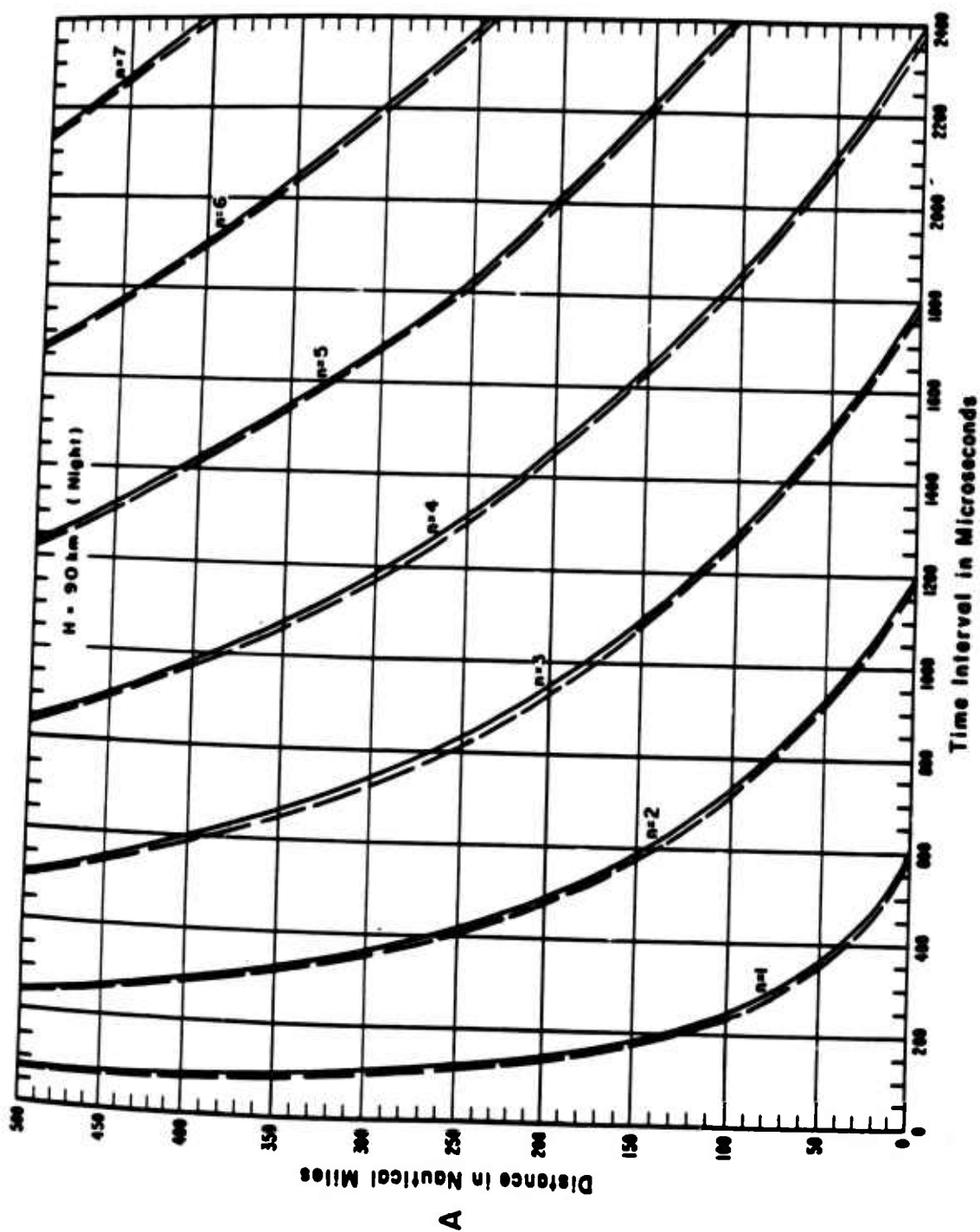
Figure 1.5 Theoretical curves relating distance between source and receiver and time interval between ground wave and nth sky wave. Ionosphere height: A, 90 km; B, 80 km; C, 70 km.
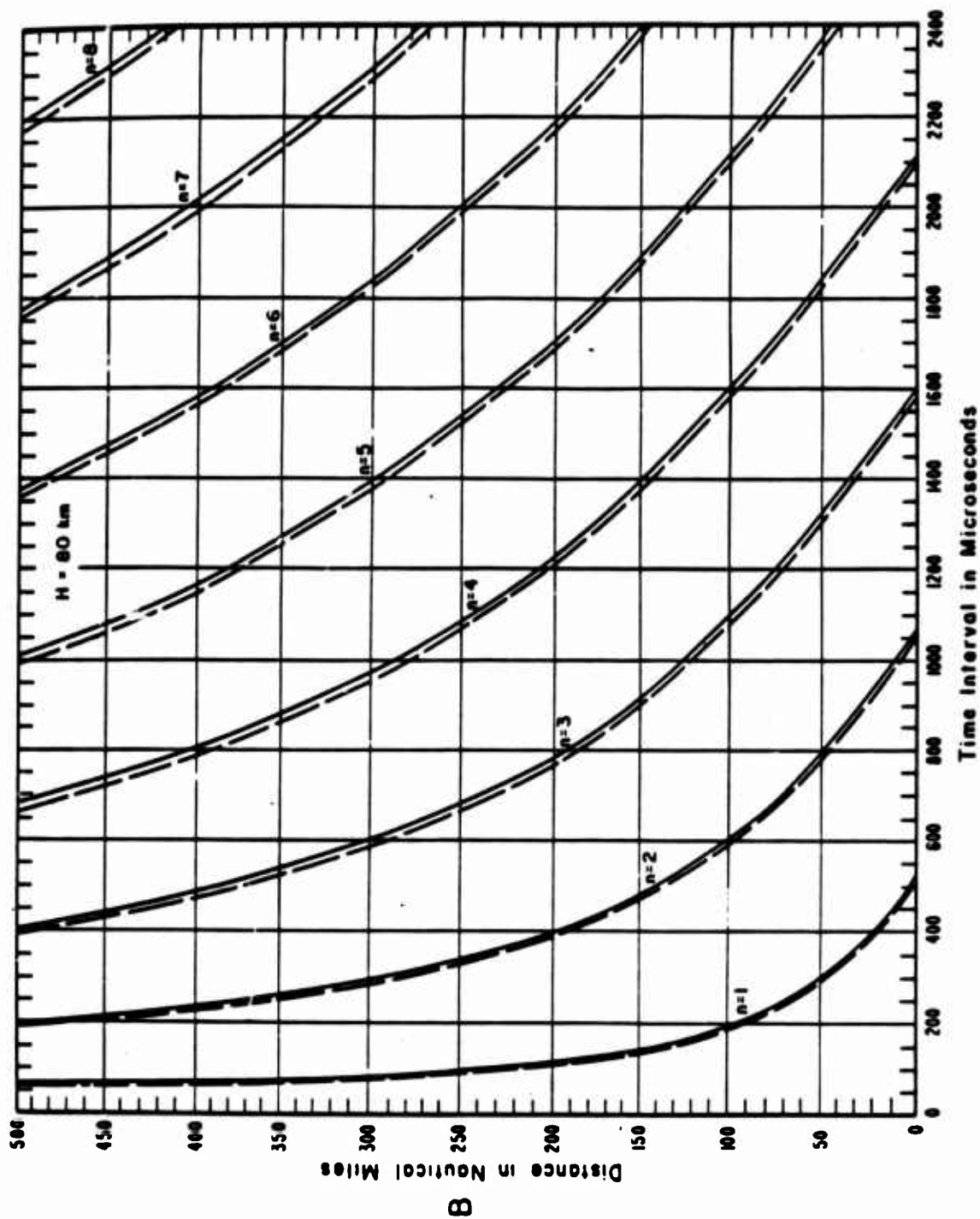
Figure 1.5 Continued.

Figure 1.5 Continued.

27
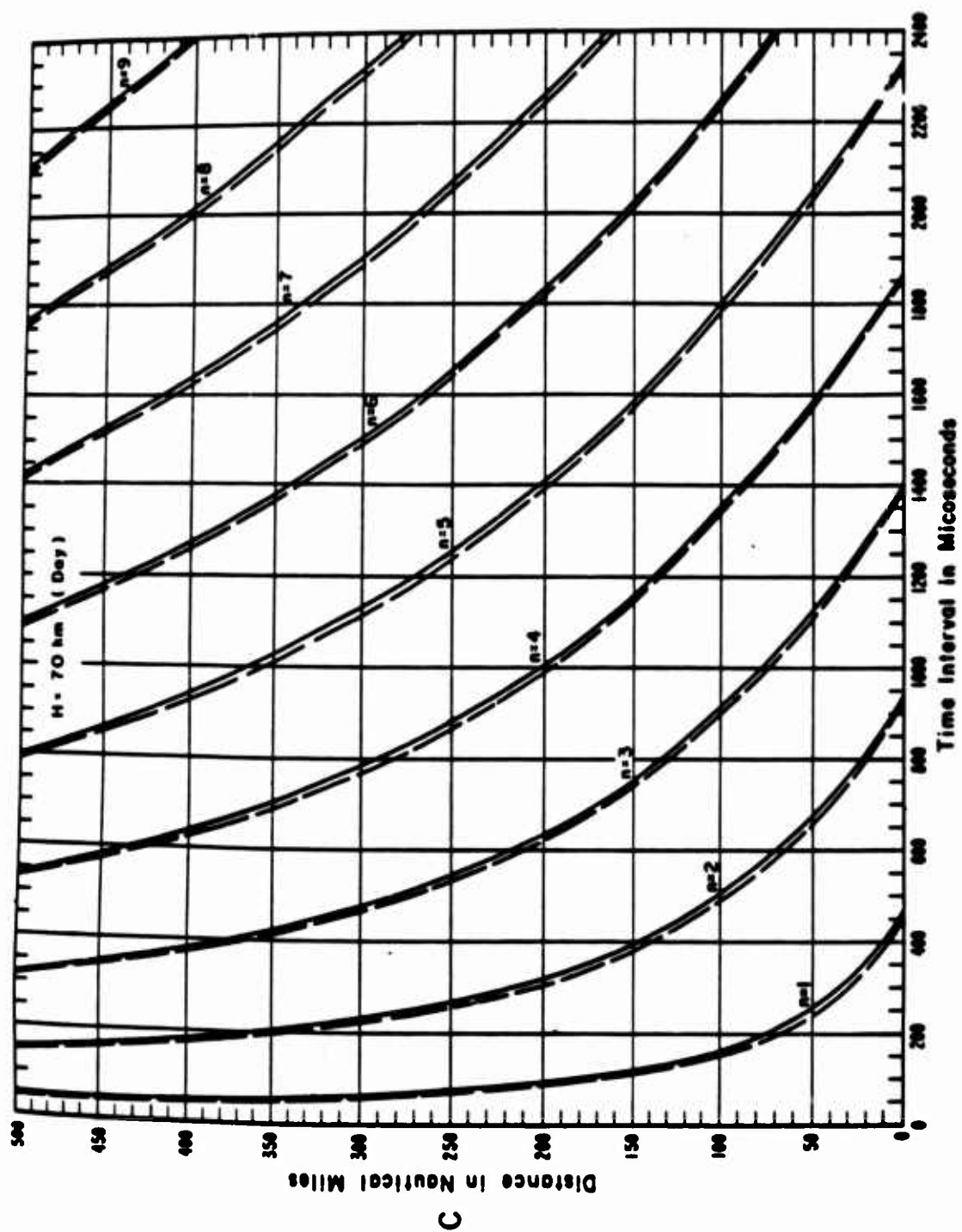
the ionosphere was by no means a perfect reflector for the frequencies contained in the electro-magnetic pulse.

In Reference 4 there is an equation giving the reflection coefficient, $R(\bar{\theta})$, for a single reflection from the ionosphere, as a function of the angle, $\bar{\theta}$, between the direction of propagation and the vertical at the point of reflection.

$$R(\bar{\theta}) = \frac{N^2 \cos\bar{\theta} - (N^2 - \sin^2\bar{\theta})^{1/2}}{N^2 \cos\bar{\theta} + (N^2 - \sin^2\bar{\theta})^{1/2}} \qquad (1.2)$$

The complex index of refraction, N, depends on the angular frequency, ω, (which equals 2π times the frequency, f), and on a quantity, ω_r, which is explained below.

$$N^2 = 1 - i\frac{\omega_r}{\omega}$$

The quantity, ω_r, is proportional to the conductivity of the ionosphere and is stated on page 769 of Reference 4 to have numerical values which are given in Equation 1.4.

$$\omega_r = 10^6 \text{ radians/sec, for night}$$
$$\omega_r = 2 \times 10^5 \text{ radians/sec, for day} \qquad (1.4)$$

The reflection coefficient has been computed for eight different values of the ratio ω_r/ω. The amplitude, $|R(\bar{\theta})|$, has been plotted in Figure 1.6 and the phase angle has been plotted in Figure 1.7. Table 1.1 gives the values of ω_r/ω which correspond to each of the curves in the two figures and also gives the frequencies, f, which are associated with each curve, for the two choices for ω_r given above in Equation 1.4.

An expression for the field strength of the nth sky wave would contain the factor $|R(\bar{\theta})|^n$, where $\bar{\theta}_n$ is the reflection angle at the ionosphere associated with the nth sky wave. It would also contain the factor $1/D_n$, where D_n is the path length traversed. In addition, factors would be needed to include any directivity in the source currents or in the receiving antenna. The ratio of the field strength of the nth sky wave to that of the ground wave would be given by such an expression as Equation 1.5.

$$\frac{E_n}{E_0} = \frac{D_0}{D_n} G_s(\theta_n) G_a(\theta_n) |R(\bar{\theta}_n)|^n \qquad (1.5)$$

The angle, θ_n, appearing in the gain factors for source, G_s, and for receiving antenna, G_a, is the angle between the direction of propagation and the vertical, as measured at the ground, where as $\bar{\theta}_n$ is the similar but slightly different angle measured at the ionosphere.

The practical application of Equation 1.5 in the reduction of sky wave data is illustrated in "Amplitude Comparison", Chapter 3.

Phase Shift of Sky Waves. Figure 1.7 shows the phase shift accompanying a single reflection from the ionosphere. The quantity plotted is the phase angle of the complex reflection coefficient given in Equation 1.2. In each case the phase shift is negative, denoting a phase lag on reflection.

At long ranges, for which the first sky wave strikes the ionosphere at an angle near grazing incidence, Figure 1.7 shows that the phase shift can approach 180 degrees. Curve A of Figure

28

1.2 illustrates such a phase reversal. The sky wave at the right of the curve starts with a positive deflection, while the ground wave at the left starts with a negative deflection. The angle of incidence at the ionosphere was about 70 degrees, for the conditions under which Curve A of Figure 1.2 was measured, and the phase shift estimated from Figure 1.7 is about −120 degrees, which is consistent with the observed result.

For conditions of Operation Redwing tests, the range was generally shorter and the angle of incidence at the ionosphere was smaller, closer to normal incidence. The phase shift was ac-
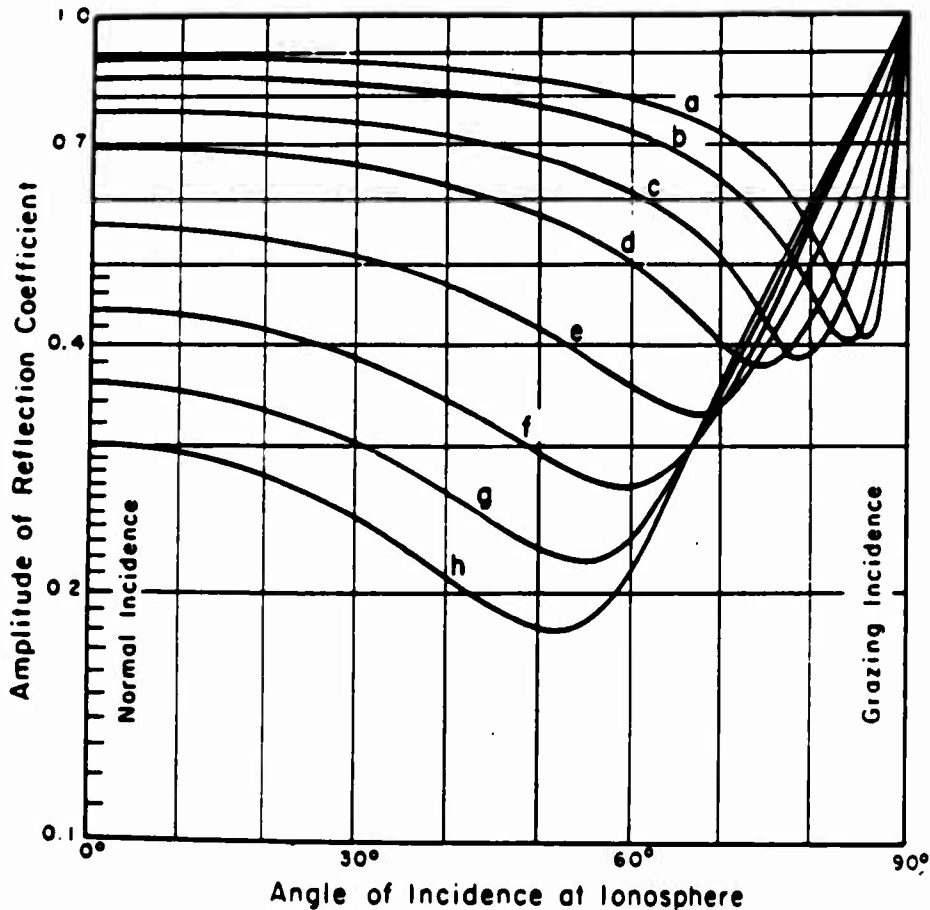
Figure 1.6 Amplitude of ionosphere reflection coefficient for vertically polarized wave. See Table 1.1 for frequency parameters.

cordingly in the neighborhood of −45 degrees or less, and the initial deflection for the first sky wave was of the same polarity as the initial deflection for the ground wave.

1.3.3 Thermal Radiation. The term thermal, as used in this report, refers to the incoherent radiation from the fireball. It has a continuous spectrum, including infrared, visible, and ultraviolet radiation. The thermal radiation is to be distinguished from the electromagnetic pulse, which is coherent and has a definite polarization and wave form involving a band of very low frequencies near 15 kc.

Timing and Yield. The temporal characteristics of the thermal radiation from the fire-

ball have been described in Reference 5 and on Pages 24 to 30 and 180 to 189 of Reference 6. In general, when observed from a distance of at least several fireball diameters, the irradiance from the detonation rises rapidly after zero time to a maximum value, decreases somewhat more slowly to a minimum value, and then rises still more slowly to a relatively long second peak, at
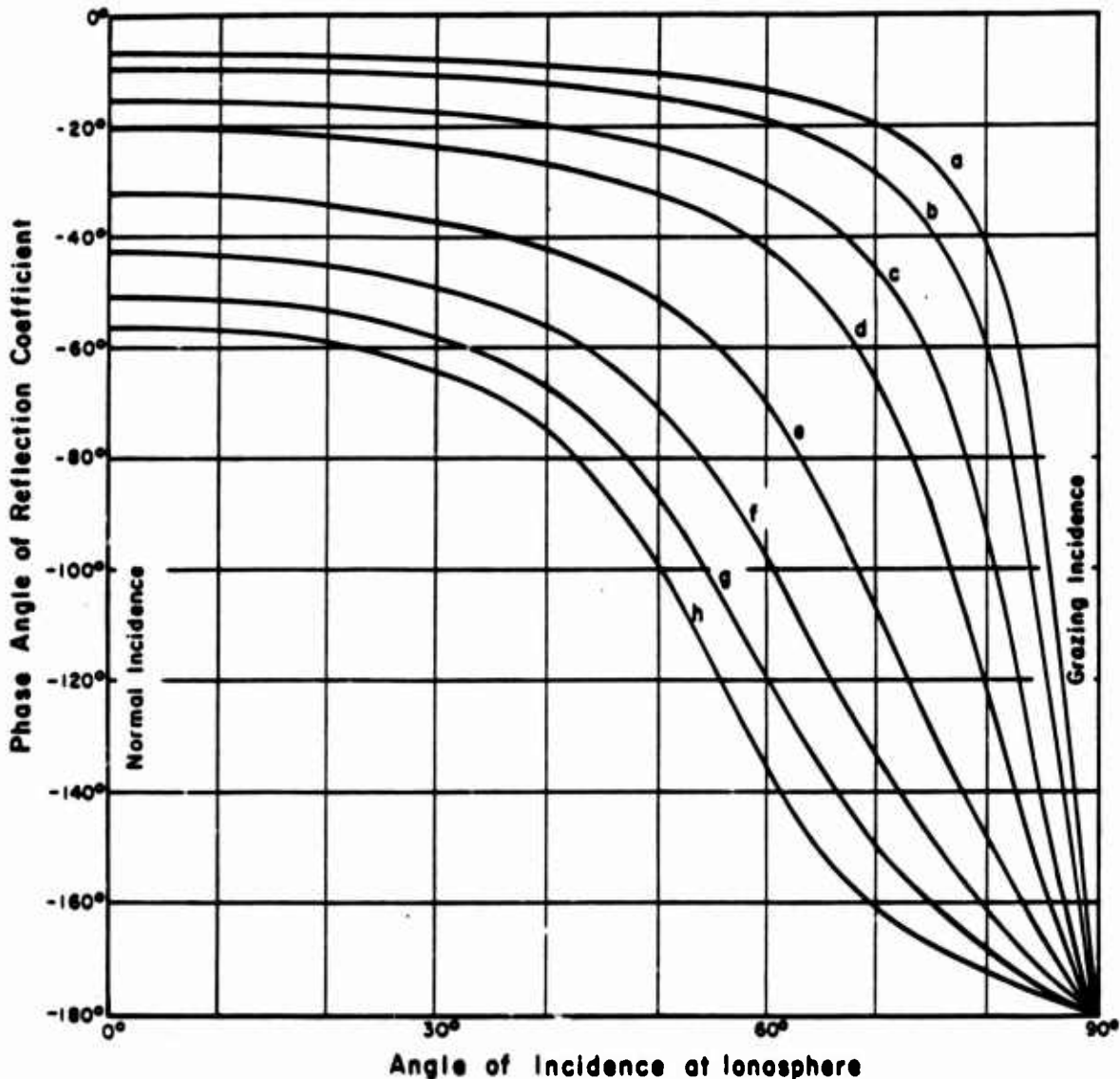
Figure 1.7 Phase angle of ionosphere reflection coefficient for
vertically polarized wave. See Table 1.1 for frequency parameters.

which there is a slow decrease to ambient level. This characteristic behavior of the observed thermal intensity has been illustrated in the upper curve of Figure 1.1, Curve C.

The time intervals (measured from zero time) to the first peak, the minimum, and the second peak, are found to be roughly in the ratio 1:10:100 and are observed to be directly related to the yield of the detonation. Each of the three time intervals varies in proportion to the square root of the detonation yield.

The longest of the three, the time to the second peak, was considered to be the most easily

measured. It was also considered to be the most accurate and the most reliable of all the detonation parameters which could have been chosen for the yield determination. Therefore, it was selected for the primary measurement of yield for the IBDA system.

Within the limitations of instrument response, and with allowance for varying weapon types, zero-point situations, and atmospheric conditions, the energy release, Y, may be determined, with an accuracy of ±20 percent, by the empirical relation given in Equation 1.6.

$$Y = T^2 \tag{1.6}$$

Where: Y = yield, megatons
  T = time to second peak, seconds

Thermal Intensities. The intensity of the thermal radiation, as observed at a given distance, depends upon the surface temperature and the radius of the fireball, as well as upon

TABLE 1.1 FREQUENCY PARAMETERS FOR CURVES IN
FIGURES 1.6 AND 1.7

Curve Identification	$\dfrac{\omega_r}{\omega}$	$\omega/2\pi = f$, (kilocycles)	
		Night: $\omega_r = 10^6$	Day: $\omega_r = 2 \times 10^5$
a	159.155	1	0.2
b	79.578	2	0.4
c	31.8310	5	1
d	15.9155	10	2
e	6.3662	25	5
f	3.1831	50	10
g	2.1221	75	15
h	1.5915	100	20

the range between source and receiver and the atmospheric attenuation along the propagation path.

The fireball temperature is initially above one million degrees K, but falls rapidly as the fireball expands and the thermal energy becomes distributed over a larger volume. The visible surface, which coincides at first with the shock front, cools more rapidly than the interior. Just after the minimum in the observed thermal intensity, the shock front has become so cool that the air is losing its ability to radiate or absorb. It then becomes transparent and allows the inner core of the fireball to become the visible fireball surface. The core is at a much higher temperature than was the shock front just before it became transparent, and the result is that the observed surface temperature rises again to a second peak, which has been described in the previous section. The surface temperature at this second peak is of the order of 6,000 K independent of detonation yield.

In practice, it is difficult to give a very precise value for the color temperature of the fireball at the second peak because the black-body spectral distribution of the fireball is modified by selective absorption in a gaseous layer which forms just outside the fireball, especially with the larger detonations (see Reference 7).

The intensity of the observed thermal radiation depends in part on the size of the fireball. The fireball radius at the moment of the second thermal radiation peak has been measured for

many test detonations. It is given as a function of yield in Figure 1.8, which has been drawn from data provided by Edgerton, Germeshausen, and Grier, Inc. Over the range covered in the figure it can be seen that the fireball radius varies approximately as the cube root of the yield. That is, the yield is proportional to the volume of the fireball at the second peak. This proportionality could be used in the IBDA system for an auxiliary estimate of yield, provided that it was possible to determine the fireball radius from the sequence photographs and to correlate the timing of the photographs, with the timing of the second peak in the thermal radiation intensity curve.

In the absence of atmospheric attenuation, the thermal irradiance at the second peak, measured at a particular range, D, from a fireball with the radius, R, is given by Equation 1.7, which is taken from page 89 of Reference 8.

$$H = W\left(\frac{R}{D}\right)^2 \tag{1.7}$$

Where: H = irradiance
W = radiant emittance
R = fireball radius at second peak
D = distance from source to receiver

The radiant emittance, W, is a function of wave length, as will be explained in more detail in the next section.

An equation of the form of Equation 1.7 could also be written to apply to the irradiance at the first peak. The radiant emittence is higher for the first peak than for the second peak because of the higher surface temperature of the fireball. However, the fireball itself is much smaller at the time of the first peak. Also, the radiated energy tends to be concentrated in the short wave lengths of the far ultraviolet. These wave lengths are quickly absorbed in the atmosphere.

It was concluded from the considerations mentioned above that the first peak would be substantially more difficult to detect than the second peak, under anticipated operational conditions. The IBDA equipment was accordingly designed to make full use of the second thermal peak, but to use the electromagnetic signal instead of the first thermal peak as the fiducial mark establishing the moment of detonation from which the second peak could be timed. Substantiation of this design philosophy was obtained during Operation Redwing.

Spectral Distributions. The radiant emittance of the fireball, given as W in Equation 1.7 is really not a single number. Instead, it is a distribution curve, $W(\lambda)$, dependent on wave length. As stated in the previous section, the fireball has a color temperature of about 6,000 K at the second peak. The black-body spectral distribution for 6,000 K, which is shown in Figure 1.9, is therefore an approximate representation of $W(\lambda)$. Figure 1.9 was plotted from data on page 84 of Reference 9.

The distribution shown in Figure 1.9 can be integrated over any particular wave-length band to give an emittance, W, referring to that band. On page 90 of Reference 8 a value is given for the radiant emittance at the second peak over the wave-length band from 3,500 to 5,000 Å, the approximate wave-length range of a phototube with S-4 response. The radiant emittance was given as the value in Equation 1.8, which is expressed in a form permitting it to be used directly in Equation 1.7.

$$W(\text{S-4 response}) = 2 \times 10^6 \text{ watts/meter}^2 \tag{1.8}$$

In Operation Redwing tests, the thermal radiation was detected photoelectrically. Two different phototubes were used. One, the 1P39, had an S-4 spectral response peaked at about 4,000 Å at the violet end of the visible spectrum, but extending partly into the ultraviolet as well as into the blue and green portions of the visible spectrum. The S-4 response curve has
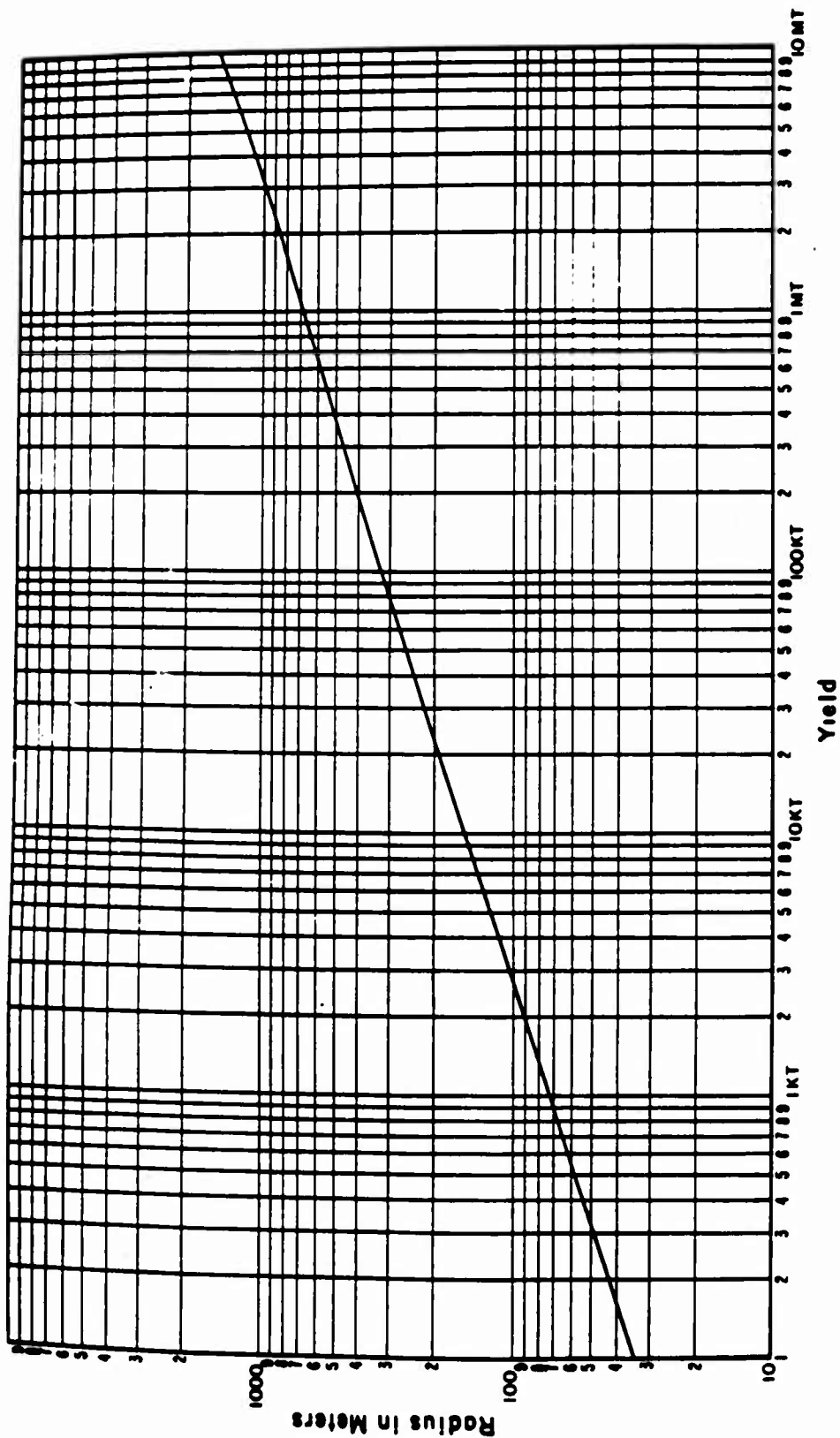
Figure 1.8 Fireball radius at the second thermal radiation intensity peak, as a function of detonation yield.
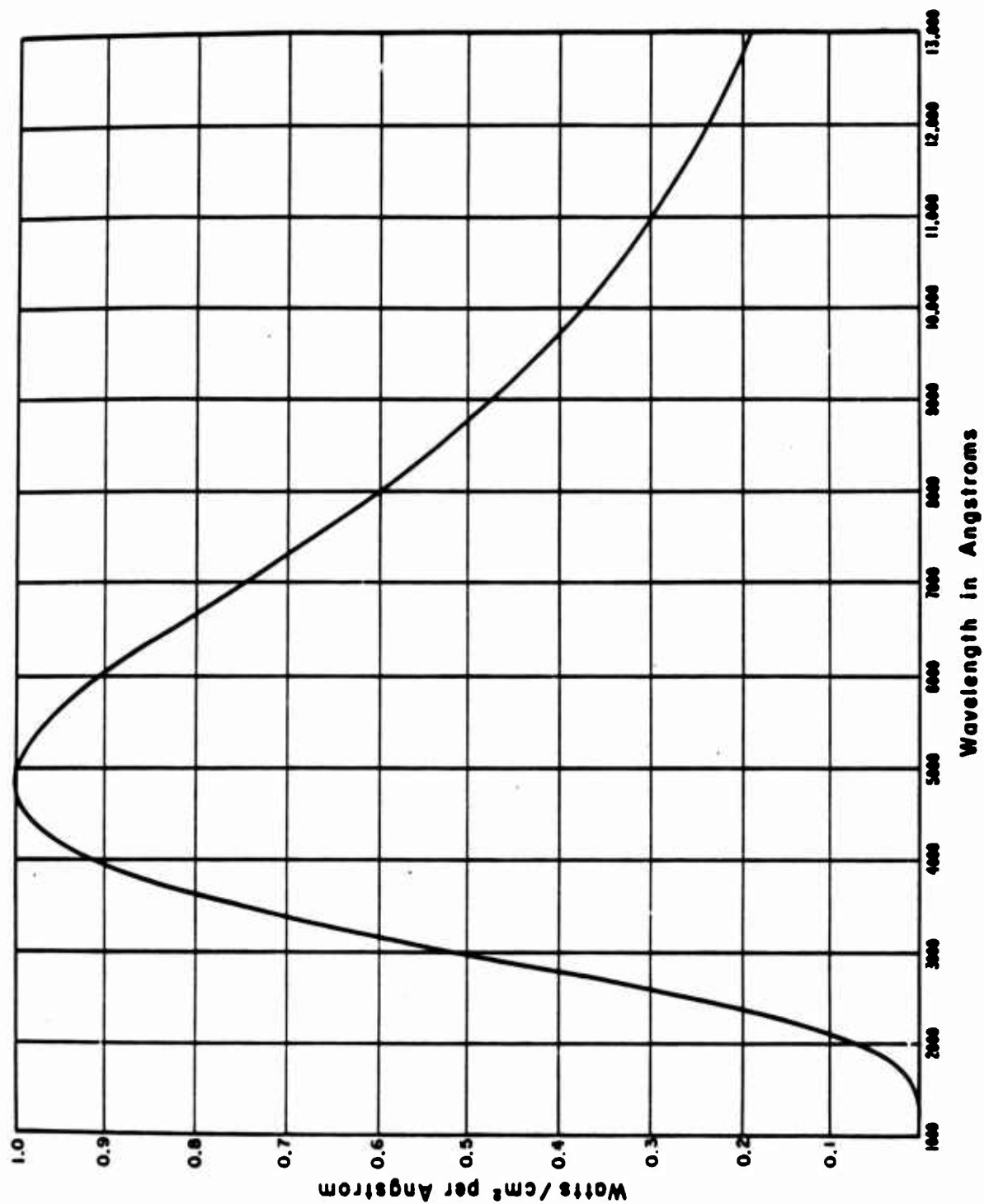
Figure 1.9 Spectral distribution of radiation emitted from a blackbody surface at 6,000 K, as a function of wave length.

34

been reproduced from Reference 10 and is included in this report as Figure 1.10. The S-4 response is sometimes called a blue-green response.

The other phototube used was the 6570, with an S-1 response curve as shown in Figure 1.11 which has also been reproduced from Reference 10. The main response peak is at 8,000 Å in
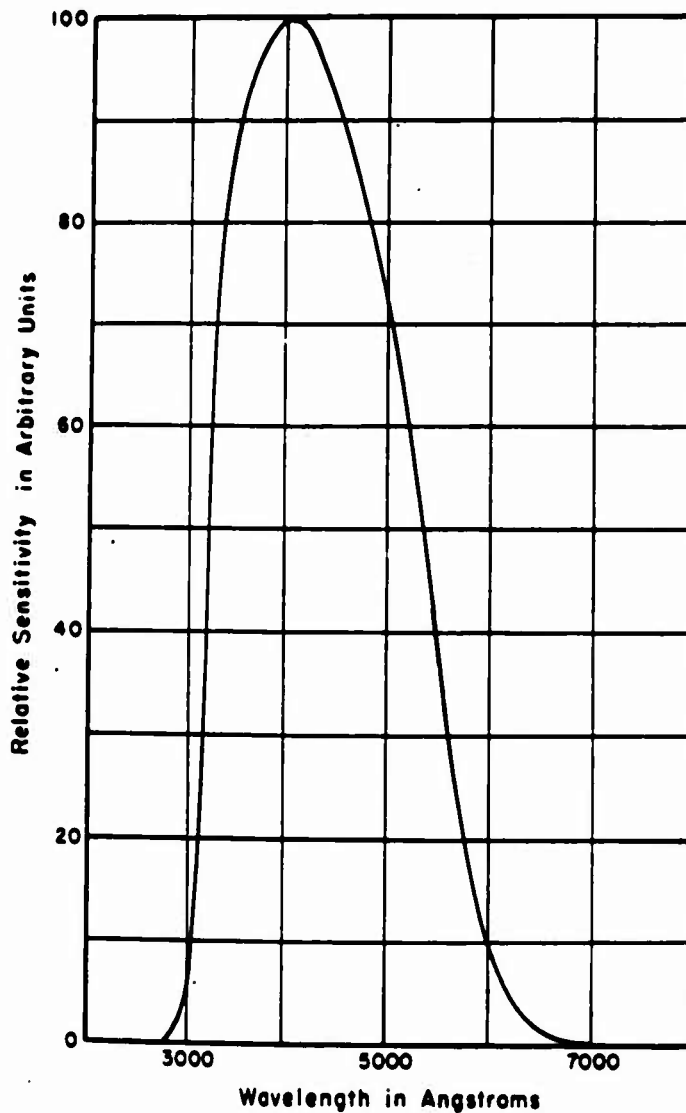
Figure 1.10 S-4 response curve (spectral sensitivity of 1P39 phototube).

the near infrared, extending somewhat farther into the infrared and also extending into the red portion of the visible region. In addition, there is a narrow response peak in the ultraviolet which is shown dashed in Figure 1.11, because neither its position nor its magnitude is held fixed from one tube to the next. However, an S-1 phototube is not marketed unless its response matches quite closely the solid part of the curve in Figure 1.11.

With the help of these response curves and the fireball distribution curve of Figure 1.9, it is possible to make an estimate of the value of W appropriate from the S-1 response. Because the
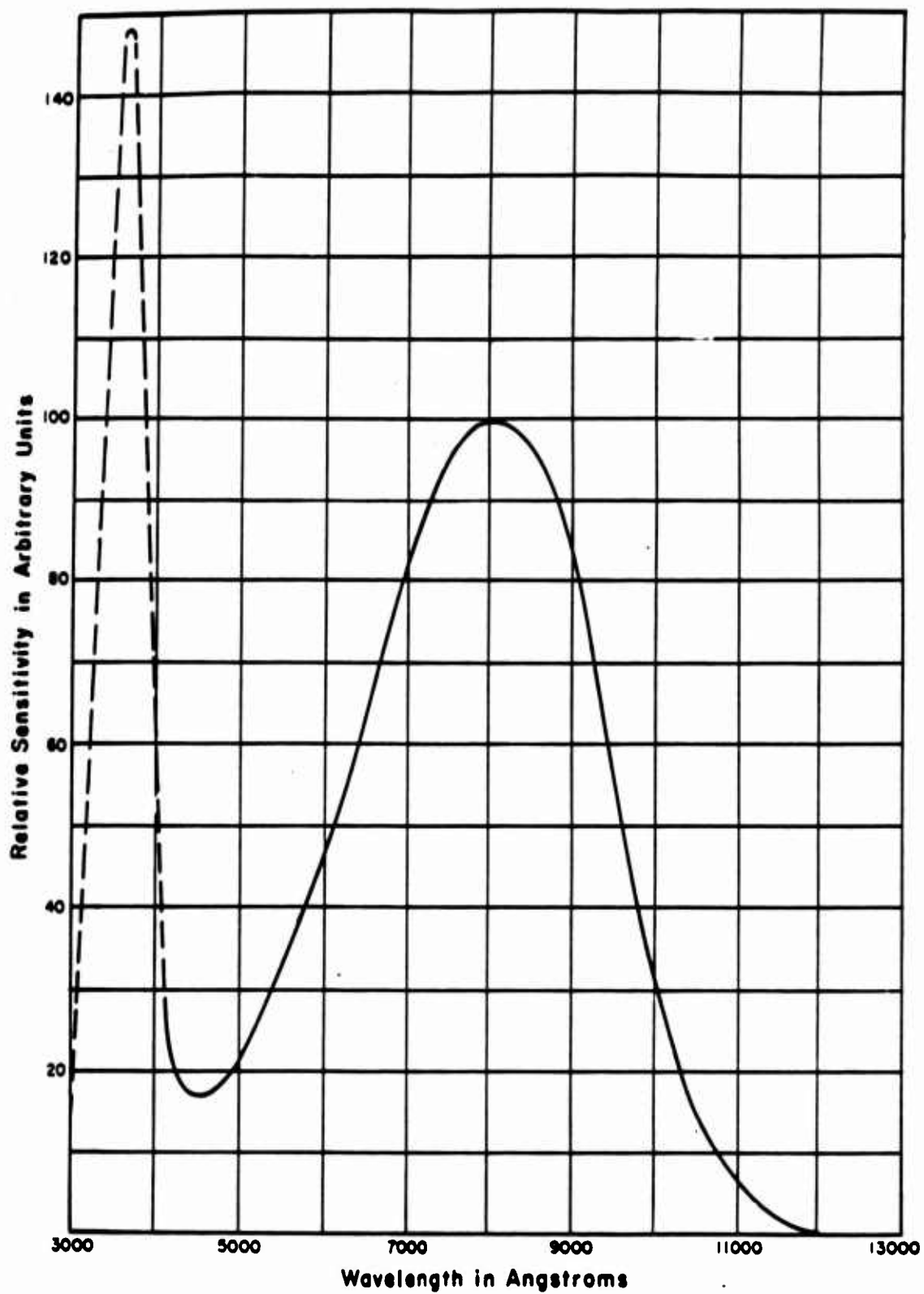
Figure 1.11 S-1 response curve (spectral sensitivity of 6570 phototube).

fireball gives about two thirds as much radiant energy near 8,000 Å as it gives near 4,000 Å, the radiant emittance, W, for the S-1 response could be expected to be roughly two thirds of the value in Equation 1.8. However, the presence of the narrow peak at 3,600 Å, shown dotted in Figure 1.11, suggests that a phototube with S-1 response will give a somewhat greater output
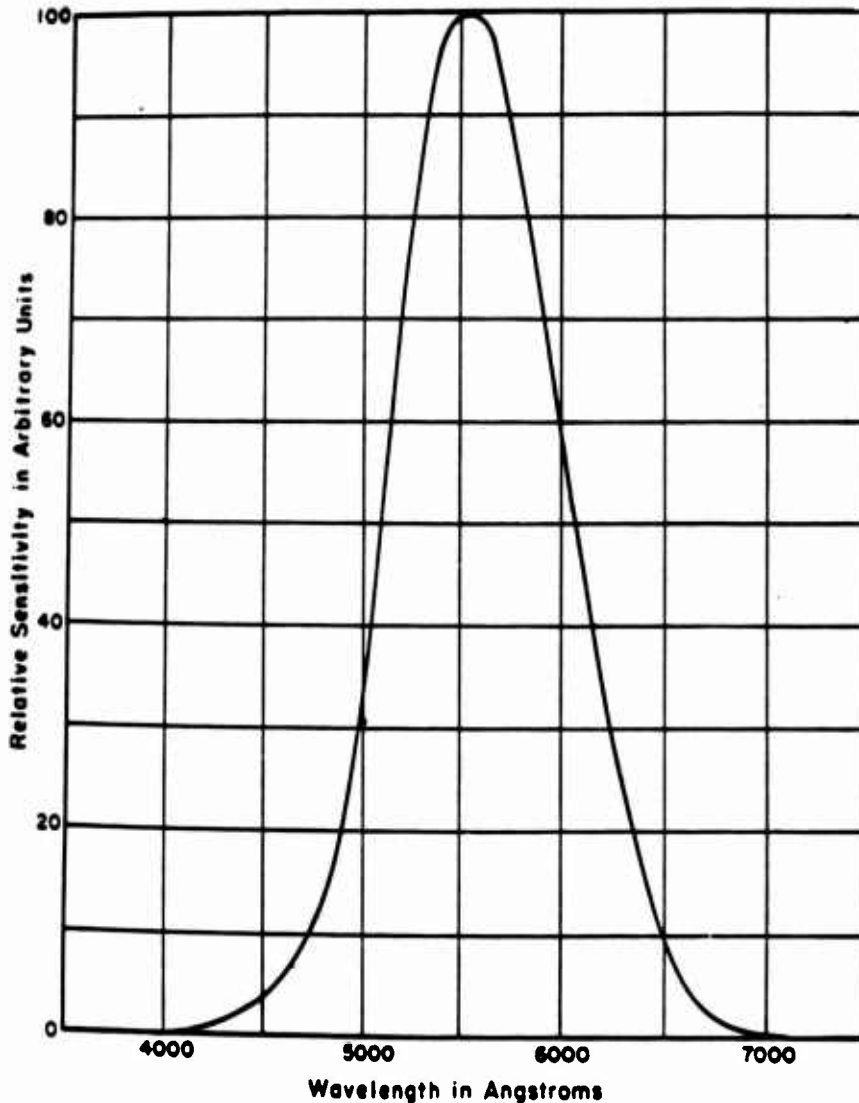
Figure 1.12 Standard luminosity curve (spectral sensitivity of average human eye).

than would be computed from the infrared peak alone. As a result, the value of W should probably be raised somewhat. The rough estimate which was made is given in Equation 1.9.

$$W(\text{S-1 response}) = 1.5 \times 10^2 \text{ watts/meter}^2 \tag{1.9}$$

For comparison with the phototube response curves, the standard luminosity curve representing the average response of the human eye is shown in Figure 1.12. (This, too, is from Refer-

ence 10.) For further comparison, the response curve for the Weston lightmeter used in some of the measurements is included as Figure 1.13 (Reference 11).

Attenuation of Thermal Radiation. Most of the earlier studies of thermal radiation from nuclear detonations had been made in a ground-to-ground environment. Several phototube bhangmeters had been operated in aircraft, but the resultant data had not yet yielded information on absolute irradiance levels. (See References 8 and 12.) During Operation Redwing it was planned to accumulate some of the needed information concerning thermal intensities under varying meteorological conditions.

Under the wide variety of operational conditions for which the IBDA system was designed, the range of thermal intensities expected from the burst covered from six to eight orders of magnitude. That is, the ratio of the largest intensity to the smallest was between 10^6 and 10^8. The possibility of heavy atmospheric attenuation over the longest path, 250 nautical miles, was primarily responsible for this wide range in expected intensities. It was necessary in the design
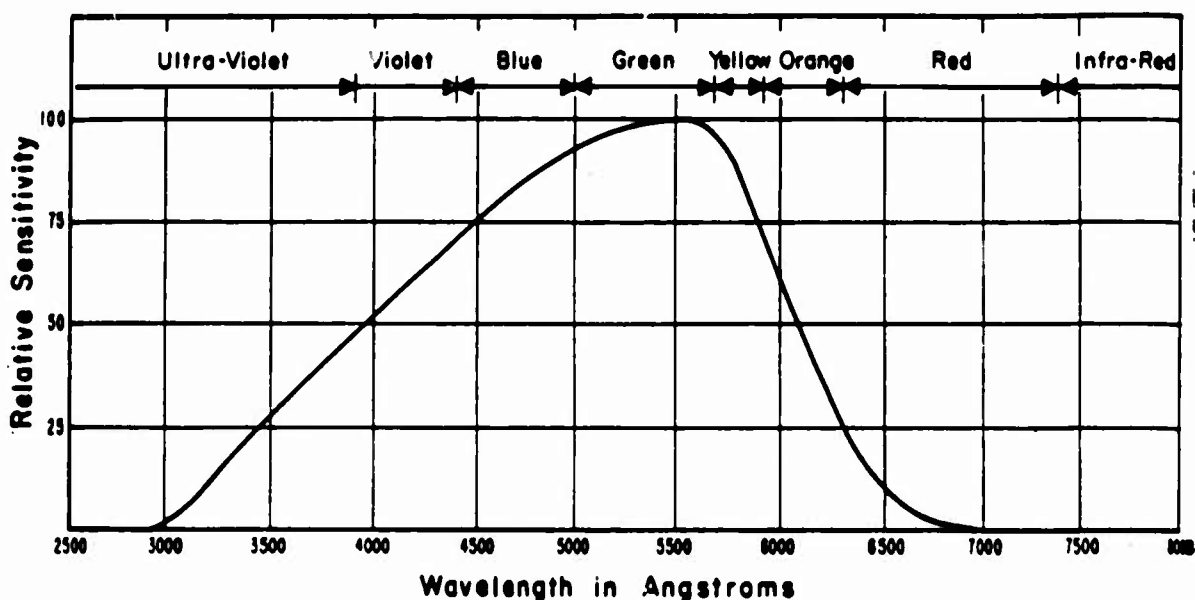
Figure 1.13 Response curve for photocell used in Weston exposure meter.

of the bhangmeter equipment to compress the intensity variation to about two orders of magnitude for convenience in recording, but it was important that the compression should not degrade the temporal characteristics of the wave form to the point where the measurement of the time to the second peak could no longer be made with sufficient precision.

The circuit devised for the compression was found to be satisfactory from the point of view of time measurements on the thermal radiation intensity curve, but it was less satisfactory for intensity measurements which could not be made with any great accuracy. Nevertheless, a number of intensity measurements were made during Operation Redwing tests. The thermal intensity at the second peak was measured for a number of different distances and yields and for varied cloud and atmospheric conditions. A comparison was made between the observed intensity and the intensity predicted from Equation 1.7. The observed intensity was less than the predicted intensity and the reduction factor was attributed to scattering and absorption by the atmosphere and by specific clouds that could be identified in the sequence photographs taken shortly after each detonation.

A difference is to be expected between the attenuation of the thermal radiation within the S-4

38

band and the attenuation in the S-1 band. Attenuation can be by scattering or by absorption. The scattering is by small particles of dust and by water droplets in cloud or haze and also by the air molecules themselves (Rayleigh scattering). The scattering is wave-length dependent in part, and is generally more severe for the shorter wave lengths. The absorption can be by small particles or by specific molecules, such as ozone or water vapor, and may be wave-length dependent in either case. Water, in particular, has strong absorption bands in the infrared. Thus, scattering should be more important in the S-4 band (blue-green) than in the S-1 band (infrared), while absorption might be more important for the S-1 band than for the S-4 band.

Both absorption and scattering will attenuate the direct beam from source to receiver, but scattering can also serve as a transmission route over an indirect path. A detonation may be hidden behind a cloud, for example, and yet be visible to the bhangmeter because of scattering of its emitted thermal radiation from haze or cloud particles in the air above it or around it. There are examples of this effect among the Operation Redwing photographs shown in Chapter 3 of this report.

Ambient Light. The ambient light intensity which reaches the phototube comes ordinarily from either the portion of the horizon sky which lies within the 20-degree field of view of the photohead optical syste..n or from sunlit clouds that drift into that field of view.

The brightness of the horizon sky is discussed on Pages 83 to 88 of Reference 8. It is concluded there that the maximum skylight reaching the phototube within its 20-degree field of view will be 1.6 watts/meter^2 in the wave-length band between 3,500 and 5,000 Å, the approximate range of sensitivity of the 1P39 phototube with its S-4 response (Figure 1.10).

The spectral distribution of sunlight is given in tabular form on Page 87 of Reference 8 and also on Pages 721 to 723 of Reference 9. It is shown in graphical form in the two curves of Figure 1.14. Curve A is for sunlight arriving at the top of the earth's atmosphere, and Curve B is for sunlight reaching the earth's surface on a clear day at a time when the sun is 30 degrees above the horizon.

The spectral distribution of direct sunlight varies with the angular height of the sun in the sky, with the altitude of the observer above sea level, and with the moisture content of the air and its content of scattering and absorbing particles. The spectral distribution of scattered skylight follows the distribution of direct sunlight to some extent but tends to have relatively more energy in the shorter wave lengths and relatively less energy in the longer wave lengths. Curve B of Figure 1.14 would indicate that there was more sunlight in the S-1 band than in the S-4 band (see Figures 1.10 and 1.11). However, the skylight is formed from scattered sunlight, and scattering is stronger in the S-4 band than in the S-1 band, so that the ambient skylight reaching the 1P39 phototube is expected to be about the same as that reaching the 6570.

The maximum light from sunlit clouds can be estimated by the following argument. As a simplified model of a cloud, consider an ideally rough white surface oriented normal to the incident sunlight and viewed from a direction making an angle, Ψ, with the normal to the surface. If D is the distance from the white surface to the photohead, and if Ω is the solid angle contained within the photohead field of view, then the area viewed will be that shown in Equation 1.10.

$$A = \frac{D^2 \Omega}{\cos \Psi}$$

(1.10)

The amount of sunlight intercepted by the area, A, will be P A, where P is the sunlight radiant flux density in watts per square meter. P is actually a function of wave length, a curve like those shown in Figure 1.14. If the surface is diffusely reflecting as assumed and obeys Lambert's law (reflected intensity proportional to cos Ψ), then the flux density in the diffusely reflected wave, at a distance, D, and angle, Ψ, will be P'.

$$P' = P A \frac{4 \cos \Psi}{4 \pi D^2}$$

(1.11)
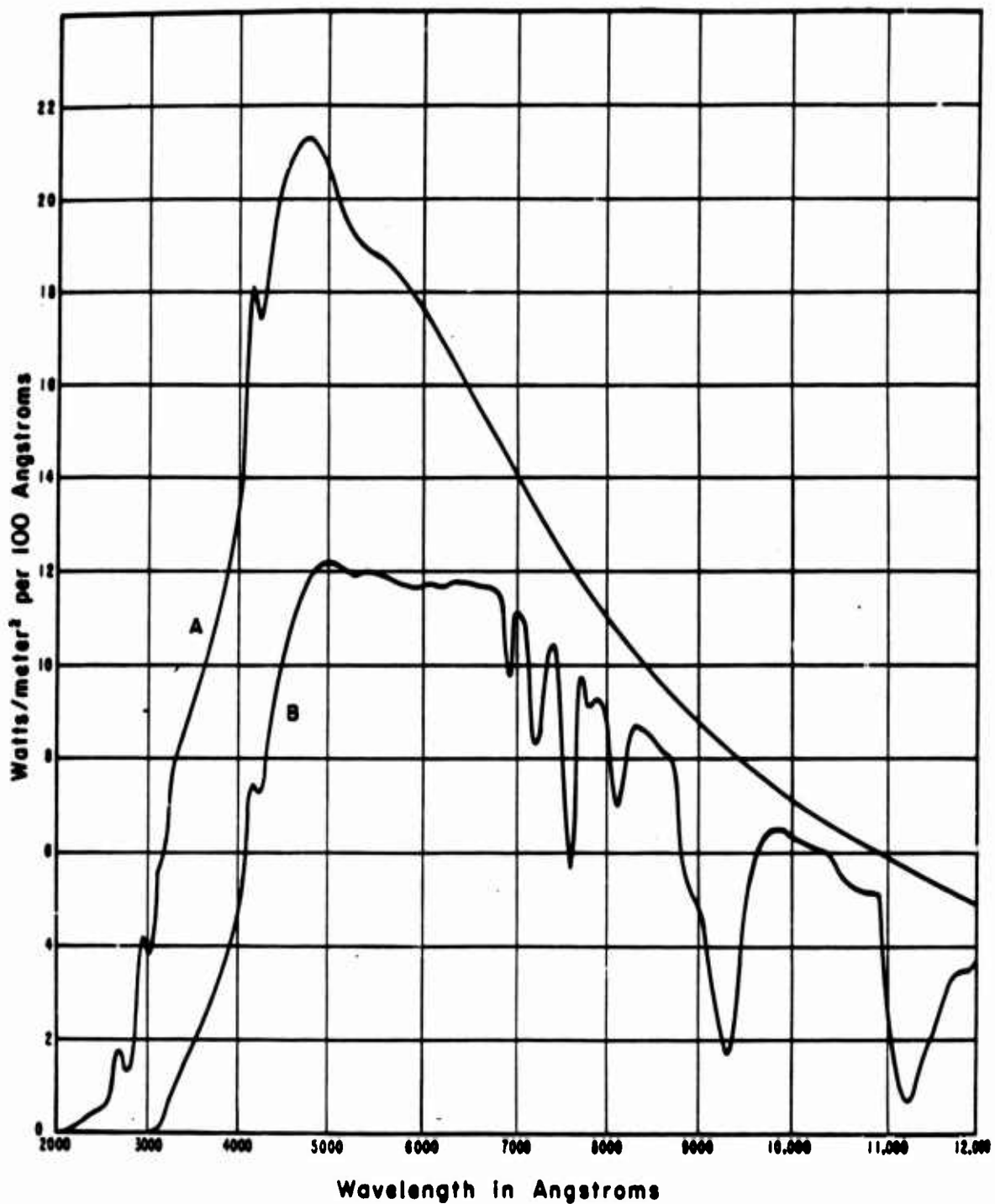
Figure 1.14 Spectral distribution of sunlight, in watts/meter² per 100 Å (0.01 micron), on a surface perpendicular to the sun's rays. (A) Outside the earth's atmosphere. (B) At sea level, with the sun 30 degrees above the horizon.

The numerical factors are so chosen that the total reflected flux, integrated over the hemisphere above the surface, will equal the incident flux, P A.

Substitution of A from Equation 1.10 into Equation 1.11 gives the result shown in Equation 1.12.

$$P' = 4 P \frac{\Omega}{4\pi} \qquad (1.12)$$

That is, the diffusely reflected flux density, P' is proportional to the sunlight flux density, P, with a proportionality factor equal to four times the ratio of the photohead solid angle, 4π.

The phototube in the bhangmeter has a 20-degree field of view, which means a conical field of view with a half angle of 10 degrees. The solid angle, Ω, enclosed in such a cone is as shown in Equation 1.13.

$$\Omega = 2\pi[1 - \cos 10 \text{ deg}] \qquad (1.13)$$

Substitution in Equation 1.12 gives Equation 1.14.

$$P' = 0.03 P \qquad (1.14)$$

An actual cloud will transmit some of the incident sunlight and absorb a further portion so that it will not act as the ideally rough reflecting surface considered above does. Equation 1.14 should, therefore, be considered as an upper bound to the light reflected from a cloud.

The result can be stated in words. The light received by the photohead from the brightest cloud will not be more than three percent of the light that would be received from the sun viewed directly.

A computation from Figure 1.14 shows that direct sunlight in the band from 3,500 to 5,000 Å amounts to about 250 watts/meter^2 at the top of the atmosphere and about 110 watts/meter^2 at sea level with the sun 30 degrees above the horizon. At 18,000 feet, at noon on a clear day, a reasonable estimate might be 190 watts/meter^2 for direct sunlight. Three percent of this, or about 6 watts/meter^2, is therefore the extreme upper limit of the radiant flux density to be expected from the brightest clouds during Operation Redwing tests. This can be compared with the estimate given earlier of 1.6 watts/meter^2 as the expected maximum light, in the same wavelength band, from the horizon sky.

1.3.4 Sequence Photographs. A 35-mm sequence camera was incorporated in the IBDA system design for the primary purpose of locating the angular position of the burst. In Operation Redwing equipment the 35-mm sequence camera served the general purpose of pictorial documentation of the measurements of light intensity. The burst pictures, taken at one frame per second, showed the cloud structure at the time of burst, but they could also be used in evaluating the probable accuracy of burst location. The burst pictures were of added usefulness in showing the fireball and the condensation cloud from which auxiliary information concerning the detonation could be derived. Later pictures of the nuclear cloud development could be used to give further detonation information.

Burst Location. In the IBDA system, the use of the sequence photographs in the location of the point of detonation requires an elaborate system of alignment synchronization and recording to ensure that a measurement on the sequence film can be properly corrected for the motion of the aircraft. This is particularly true for changes in aircraft heading.

In Operation Redwing tests the orientation system mentioned above was not being tested. However, Operation Redwing burst pictures were themselves of importance to the IBDA evaluation program since the accuracy of burst location can be no better than the precision with which the burst center can be determined on the sequence photographs.

There are several methods which can be used to locate the detonation point from the sequence photographs. Where the fireball itself is visible, the location of its center is not difficult. When

41

the fireball is hidden but the condensation cloud can be seen, the center of the condensation dome can be used as the burst point. If both fireball and condensation dome are obscured by clouds, there may be rays of light penetrating through openings in the clouds and appearing as radial streaks on the picture. The central intersection of these rays of light then can be taken as the point of burst. Pictorial examples are included in Chapter 3 of this report.

Fireball Growth. Figure 1.8 shows the radius attained by the fireball at the time of the second peak (t_2) in the thermal-radiation curve. Later, at 10 t_2, the fireball radius has increased to between 1.2 and 1.3 times the value given in Figure 1.8 and has then reached its maximum size. Earlier, at the time of the minimum (0.1 t_2), the fireball radius is roughly 0.6 as large as the value given in Figure 1.8.

When the fireball is visible on one of the sequence photographs and when the approximate time of the photograph is known with respect to the time of detonation, the fireball radius can be used to give an auxiliary estimate of yield if the range is known. Conversely, if the yield is known from other measurements such as the measurement of the time to the second peak, the fireball radius, as scaled off the sequence film, can be used, together with the knowledge of the focal length of the camera, to give an estimate of the range to the detonation.

Condensation Cloud. When there is sufficient moisture content in the air, the rarefaction wave which follows the shock front can cool the air sufficiently to cause the moisture to condense into a visible cloud. Since the condensation process is similar to that in a Wilson cloud-chamber, the condensation cloud has been described as a cloud-chamber effect. (See Pages 26 to 38 of Reference 6.)

The condensation cloud, forming a dome above the fireball, is lighted from within by the fireball and may itself be mistaken for the fireball on a photograph. It may be distinguished from the true fireball by its size because it generally becomes two or three times as large as the fireball. It may also be distinguished by the characteristic horizontal striations into which it breaks as it fades in successive sequence photographs. The striations are believed to be caused by alternating layers of moist and dry air which characterize the lower atmosphere, at least in the areas of the Pacific where Operation Redwing tests took place.

The condensation cloud does not form immediately. It is necessary for the shock front to move beyond the fireball far enough to develop the cooling rarefaction wave or negative phase, which is discussed on Pages 46 to 51 of Reference 6. Even then, the condensation will not take place unless the humidity is sufficiently high. During Operation Redwing tests in the Pacific, the humidity was very high and many of the burst photographs in Chapter 3 show the condensation cloud very clearly.

The rate of growth of the condensation dome is related to the velocity of the shock wave moving away from the fireball. At first the shock wave moves very rapidly. Then later it slows down as described in detail in Reference 6. From the sequence photographs, the growth of the condensation dome could be measured and these measurements could be used in much the same way as the fireball growth measurements to give auxiliary information about the yield of the detonation, when the range was known, or to give range information when the yield had been determined by other measurements.

Nuclear Cloud Development. When the detonation takes place during the day, it may be possible to photograph the development of the nuclear cloud. Both the rate of rise of the nuclear cloud and the maximum height reached by it have been found to be correlated with the yield of the detonation, though with so much scatter in the data that the correlation can be considered only an auxiliary method for yield determination, not a primary one. The experimental correlation is described on pages 16 to 28 of Reference 8, where a similar correlation is also shown between the yield of the detonation and the lateral growth rate and maximum diameter of the nuclear cloud.

Most of Operation Redwing tests took place at dawn when there was insufficient light to photo-

graph the developing nuclear cloud from the range at which the aircraft was usually flying. Photographs were taken later in the day, as shown in Chapter 3, but the nuclear cloud by that time had lost some of its distinctive structure.

Ambient Conditions. For aid in measuring and evaluating the ambient light conditions which could be anticipated in operational situations, the sequence camera was used in synchronization with the photohead equipment. Photographs were made of the horizon sky and of various cloud configurations at the same time that the intensity of the thermal radiation was being measured in the spectral bands of the two phototubes. These measurements are included in Chapter 3.

Chapter 2
PROCEDURE

The requirement for Ultrasonic Corporation (now Advance Industries, Inc.) to participate in nu-clear tests had been a contractual obligation for some time prior to Operation Redwing. Initially, permission was requested to attend the fall tests of 1955. When those tests were cancelled, per-mission was requested for participation in Operation Redwing. Authorization to proceed with confidence was received during February 1956, and a project number was assigned, Project 6.4. About six weeks remained for the procurement and fabrication of equipment, formulation of test plans, and installation of equipment in the aircraft. The instrumentation and operations describe below are not considered to be optimum. More extensive preparation would have led to the re-covery of more data.

2.1 OPERATIONS

The aircraft used in the operations was a C-97 military cargo plane, which flew primarily to satisfy the objectives of another project, Project 6.3. Since Project 6.4 participated in the use of the aircraft on a non-interference basis, the experiments described in this report had to be curtailed to conform to the requirements of Project 6.3. As a consequence, most of the data refer to the larger detonations of the series, and the range is generally not as great as would have been selected if only Project 6.4 had been using the aircraft. On the other hand, the air-craft was flying at its maximum altitude, broadside to the burst, in accordance with the needs of Project 6.4.

2.1.1 Flight Plans. The flight plans for an actual burst were regulated closely by the opera-tional group at the Pacific Proving Ground (PPG). The major requirement presented by Project 6.4 was that the aircraft be broadside to the burst at H hour, with the burst to starboard. Figure 2.1 shows the geographical position of the aircraft for the bursts on which data were successfully recorded in the air. For four shots the aircraft was not available for flight, and measurements were made from ground sites. These sites are included in Figure 2.1 with an asterisk for iden-tification.

2.1.2 Operating Procedure. In Chapter 1, three categories of burst-generated phenomena were considered. These were the electromagnetic signal, the thermal radiation, and the picto-rial aspects of the burst. The Project 6.4 equipment for measuring these phenomena is describe in detail in Section 2.2, Instrumentation.

For the purpose of describing the operational procedure, it is sufficient to list the equipment used for each kind of measurement. For the measurement of the electromagnetic signal, there were two magnetic antennas (fiducial antennas) and one whip antenna, together with amplifiers, oscilloscopes, and scope cameras. To measure the thermal radiation, there were two photoheads and a Heiland recorder. A sequence camera was used for the photographic record. During the series of test shots, the equipment was operated in several different ways. These are described in the following three sections.

Automatic Operation. The system design included a synchronizer package which was intended to make the operation of the equipment as automatic as possible and to present the opera-

All Times Are in Local
ENIWETOK Time

RONGELAP

ALINGINAE

BIKINI

Navajo
0556
11 July

WOTHO

Dakota
0606
26 June

Tewa
0546
21 July

Cherokee
0551
21 May

Zuni
0556
28 May

UJAE

Inca
0956
18 June

Yuma
0756
28 May

Apache
0606
9 July

Blackfoot* Kickapoo*
0626   1126
12 June   14 June

Lacrosse* Osage*
0629   1314
5 May   16 June

ENIWETOK

Mohawk
0606
3 July

UJELANG

Huron
0616
22 July

Shot	Range Naut. Miles	Bearing Degrees
Lacrosse*	12	062
Cherokee	98	339
Zuni	99	341
Yuma	58	231
Blackfoot*	9	353
Kickapoo*	14	347
Osage*	12	004
Inca	67	230
Dakota	98	341
Mohawk	41	014
Apache	44	102
Navajo	55	022
Tewa	96	338
Huron	135	014

Figure 2.1 Geographical position of the receiving equipment for shots in which Project 6.4 participated. Starred bursts refer to observations made on the ground; all other observations were airborne, usually at an altitude of 18,000 feet.

tor with the least amount of work at the critical time. However, in anticipation of the need for flexibility, the synchronizer provided a semiautomatic mode of operation as well as an automatic mode. In either mode, the synchronizer provided simultaneous operation of the two photoheads, the recorder, and the sequence camera. In the automatic mode, the oscilloscope cameras were operated automatically along with the photoheads, recorder, and sequence camera. In the semi-automatic mode, either the photohead system and sequence camera, or the fiducial system, with the two scope cameras, could be operated independently. The synchronizer also provided means by which the recorder and oscilloscopes were calibrated in time and in amplitude, and provided counters whose numbers could be recorded for correlation of the data from the various instruments.

It was originally planned to operate in the following manner. The semiautomatic mode would be used by the operator for calibrating the equipment and recording the calibration results on film. The equipment would then be switched to the automatic mode. When the count-down for H hour was broadcast, preset counters in the synchronizer would allow the operator to synchronize his equipment with the count-down, approximately 30 seconds before H hour. Operation would then become completely automatic. At minus five seconds, the oscilloscope cameras would open, the Heiland recorder would start, the sequence camera would begin taking pictures, and the relays in the photoheads would activate. At plus two seconds, the scope cameras would automatically close. At plus 12 seconds, the recorder would stop running, and the photohead relays would de-activate. The sequence camera, however, would continue to run to take pictures of the nuclear cloud. After several minutes, the operator would switch back to semiautomatic operation and recalibrate his equipment. The above procedure was used for the first four shots.

Ground Station. The aircraft was not available at the proving grounds for the fifth and sixth shots. Upon returning to the PPG, it encountered difficulty and was unable to participate in the next four shots. However, part of the equipment was removed from the aircraft and set up in a tent on Site Elmer (Parry Island, Eniwetok Atoll). The testing of the fiducial antenna was the objective of highest priority, and the equipment set up at the ground station was concerned with this objective. Included were one dual-beam oscilloscope (Dumont Model 333), two fiducial antennas, a scope camera, and the necessary power supplies and cables.

At the ground station the equipment was operated manually. The shutter of the scope camera was opened at minus two seconds and closed at approximately plus one second. Because the magazine of the scope camera had given difficulty on the earlier shots, it was replaced by a Polaroid film magazine for operation at the ground station and for airborne operation during the later tests.

Manual Operation. When the aircraft was ready for further participation, the equipment which had been taken out was reinstalled. Based on experience gained during the first four shots and during the operation at the ground station, the automatic operation was replaced by a procedure which was almost entirely manual. It had been found, for example, that the switching action in the synchronizer and in the sequence camera caused interference that was picked up by the sensitive fiducial and photohead circuits. Because there was not enough time to install sufficient shielding and filtering, the procedure was changed instead.

The procedure for manual operation was the following. At the count of minus five seconds, the Heiland recorder was turned on and the relays in the photohead were activated. At the count of minus 2 seconds, the scope camera shutters were opened. The shutters were held open until either the fiducial signal was seen on one of the scopes or the visible light from the detonation was observed through the windows of the aircraft. Immediately after the burst, the sequence-camera switch on the synchronizer was turned on to start the sequence camera which took pictures at one frame per second. At plus 15 seconds, the Heiland recorder was turned off. At plus 60 seconds the sequence camera was turned off, since the aircraft changed heading at this time and the nuclear cloud was no longer in view. The equipment was then calibrated.

46

2.1.3 Data Sheets. Each time a scope picture was taken, a notation was made on a data sheet, giving the time, the exposure number on the film, the oscilloscope type (333 or 324), the sweep length and gain settings, and pertinent information concerning the content of the picture. Similar notations were generally made for each interval of operation of the Heiland recorder and for each series of frames on the sequence camera.

Figure 2.2 illustrates a sample four-page data sheet containing the notations for the scope pictures during Shot Navajo (Page 1), sequence camera data and Heiland recorder data during Shot Navajo and for cloud studies (Page 2), camera and recorder data for further cloud studies (Page 3), and photohead calibration data taken on the ground after the shot (Page 4). The additional notations needed to identify the particular shot, the film rolls, the geographic location of the aircraft with respect to the burst, and other similar details concerning the mission are shown at the top of Page 1 of the data sheet.

2.1.4 Cloud Measurements. An important source of ambient light is the reflection of sunlight from clouds that lie within the field of view of the photohead. Quantitative data was needed on the brightness of the clouds and on the fluctuations of the light from clouds as the aircraft flew near or through them.

On several flights, the light received from clouds was recorded on the Heiland recorder, and synchronized photographs were taken by the sequence camera, so that the changing appearance of the clouds could be correlated with the varying output of the photoheads. The data sheet in Figure 2.2 includes notations concerning such cloud measurements made with the two photoheads and the sequence camera.

2.1.5 Photohead Calibrations. So that the deflection of the Heiland recorder trace might be used as a quantitative measure of light intensity, a number of calibration measurements were made on the ground. A light bulb was placed at one end of a specially constructed cylindrical tube. One of the photoheads was placed at the other end, with its output connected to a channel of the Heiland recorder. The bulb was turned on and off while the recorder was operating, and the resulting Heiland recorder deflection was compared with the setting of a Variac which controlled the brightness of the bulb. A comparison was also made with the reading of an exposure meter which was substituted for the photohead to give a measure of the incident light from the bulb. Some of these calibration measurements are noted on the data sheet in Figure 2.2.

Two bulbs were used, one a photoflood bulb giving white light, and the other, an infrared bulb. To some extent, however, the filament temperature of such a bulb depends on the Variac setting, and the spectral distribution of the emitted light depends, in turn, on the filament temperature. The spectral distribution of the light source was, therefore, changed whenever the intensity was changed.

The two photoheads and the exposure meter all had different spectral response curves, as shown in Figure 1.8. As a result, the photohead calibration measurements were not as easily interpreted as had been expected. They could, nevertheless, be used in the translation of some of the Heiland deflection readings into values of light intensity.

A different kind of measurement of the photohead response was carried out after Operation Redwing test detonations were over. The output current to the Heiland recorder was measured as a function of the current through the phototube itself when the light striking the phototube was varied. Several levels of ambient light were simulated, and several characteristic curves were therefore obtained. (The curves are shown later in this report in Figure 2.19.)

2.2 INSTRUMENTATION

The primary data to be gathered in Project 6.4 consisted of records of the electromagnetic

Page 48 Deleted

OPERATOR _____ DATE _____ 1956

SHOT TITLE __Navajo__ TIME _____ YIELD(OFF.) _____ RANGE _____ MI. ALTITUDE _____ FT

METEOROLOGICAL CONDITIONS _____

AZIMUTH HEADING _____ ° LOCATION _____ ° ' LAT. _____ ° ' LONG.

SEQUENCE CAMERA FILM NO. _____ MAG.NO. _____ FOCUS _____ f FILTER _____ FRAME ↗

RECORDER PAPER # _____ PHOTOHEAD FILTER _____ (333) MAG.NO. ____ FILM ROLL ____ (324) MAG.NO. ____ FILM ROLL ____

UNIT	FUNCTION	TIME	VISUAL COUNTER NO's.	LIGHT μa	RECORDER PAPER IDENT	RECORDER CHAN	RECORDER POS	CAL μa	SWEEP LENGTH μ SEC	GAIN SETTINGS VAR.	GAIN SETTINGS FIXED	SCOPE & TRACE IDENT
Sequence Camera	Shot	0556	1-39	f 22	N.D.filter		2.0					
"	Bomb cloud	0606	40-44, 45-55	f 1.9	No filter							
"	"	0627	56-238	f 4.0	No filter							
Rec & Photo	Shot	0556		-		2	Upper					Blue green Navajo shot
"	"	0556		-		3	Lower					Infra-red Navajo shot
Recorder	Calibrate	0603		-		1,2,3,4,5		69 thru 5 channels				
Recorder Photohead	Clouds	0655		4		2	U					
"		0655		1		3	L					
Sequence Camera		0655	239-252	f 16	No filter							
"		0658	253-292	f 16	No filter							
Recorder & Photohead		0701		6		2	U					
"		0701		1		3	L					
Sequence Camera		0701	293-300									
Recorder Photohead		0705		8		2	U					
"		0705		2		3	L					
Sequence Camera		0705	101-312									

REMARKS

Figure 2.2 Continued.

OPERATOR _____ DATE _____ 1956

SHOT TITLE _Navajo_ TIME _____ YIELD(OFF.) _____ RANGE _____ Mi. ALTITUDE _____ FT.

METEOROLOGICAL CONDITIONS

AZIMUTH HEADING _____ LOCATION _____ ° LAT. _____ ° LONG.

SEQUENCE CAMERA FILM NO. _____ MAG. NO. _____ FOCUS _f_ _____ FILTER _f#_ _____ FRAME _f#_ _____

RECORDER PAPER _#_ PHOTOHEAD FILTER _____ (333) MAG. NO. _____ FILM ROLL _____ (324) MAG. NO. _____ FILM ROLL _____

UNIT	FUNCTION	TIME	VISUAL COUNTER NO's.	LIGHT μa	RECORDER PAPER IDENT	RECORDER CHAN	POS.	CAL μa	SWEEP LENGTH μ SEC	GAIN SETTINGS VAR.	FIXED	SCOPE & TRACE IDENT.
Recorder Photohead	Clouds	0755		10		2	U					
"		0755		2		3	L					
Sequence Camera		0755	313-324	f 22	N.D. 0.5	filter						in cloud
Recorder Photohead		0800		22		2	U					
"		0800		2		3	L					
Sequence Camera		0800	325-367	f 22	N.D. 0.5	filter						in & out of cloud and the right bank
Recorder Photohead		0805				2	U					Blue-green
"		0805			Clouds	3	L					Infra-red
Sequence Camera		0805	368-378	f 22	N.D. filter	0.5						
	Calibrate	0807				1,2,3,4,5		69 thru 5 channels				

REMARKS _____

OPERATOR _____ DATE _____ 1956

SHOT TITLE _Navaho_   TIME _____ YIELD(OFF.) _____ RANGE _____ MI. ALTITUDE _____ FT

METEOROLOGICAL CONDITIONS _____

AZIMUTH HEADING _____ °   LOCATION _____ ° _____ ' LAT. _____ ° _____ ' LONG.

SEQUENCE CAMERA FILM NO. _____ MAG. NO. _____ FOCUS _____ FILM ROLL _____ FILTER _____ FRAME [#]

RECORDER PAPER [#] _____ PHOTOHEAD FILTER _____ (333) MAG. NO. _____ (324) MAG. NO. _____ FILM ROLL

UNIT	FUNCTION	TIME	VISUAL COUNTER NC's.	LIGHT μa	RECORDER PAPER IDENT	RECORDER CHAN	RECORDER POS	CAL μa	SWEEP LENGTH μ SEC	GAIN SETTINGS VAR.	GAIN SETTINGS FIXED	SCOPE & TRACE IDENT
Recorder & Photohead	Calibrate	1330	Variac Setting		Calibrate					Light	Meter	
			44	14		2	U			375		White Bulb
			48	20		2	U			450		
			57	40		2	U			825		
			60	50		2	U			1175		
		1345	67	14		3	L			13		Infra-red Bulb
			79	20		3	L			23		
		.	104	40		3	L			75		
			116	50		3	L			100		
		1350	135	1	with 1% filter on photohead	3	L			150		White Bulb
		1355	135	5		2	U			1000 with		
				with 1% filter on photohead						N.D. 1.0 on light meter		

REMARKS _____

Figure 2.2 Continued.

pulse and the thermal intensity and pictures of the fireball and the nuclear cloud. In no case was there anything to be transmitted, and the instrumentation was accordingly all of the passive type, designed for reception only. Specially built detection instruments, including prototype equipment for the IBDA system, were combined with standard laboratory test equipment and installed in the aircraft, a C-97 military cargo plane. The principal requirement placed on the aircraft installation was that the detection equipment be provided with a clear line of sight to the nuclear explosion.

2.2.1 Block Diagram. Figure 2.3 is a block diagram showing the connections linking the more important pieces of equipment. The specially built detection instruments are indicated in the blocks at the top of the figure. The remaining blocks show the power sources, the synchronizer, and the instruments necessary for presenting and recording the electromagnetic and thermal signals.

A whip antenna was included in Operation Redwing equipment for comparison with the loop antennas. For all shots, the whip antenna was connected to its cathode follower, as shown in Figure 2.3, and the two ferrite-core loop antennas were connected to the fiducial amplifiers. However, for some shots the three outputs were presented on the three channels of the two oscilloscopes with connections that were different from those shown in the block diagram. For example, the dual-beam oscilloscope was sometimes used to present the signals from the two ferrite antennas, leaving the whip antenna signal for presentation on the single-beam oscilloscope. Two scope cameras were used to make a permanent record of the presentation.

Two photoheads were used, one containing a 1P39 phototube and the other containing a 6570 phototube. The outputs from the two photoheads were fed to separate channels of the six-channel Heiland recorder, which recorded directly onto a moving strip of light-sensitive paper. On some early shots, there was an extra connection to the Heiland recorder. A pulse from the sequence camera was introduced onto a third Heiland channel, to indicate the time at which each frame was exposed, for correlation of the sequence photographs with the varying output currents from the photoheads.

The primary power source, as indicated in Figure 2.3 was a 115-volt, 400-cycle inverter, which was powered by the 28-volt, direct-current power from the aircraft generator (or from an auxiliary power unit during ground operation). The 400-cycle power was used for the direct-current power supplies and also for the alternating-current power requirements of all the instruments.

The synchronizer was designed to throw switches, controlling the other pieces of equipment, at predetermined times relative to the time of burst. The switch controls are shown as dashed lines in Figure 2.3. The procedure was changed midway through the program of test detonations and a number of automatic functions of the synchronizer were transferred to manual operation. For example, the operation of the two scope cameras was made manual, although the timing of the sequence camera exposures, at one per second, was left under the control of the synchronizer.

2.2.2 Installation. The installation of the equipment in Aircraft C-97A S/N 49-2596 was conducted at the Air Force Cambridge Research Center, Laurence G. Hanscom Field, Bedford, Massachusetts. Details of the installation are contained in Reference 13.

Figures 2.4 to 2.11 show the equipment and its installation in the C-97 aircraft. Most of the primary equipment is shown in Figure 2.4, with the exception of the antenna and its cathode follower. In the category of secondary equipment are the inverter, the power supplies, the various cables and the junction boxes. Figure 2.5 is a sketch of the C-97 showing the location of the main items of equipment used by Project 6.4.

Power. The 400-cycle inverter was located beneath the forward crew compartment. Direct-current power for the inverter could come directly through the aircraft 28-volt supply, which was powered either by the aircraft generators or by an auxiliary power unit (APU) plugged into the air-
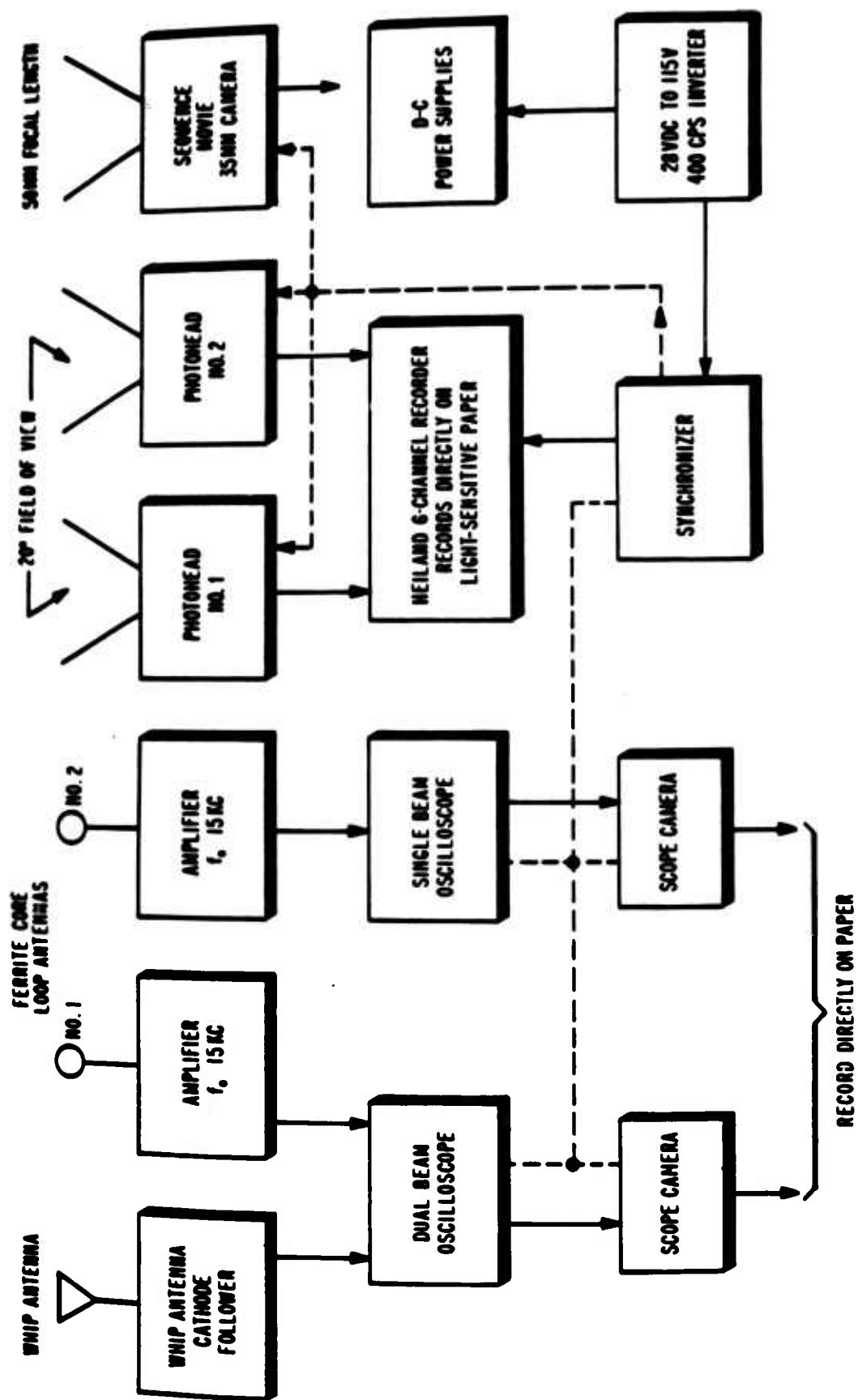
Figure 2.3 Block diagram of instrumentation.

craft for ground operation of the aircraft's electrical system. Alternatively, for ground operation of Project 6.4 equipment only, an APU could be connected to a power receptacle provided on the project relay box, located inside the aircraft just forward of the forward entry door. The direct-current power source to be used (aircraft power or external power) was selected by a switch at the power control box, located on the forward left-hand side of the upper cargo compartment. Alternating-current power from the project inverter was routed through the power control box to the power distribution box, which was installed on the lower forward end of the main equipment rack at the operator's position (Figure 2.6). From this point, the alternating-current ' power was distributed to the individual project components.

All direct-current power requirements for Project 6.4 were satisfied through the use of power supplies and rectifiers operating from the 400-cycle inverter output. In order to avoid
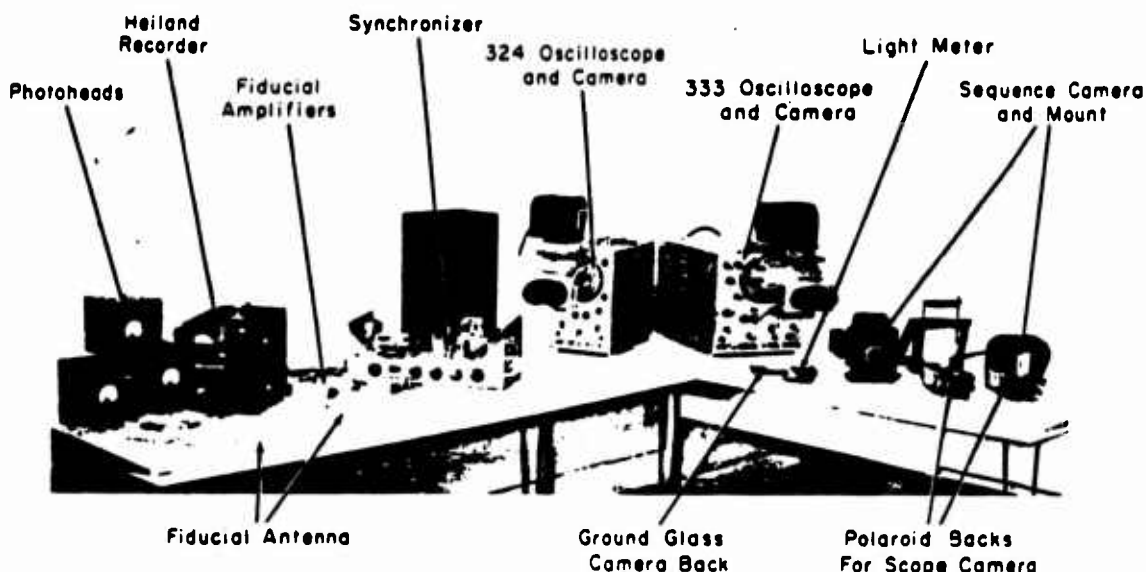
Figure 2.4 Primary equipment.

interference with Project 6.3, which used equipment particularly sensitive to any voltage fluctuation on the 28-volt, direct-current line, there was no direct use of the 28-volt, direct-current aircraft power except for the operation of the inverter itself. The inverter could be turned off, and all Project 6.4 wiring de-energized, by means of an on-off switch on the flight engineer's panel, for the flight engineer's use whenever the need might arise.

Equipment Racks. In addition to the power distribution box, the main equipment rack at the operator's position (Figure 2.6) also contained the two direct-current power supplies, for −150 volts and +250 volts, on the left and right sides, respectively, of the lower shelf. The Heiland recorder was located in the center of the lower shelf, between the two power supplies, and the synchronizer was in the center of the upper shelf, between the two oscilloscopes.

The main equipment rack held most of the equipment needed for presenting and recording the received information. However, most of the instruments used for the actual detection were located a short distance away on a smaller rack designed to hang just inside one of the aircraft windows. This window provided the sequence camera and the two photoheads with a clear view in the direction of the nuclear detonation when the aircraft maintained the correct orientation. The window used was the one farthest aft on the starboard side of the aircraft. The operational location of the window equipment rack is indicated in Figure 2.5.

This window was also used by a crew member for scanning purposes during takeoff and land-
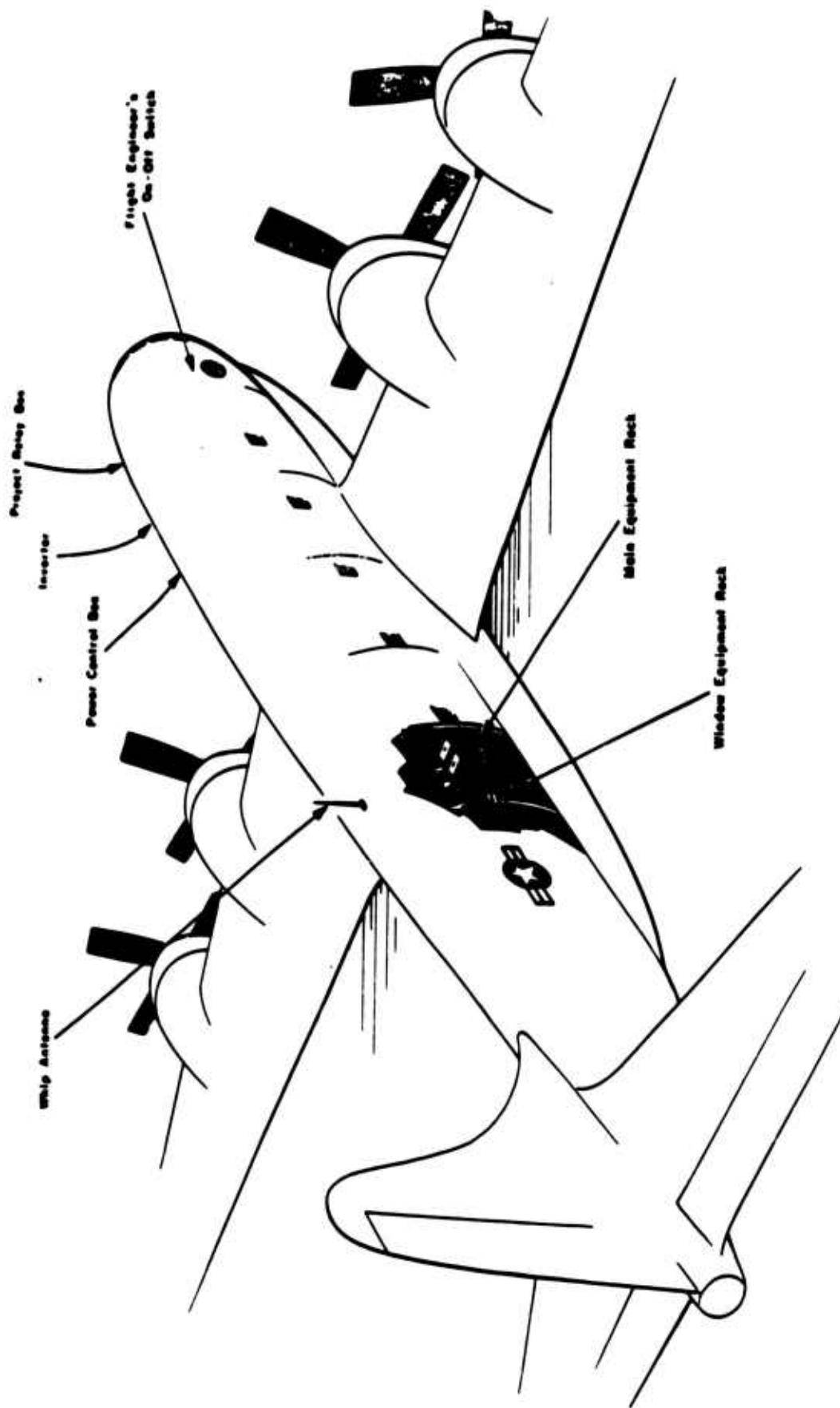
Figure 2.5 Sketch of C-97 aircraft showing location of equipment for Project 6.4.
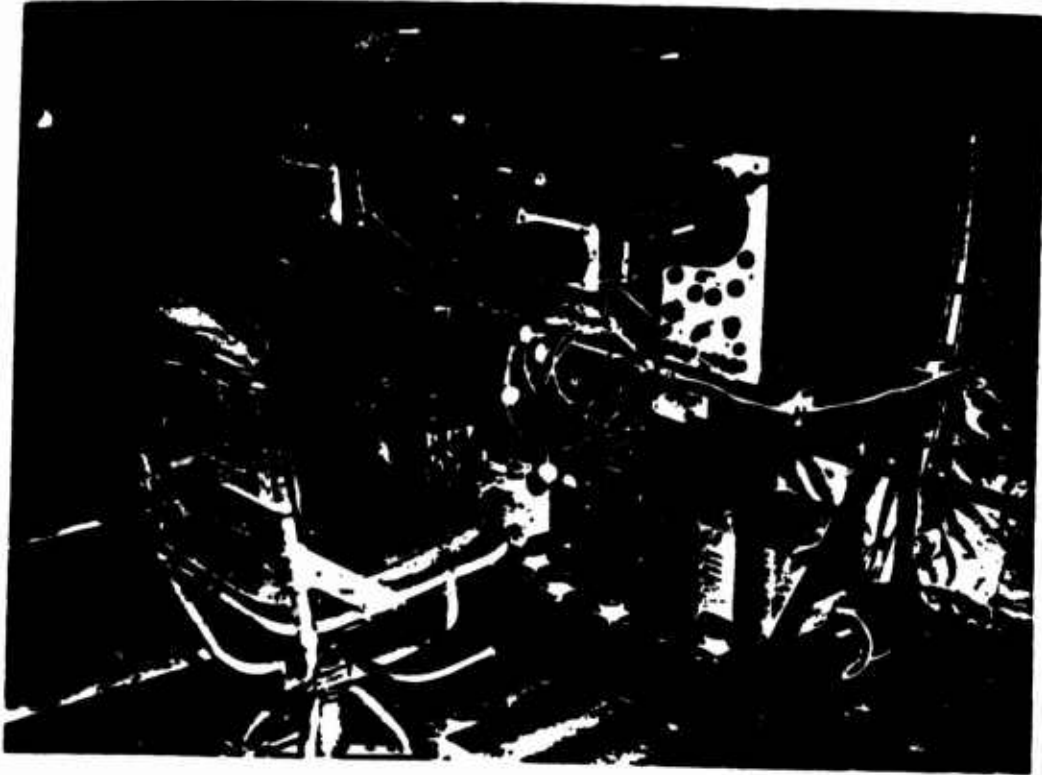
Figure 2.6 Main equipment rack.
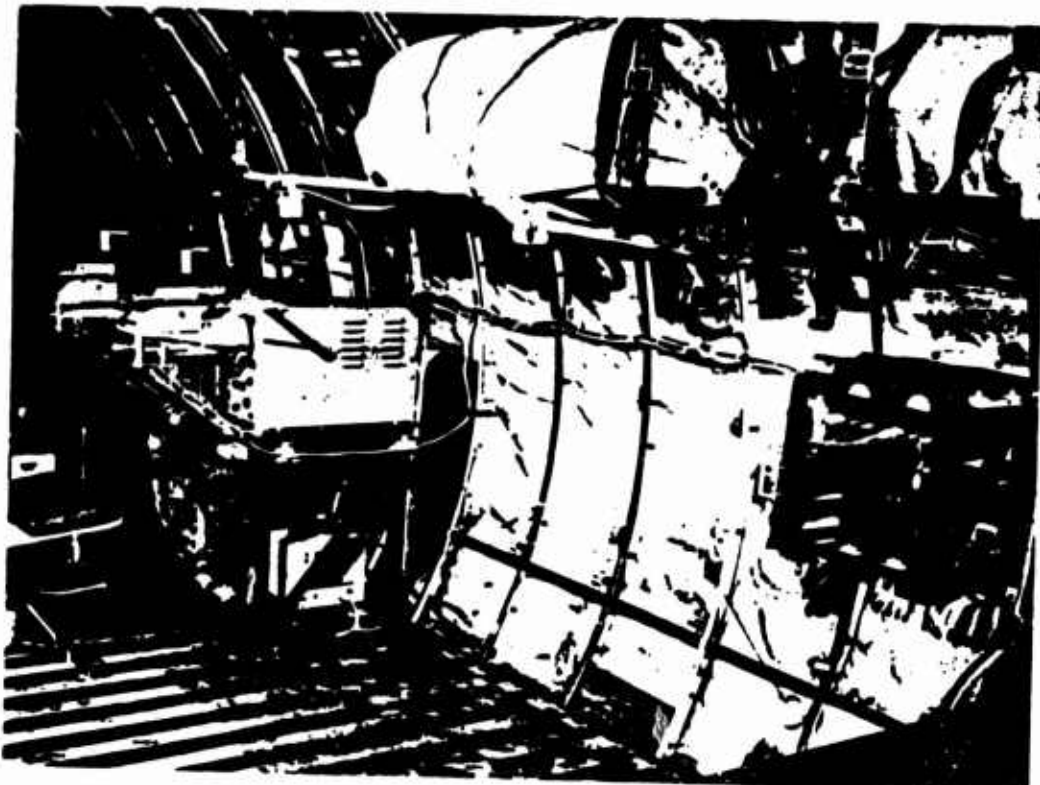
Figure 2.7 View of C-97 installation.
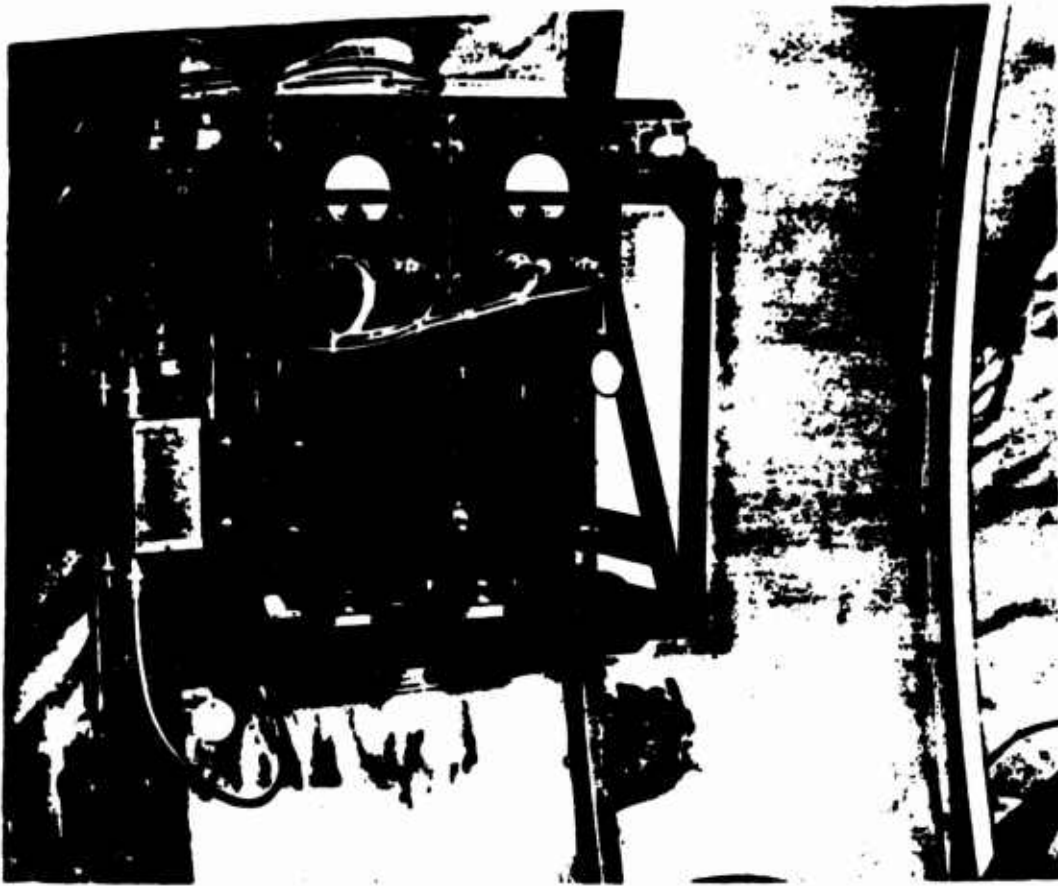
Figure 2.8 Window equipment rack.

Figure 2.9 Fiducial antennas.

ing of the aircraft. Therefore, an alternate position for securing the window rack was provided several feet forward. Figure 2.7 shows the location of the main equipment rack and the location of the window rack for normal operation. Between the racks, on two of the aircraft ribs, can be seen the lugs for the alternate mounting position of the window rack.

Figure 2.8 is a close-up view of the window rack. The two photoheads are at the top of the rack, the sequence camera is below them, and the two fiducial amplifiers are on the outside of the rack, at the left side of the figure. The two fiducial antennas were mounted close to the window, above and below the sequence camera lens.

Antennas. The two fiducial antennas are pictured in Figure 2.9. Each was mounted with its longest dimension horizontal, and with the partly curved surface facing the window. The larger antenna was above the smaller one, with about three inches of separation between them.
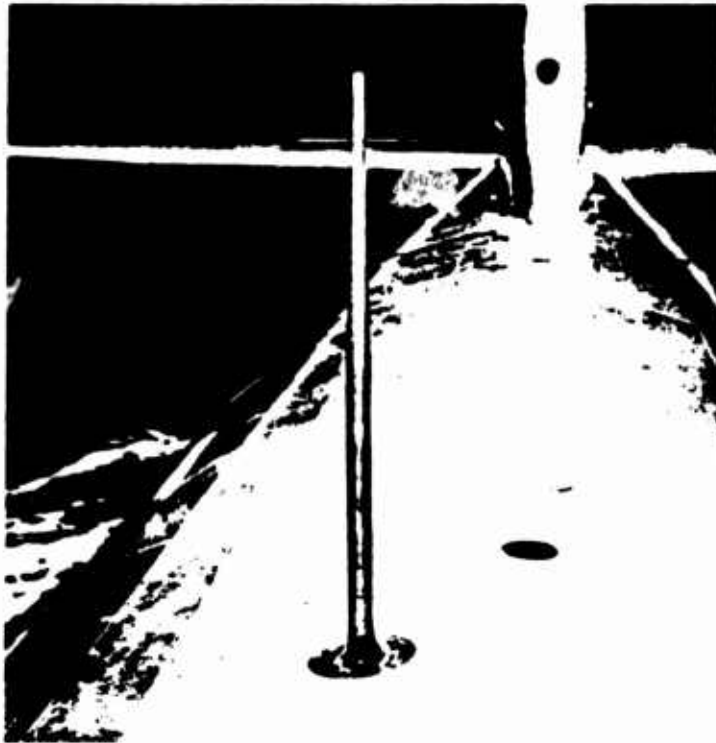
Figure 2.10 Whip antenna on top of C-97 fuselage.

Previous laboratory measurements had established that coupling between two fiducial antennas was unimportant for this configuration.

Plans had been made for mounting the fiducial antennas outside the aircraft, in case the initial tests indicated poor performance by the antennas in their locations just inside the window. For the last six shots, one of the two antennas was mounted outside, with its output brought through the pressurized skin of the aircraft by means of a coaxial connection. The antenna was positioned with its curved side outward, as in the window location. However, the antenna was turned end for end when it was mounted outside. The output connector from the antenna appeared at the upper rear corner, whereas it was at the lower forward corner in the window installation. The 180-degree rotation from the inside location to the outside resulted in a 180-degree phase shift in the received electromagnetic pulse. (See "Polarity and Wave Form", Chapter 2, and "Polarity" in Chapter 3.)

The whip antenna was installed on top of the C-97 aircraft as shown in Figure 2.10. The base

of the whip antenna can be seen in Figure 2.11, penetrating the roof of the upper cargo compartment of the C-97. The whip antenna itself is the conducting rod shown encased in the plastic bearing whose oval cross section appears in the illustration. A wire leads directly from the base of the whip antenna to the cathode follower a few inches away. Two cables lead down from
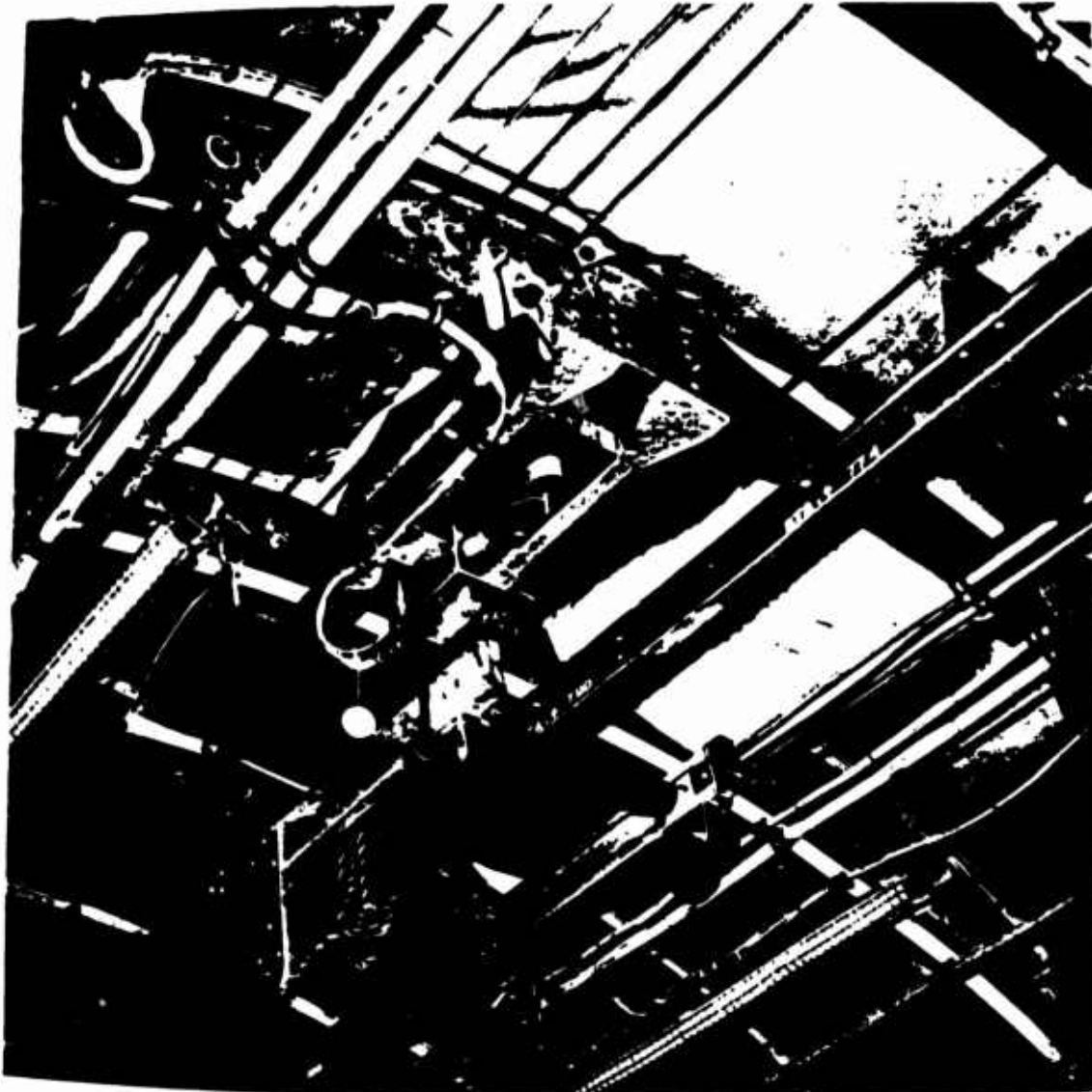
Figure 2.11 Base of whip antenna installation,
on ceiling of C-97 compartment.

the cathode follower, one to the synchronizer for voltages needed by the cathode follower, and the other to an oscilloscope for presentation of the received pulse.

Interference. The fluorescent bulbs shown in Figure 2.11 were part of the aircraft lighting system. However, it was discovered that they caused interference with Project 6.4 equipment; therefore, they were turned off while the project instruments were in operation. The

other electronic equipment in the aircraft, belonging to Project 6.3, also was found to cause interference which could not be removed by field modifications of the project installation. This latter interference was serious during the first four shots. For the later shots, the Project 6.3 equipment was not in operation during the time interval from two minutes before detonation time until two minutes after detonation.

Other interference picked up by the antenna systems came from the switches and solenoids used for automatic operation of the scope cameras and the sequence camera. To remove this interference, the scope cameras were operated manually and the sequence camera was not turned on until just after the time of burst, when the electromagnetic pulse had already been received and photographed.

2.2.3 Fiducial Antenna Systems. Figure 2.9 shows the two types of fiducial antenna used in the tests. Except for form factor, they were nearly identical, with the same cross sectional area, the same length, and the same number of turns. Each antenna had a core of Ferramic "Q", Part No. F-429, made by General Ceramics Corporation, Keasbey, New Jersey. This is a ferrite-core material whose initial (ring) permeability is known to be nearly constant over the large temperature range to which the planned IBDA system could be subjected in operation. Each core contained ten ferrite bars, measuring $7\frac{1}{2}$ inches by $\frac{3}{4}$ inch by $\frac{9}{64}$ inch. For the smaller or narrower antenna, the one at the lower left of Figure 2.9, the ten bars were simply stacked to a width of ten times $\frac{9}{64}$ inch, or $1\frac{13}{32}$ inches. For the larger or wider antenna in Figure 2.9, the bars were arranged in two flat layers of five bars each, to form a slab $3\frac{3}{4}$ inches wide and $\frac{9}{32}$ inch high. Each core had a length of $7\frac{1}{2}$ inches and a cross sectional area of slightly more than 1 in^2.

Two thousand turns of No. 42 wire were wound around each core in the form of a single-layer solenoid. Core and solenoid were then impregnated in a thermosetting plastic for physical protection. The antennas were mounted so that the axis of the loop was horizontal with respect to the earth and normal to the direction of propagation of the burst radiation when the aircraft was properly oriented to give the photoheads and the sequence camera the desired view of the burst.

The wider antenna, when so mounted, presented to the incident wave a greater area than did the narrower antenna. According to theory, the loop antenna should behave as a simple magnetic dipole, and the intercepted area should not be a significant variable. The two shapes were built and tested in order to check the theoretical prediction.

There were, however, certain other differences between the narrow and wide antennas. For the wider antenna, the greater perimeter of the core required a longer length of wire for each turn and resulted in a larger direct-current resistance for the winding, 2,500 ohms for the wider antenna as compared with 1,600 ohms for the narrower antenna. There was also a difference in inductance, 0.52 henry for the wider antenna, 0.4 henry for the narrower one.

There is a small turn-to-turn capacitance in the winding, and it resonates with the inductance of the solenoid to give the unloaded antenna a highly peaked response, centered at about 50 kc, with a Q of about 30. Addition of a terminating network, consisting of a 150-$\mu\mu f$ capacitance and a 56-kilohm resistance in parallel, moves the peak response to about 15 kc and reduces the Q to the order of unity. Figure 2.12 (left portion) is a simplified illustration of the response curve that would be obtained from a fiducial antenna so terminated, if the voltage picked up by the loop were constant with frequency. However, the voltage induced in a loop antenna is actually proportional to the time derivative of the incident magnetic field and, therefore, increases in proportion to the frequency if the peak field strength produced by the energy source is kept constant and only the frequency is varied. The response is then as shown in Figure 2.12 (right portion).

When terminated as described above, the fiducial antenna was designed to give an output of 10 mv for a peak input magnetic field equal to 0.0027 ampere-turns/meter, oscillating at a frequency of 15 kc. This is the peak value of magnetic field associated with an electromagnetic
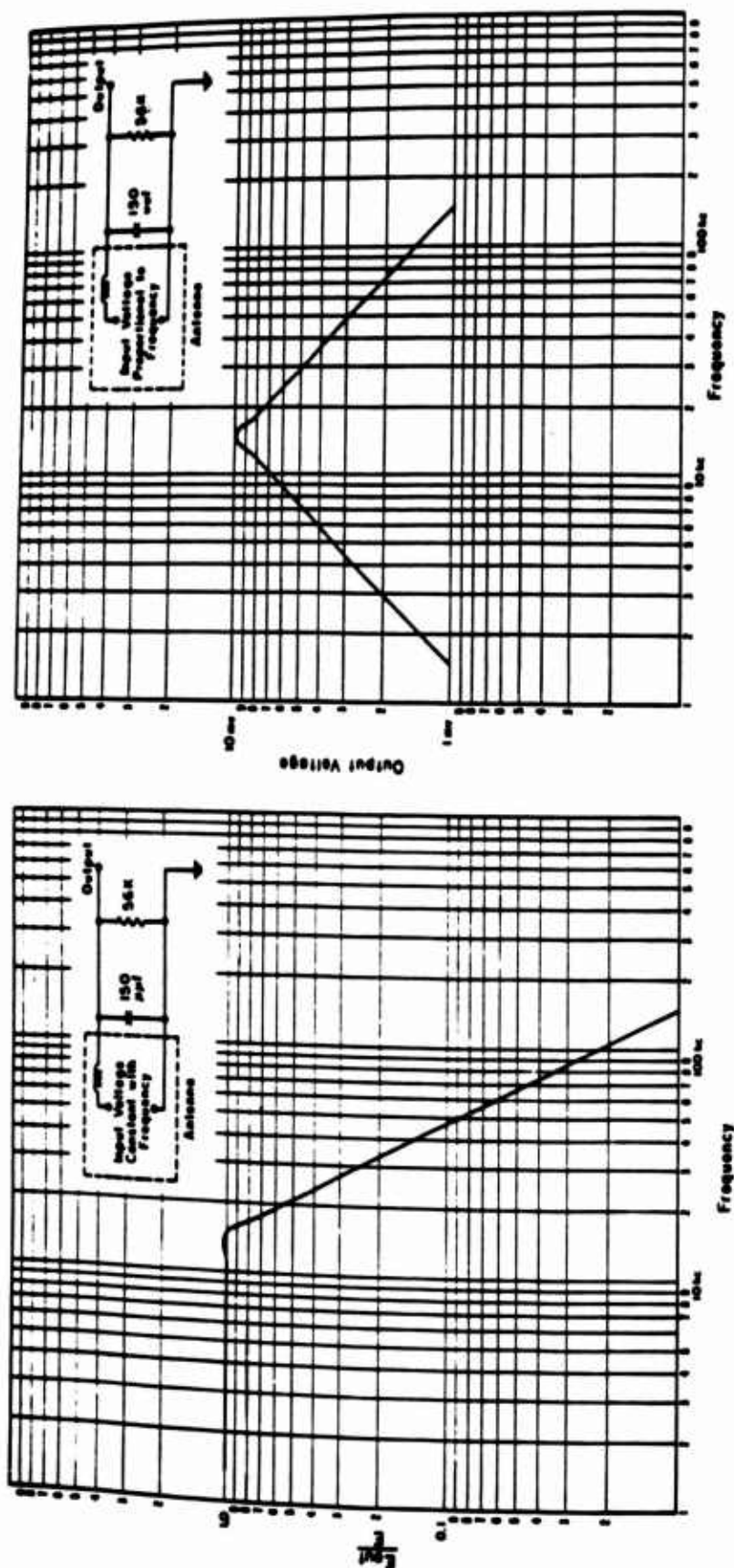
Figure 2.12 Response curve (idealized) for terminated fiducial antenna. Curve at left shows E_out (output voltage) divided by E (induced input voltage) versus frequency for input voltage constant with frequency. Right curve shows E_out versus frequency for input voltage proportional to frequency. (Output scale chosen to correspond to incident wave with peak electric field of 1 volt/meter.)

wave having a peak electric field strength of 1 volt/meter. For laboratory calibration of the antenna, the magnetic field was generated by an oscillatory current from a laboratory signal generator fed through a standard loop of 15 turns with a mean diameter of 10 inches. (See Reference 14 for descriptions of the standard loop and test procedure.)

Antenna Shields. When installed on the window rack, the ferrite-core loop antennas were very close to the aircraft window, but enough space was left to allow each antenna to have experimental metallic shields placed over it or around it. Plans had been made for a study of the effect of electrostatic shielding on the performance of the fiducial antennas. However, because of the many difficulties encountered and because of the absence of data from the first few shots, the shielding study program was not carried out.

Polarity and Wave Form. The polarity of the signal received by a magnetic antenna depends on the way it is connected and on its orientation in space. As pointed out on Page 13 of Reference 1, the electric vector in the pulse radiated from a nuclear detonation is initially pointing upward in space, tending to drive positive charge to the top of a whip antenna, negative charge to the bottom. The pulse received by a whip antenna is usually viewed on an oscilloscope which is connected to the bottom of the whip and, as a result, the initial scope deflection is negative as in Curve A of Figure 1.2.

Associated with the initial upward-pointing electric vector there is an initial magnetic vector which points horizontally, at right angles to the electric vector and to the direction of propagation In Operation Redwing tests, with the aircraft positioned so that the burst was directly to starboar the initial magnetic vector pointed forward along the axis of the aircraft.

Each of the two ferrite-core loop antennas was checked in the laboratory to establish the polarity of its solenoid. A 150-volt battery was connected to the antenna, sending a direct current of 0.1 ampere or less through the antenna winding. The resulting magnetic field was examined with a small pocket compass. With the positive terminal of the battery connected to the inner conductor of the antenna cable, it was found that the antenna behaved as an electromagnet with its north pole at the same end as the cable connection. For the inside mounting position on the window rack, the cable connection was on the forward end of the antenna. The direction of the winding, as determined with the pocket compass, is indicated at the left of Figure 2.13.

Figure 2.13 also shows the direction of the initial electric vector and the direction of the initial magnetic vector. The loop antenna gives a voltage output which is proportional to the time rate of change of the magnetic field. The induced voltage tends to drive a current whose magnetic field opposes the change in magnetic field within the loop caused by the incident wave. With the polarities as shown in Figure 2.13, the initially induced output voltage is positive. For the outside mounting position, the antenna is turned over, with the cable connection toward the rear of the aircraft, and the initial output voltage is negative.

The loop antenna gives an output pulse which is the first derivative of the pulse received by a whip antenna if the frequency is less than 15 kc. The differentiation is expressed in Figure 2.12 (right portion) by the 45-degree upward slope of the left-hand part of the response curve, and by the phase response, which has not been included in the figures. Above 15 kc the downward slope indicates an integrating action introduced by the inductance and capacitance in the antenna circuit. The received pulse from the burst contains a band of frequencies, including frequencies on both sides of 15 kc. At least in the case of a detonation larger than 500 kt, whose period would ordinarily exceed 67 μsec (Figure 1.3), the wave form received by a loop antenna should resemble the first derivative of the wave form received by a whip antenna. Any high-frequency components, such as the superimposed spikes discussed in Reference 1 and illustrated in Figure 1.1 A, would tend to be smoothed out by the integrating action at the higher frequencies.

Curve A of Figure 1.2 is actually a wave form with a period near 50 μsec and, therefore, with a frequency band centered near 20 kc. Figure 2.12 (right portion) shows that for such a

frequency band the loop antenna circuit does not simply differentiate the incident wave form. However, for larger detonations such as Shot Tewa (see Chapter 3), the frequency band is centered near 10 kc and simple differentiation is a more adequate representation of the action of the fiducial antenna circuit. For such detonations, Curve B of Figure 1.2 is a close approximation to the type of wave form actually received on one of the fiducial antennas.

In Curve B of Figure 1.2 the differentiated wave form is drawn with the initial deflection negative. This corresponds to the outside mounting position for the fiducial antenna. The
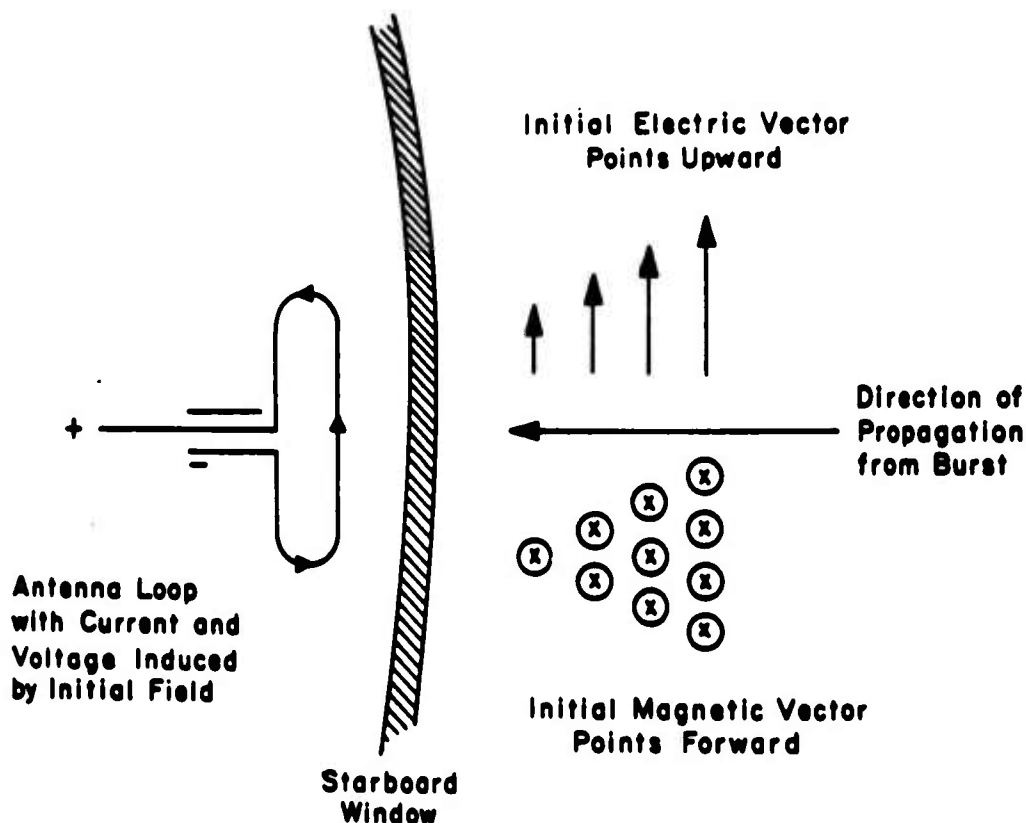
Figure 2.13 Polarity relationships for loop antenna, in its position just inside starboard window. Sectional view is toward nose of aircraft, with antenna on left and incident wave arriving from right.

wave form expected from a magnetic antenna mounted inside on the window rack would be the negative of the wave form of Curve B of Figure 1.2.

Metallic Reflection. The magnetic field which reaches the fiducial antenna in its inside mounting position, Figure 2.13, is essentially the incident field arriving directly from the burst. Some local distortion is to be expected from currents in the mounting brackets and from diffraction of the wave by the window aperture. Operation Redwing tests showed that the distortion of the fields had no great effect on the response of the fiducial antenna.

In the outside mounting position the fiducial antenna is backed by the skin of the aircraft, which acts to some extent as a reflector to the incident wave, increasing the voltage induced in the antenna. Also, because of the local distortion of the magnetic lines of force, the metal skin can affect the impedance of the fiducial antenna and this impedance change can result in a modification of the strength of the signal reaching the fiducial amplifier.

Fiducial Amplifiers. In the IBDA system the fiducial signal is used for triggering a

63

one-shot multivibrator which operates a relay. A minimum of ten volts is needed for this purpose, whereas the minimum antenna output was expected to be only 10 mv. Accordingly, the fiducial amplifier was designed to have a gain of 1,000.

The schematic of the amplifier, Figure 2.14, shows two stages of amplification, each with a gain of between 30 and 33, leading to a cathode follower for a low impedance output. For application to Operation Redwing tests, the output went directly to the oscilloscope presentation.

The actual termination of the antenna in Figure 2.14 is not quite as indicated earlier in Figure 2.12. The shielded cable from the ferrite rod antenna introduces a capacitance to ground of about 50 μμf, leaving only 100 μμf to be included as a lumped shunt capacitance at the amplifier input. An added series capacitance of 1,000 μμf is used in Figure 2.14 to protect the grid of the first stage and to reduce the low-frequency response of the terminated antenna.

Between stages in the amplifier the capacitor combination of 100 μμf in shunt and 1,000 μμf in series is repeated to give the amplifier a bandpass characteristic. In combination with the resistor values used in the circuit, the series capacitors tend to block the frequencies below
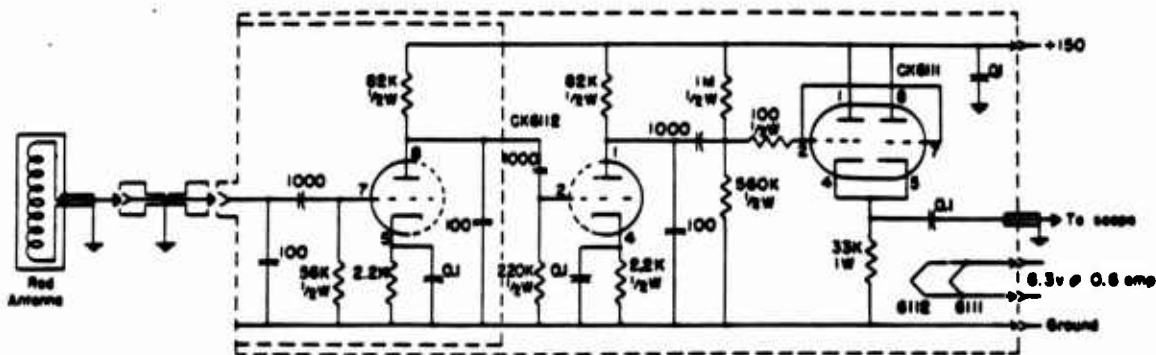
Figure 2.14 Schematic diagram of fiducial amplifier.

about 5,000 cycles while the shunt capacitors short out the frequencies above about 100 kc. The resulting response curve of the amplifier alone is approximately as sketched in Figure 2.15 (left portion). Each of the three series capacitors contributes 6 decibels per octave of low-frequency attenuation, and each of the two shunt capacitors following the amplifier stages contributes 6 decibels per octave of high-frequency attenuation. The amplifier characteristic thus cuts off at 18 decibels per octave below its passband and 12 decibels per octave above the band. The third shunt capacitor, at the input to the first stage, has been included in Figure 2.12 as part of the antenna termination and should not be considered part of the amplifier.

The product of the amplifier response, Figure 2.15 (left portion) and the response of the terminated antenna, Figure 2.12 (right portion), is the combined characteristic shown in Figure 2.15 (right portion). Although largely a calculated curve, it does not differ greatly from measured curves over the frequency ranges covered by the measurements.

The fiducial amplifiers used in Operation Redwing tests appear in Figure 2.4 and at the left side of the window rack in Figure 2.8. The output cables from the fiducial amplifiers lead directly to the oscilloscopes on the main equipment rack at the operator's position.

Saturation. The fiducial amplifier was designed for a specific function, the generation of an output signal of at least 10-volts amplitude from an input which might be as small as 10 mv, corresponding to an incident electromagnetic wave with a field strength of about 1 volt/meter. In Operation Redwing tests, the incident field was usually much greater than the minimum. The fiducial amplifier was not designed for linearity over a large dynamic range of input signals because linearity was not important for the IBDA application. As a result the amplifier often sat-
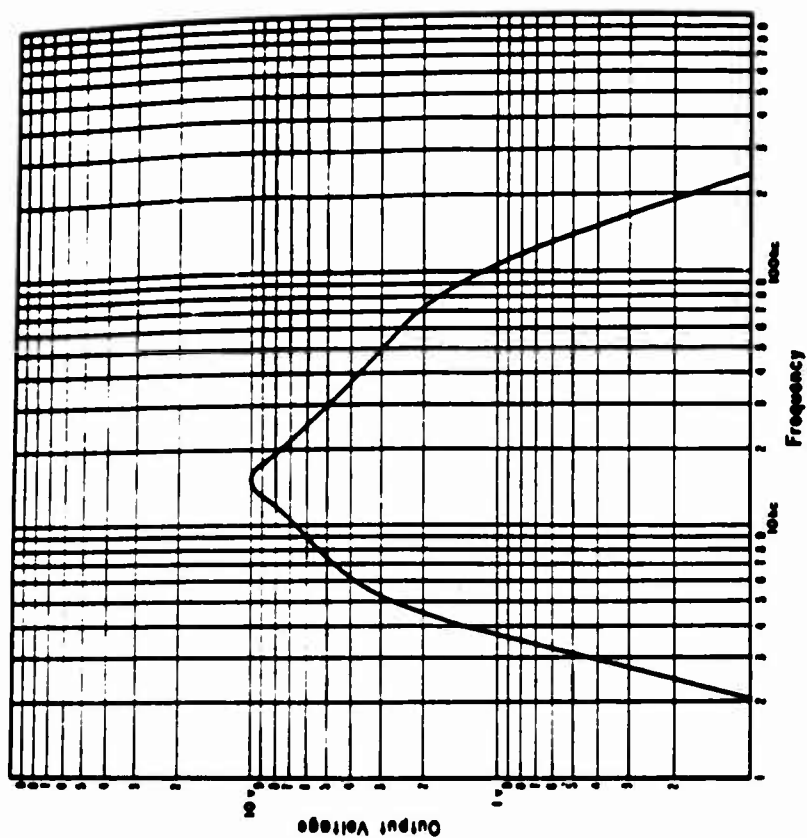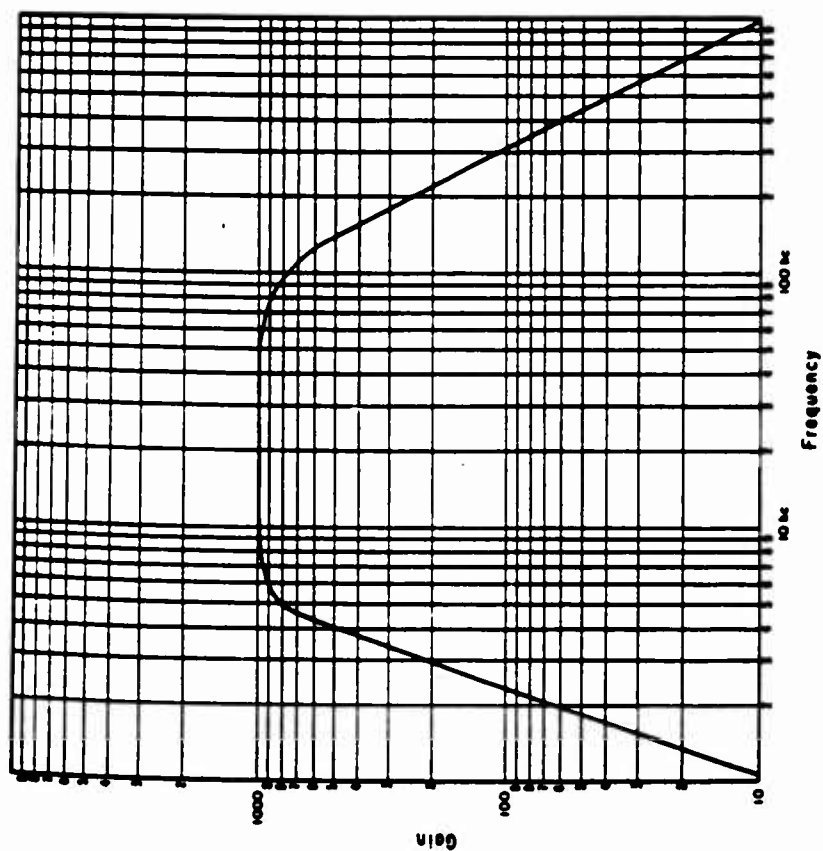
Figure 2.15 Response of fiducial amplifier, shown at left, and combined response of fiducial antenna and amplifier, shown at right. Output scale corresponds to incident wave with peak electric field of 1 volt/meter.

urated on the strong signals received from the detonations of Operation Redwing. The saturation would have been less severe if the aircraft had been flying near the extreme range (250 nautical miles) of the IBDA design requirements, but the needs of Project 6.3 kept the aircraft restricted to shorter ranges.

In practice, with a fiducial amplifier of the design shown in Figure 2.14, saturation generally occurs in the second stage of amplification, after the signal from the antenna has been amplified by the first stage with its gain of about 30. A positive input voltage from the antenna is converted by the first stage into an amplified negative voltage which is applied to the grid of the second stage. When this applied grid voltage reaches a level of about −1.5 volts, the second stage is cut off. A negative input from the antenna, on the other hand, becomes a positive voltage on the grid of the second stage. If this applied grid voltage exceeds + 1 volt, grid current flows in the second tube. The grid current will charge the 1,000-$\mu\mu f$ condenser and may make the grid bias considerably more negative than its normal value of about −1 volt.

The charged 1,000-$\mu\mu f$ condenser can discharge through the 220-kilohm resistor and the plate circuit of the first tube, but the time constant for discharge is several hundred μsec. During this interval, the extra bias voltage will distort the response of the second stage. The tube will be nearly cut off, so that negative input voltages to the second-stage grid will have only the effect of cutting off the tube somewhat more firmly. A positive input to the grid will have a large voltage swing available, since it must first overcome the extra bias voltage before it can drive the grid to the point where grid current can flow again.

Each of the two stages of amplification inverts the polarity of the signal. The final cathode-follower stage has a gain approximating unity and does not invert polarity. When the saturation phenomena are expressed in terms of the amplifier output voltage (the signal that is carried to the oscilloscope), it is found that the maximum positive swing of the output voltage, occurring when the second stage is entirely cut off, is about + 40 volts. A negative swing of the output voltage to − 30 volts will mean that grid current is drawn at the second stage, preventing a greater negative deflection of the output during the time that the 1,000-$\mu\mu f$ condenser is charging. The extra grid bias results in a positive displacement of the output voltage, even when there is no input signal to the amplifier. The positive displacement, which can be no larger than + 40 volts, drops back toward zero with a time constant of several hundred μsec while the 1,000-$\mu\mu f$ condenser is discharging, and serves as a slowly falling base line for any succeeding signals that may be received.

The electromagnetic signal for Shot Tewa, which is discussed in detail in Chapter 3, shows the effects of amplifier saturation which have been described above.

Oscilloscopes. Two DuMont oscilloscopes were used for Project 6.4 instrumentation. Both were fitted with cathode-ray tubes having P-11 phosphors to facilitate photographic recordings. One oscilloscope was a Type 324, with a single beam, and the other was a Type 333, with a dual beam. The dual beam oscilloscope had two inputs, Channels A and B, with separate vertical amplifiers, but with only one horizontal sweep control.

From measurements made after Operation Redwing, it was found that the sweep speed on the Type 324 oscilloscope was sensitive to the voltage level of the 400-cycle power. When the sweep speed was set at 100 μsec/inch, or 400 μsec for the full sweep length (four large divisions), it was found that the time required for the trace to travel the four large divisions changed somewhat as the line voltage was varied. For 400-cycle line voltages of 115, 110, 105, and 100 volts the time per sweep length was 403, 400, 384, and 354 μsec, respectively.

The Type 333 oscilloscope was also examined after the tests, but unfortunately not until after changes in tubes and in screwdriver adjustments had altered its sweep lengths to some extent. It was found to be more stable with changes in line voltage but consistently slower in its sweep velocity than the dial setting indicated. Furthermore, the two channels showed somewhat different sweep speeds. For the same four values of line voltage, and with the dials again set for

a nominal sweep time of 400 μsec, the actual times per sweep length were measured to be 420, 422, 423, 420 μsec for Channel A, and 412, 413, 413, 411 μsec for Channel B. At the beginning of the sweep, the spot for Channel B was a short distance to the left of the spot for Channel A. About one small division (one-fifth of a large division, one-twentieth of the full horizontal scale) to the right of the center line, the two spots were even, and at the right-hand end of the sweep. Spot B had moved beyond Spot A. This detailed comparison between the two channels is of importance in the interpretation of some of the results, particularly in the scope photograph of the Type 333 oscilloscope presentation for Shot Tewa.

The horizontal sweep on the Type 333 oscilloscope could be set to trigger either from a signal on Channel A or from a signal on Channel B. During the tests it was always set to trigger on Channel B, and Channel B was always adjusted to have its base line just below the center of the scope, while the base line for Channel A was set just above the scope center.

On both the Type 324 and the Type 333 oscilloscopes, the triggering could be set either for a positive signal or for a negative signal, but not for both. For some of the scope pictures the polarity of the triggering was opposite from the polarity of the initial signal deflection. The first lobe of the signal on these pictures was unfortunately lost.

Audio Generator. A calibration signal was used to check the gain of the fiducial amplifier, the gain of the scope amplifiers, and the speed of the scope sweep circuits. For generation of the calibration signal a Heathkit audio generator, Model AG-8, was used. A laboratory check showed that the frequency of the Heathkit was insensitive to 400-cycle line voltage fluctuations over the range 102 volts to 115 volts, but that the dial settings were not accurate. The dial settings of 10, 12, and 15 kc actually gave output sine waves with frequencies of 9.6, 11.5, and 14.4 kc, respectively. Since these were steady with changes in line voltage, they were satisfactory as calibration frequencies to check variations of the oscilloscope sweep speeds under operational conditions.

Artificial Signal Generator. For aid in servicing and adjusting the equipment on the ground, a simple, self-contained artificial signal generator was constructed. It contained a small battery, a pushbutton switch, a spare fiducial antenna and a condenser. The capacitance of the condenser was chosen to resonate with the inductance of the loop antenna at a frequency of about 15 kc. When the switch was closed, a damped sinusoidal current, about six or eight cycles long, passed through the winding of the antenna. When the switch was opened, a similar train of six or eight oscillations passed through the winding.

The spare antenna was held parallel to the antenna in the bhangmeter equipment and about a foot or two away from it. The magnetic coupling between the two antennas was sufficient to produce an oscillatory trace on the oscilloscope in the fiducial system when the switch on the artificial signal generator was operated. From the size and shape of the trace it could be determined whether the fiducial system was in adequate working order and whether the scope adjustments were satisfactory.

2.2.4 Whip Antenna. The whip antenna was included in the installation to provide a correlation with measurements by other organizations on this series of tests and on earlier tests. It was intended to be used as a reference antenna, so that the performance of the magnetic antennas could be evaluated by comparison with an electric antenna of conventional design.

The whip antenna was a quarter-inch aluminum rod housed within a fiberglass mast. There was an external length of 33 inches projecting vertically upward from the aircraft (Figure 2.10). The induced voltage at the base of the antenna was fed directly to the cathode follower, located about four inches away, as shown in Figure 2.11. The output of the cathode follower was carried through approximately 25 feet of regular coaxial cable to one of the oscilloscope channels on the main equipment rack (Figure 2.6).

The schematic of the cathode follower is given in Figure 2.16. The input impedance of the

circuit is high and the gain is slightly less than unity. Without the cathode follower, the whip antenna would have been loaded down with the distributed capacitance of the 25-foot cable and the output voltage reaching the oscilloscope would have been considerably reduced. If there were no loading whatever at the base of the whip antenna, the output voltage would be the product of the incident field, in volts per meter, and the effective height of the antenna, in meters. The effective height of a short antenna is about one half its physical height. The field strength of the incident wave will be modified by the shape of the aircraft. The reflection of the wave by the curved surface of the aircraft, just below the whip antenna, should nearly double the effective field reaching the antenna, but there could also be a partial shielding of the antenna caused by the concentration of the vertical electric lines of force on the high tail of the aircraft, and perhaps also on the radio antenna wires which run from the forward part of the plane to the top of its tail surface.

Of more importance, however, in affecting the voltage delivered by the whip antenna, is the terminating circuit at its output. Because of the voltage drop across the internal impedance of
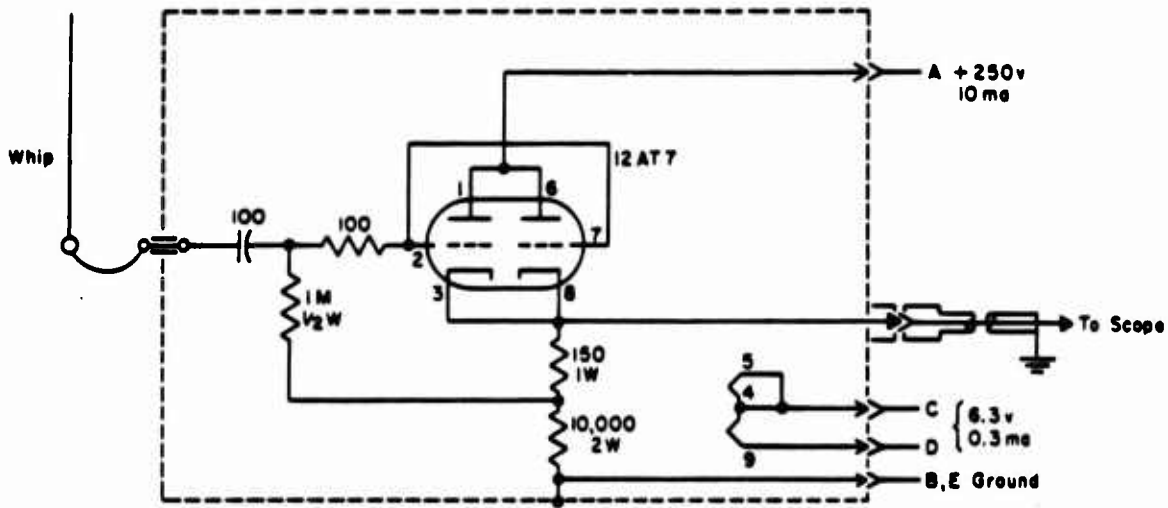
Figure 2.16 Schematic diagram of cathode follower for whip antenna.

the antenna, when the antenna is loaded down by an output impedance, only a portion of the received voltage will appear across the load. The internal impedance of the whip antenna is computed to be a capacitance of about 9.4 $\mu\mu f$, in series with a radiation resistance of the order of 10^{-4} ohms, which can be neglected, and an impedance associated with the fields inside the wire, which can also be neglected.

The antenna capacitance was computed from Equation 2.1, which is a modified form of Equation 46 on page 147 of Reference 15. The modified form is only valid for antennas which are very short compared to the wave lengths included in the received or transmitted radiation.

$$C_{antenna} = \frac{h}{9 \times 10^5} \frac{\left[2 \log_e\left(\frac{2h}{a}\right) + 2 + 2 \log_e 2 \right]}{\left[2 \log_e\left(\frac{2h}{a}\right) \right]^2} \tag{2.1}$$

Equation 2.1 applies to linear antennas perpendicular to a conducting plane. The antenna height, h, and radius, a, are to be expressed in meters, and the capacitance will then be given

68

in farads. A center-fed antenna of height 2h with no ground plane will have one half the capacitance given by Equation 2.1.

An expression for the radiation resistance, valid only for very short antennas, can be obtained in a similar way from Equation 4a, Page 147, Reference 15.

$$R_{radiation} = 10\left(\frac{2\pi h}{\lambda}\right)^2 \frac{\left[2 \log_e\left(\frac{2h}{a}\right) + 4 + 4 \log_e 2\right]}{\left[2 \log_e\left(\frac{2h}{a}\right) + 2 + 2 \log_e 2\right]^2} \tag{2.2}$$

Equation 2.2 gives the radiation resistance in ohms of a linear antenna of height h over a reflecting ground plane. A symmetrical, center-fed antenna of height 2h will have double the radiation resistance given by Equation 2.2.

As stated above, the internal impedance of the whip antenna is almost entirely capacitative, a capacitance of about 9.4 μμf in series with the voltage induced by the incident electric field. At 15 kc, this is an internal reactance of 1.13 megohms. The output loading at the base of the antenna is partly capacitative, partly resistive. The capacitances associated with the wiring from the antenna to the cathode follower and the input capacitance of the cathode follower are believed to total no more than 10 μμf. There are leakage resistances associated with the dielectrics around the antenna and the insulators in the cathode follower. The leakage resistances vary with humidity, and the humidity is often very high. Even so, provided that the dielectrics had not deteriorated seriously, the resistive loading of the whip antenna is believed to have been equivalent to a leakage resistance of at least a megohm.

The loading mentioned above could reduce the effective output voltage to as little as one third of the open-circuit voltage. However, such a reduction does not account for the complete lack of an observed signal large enough to be recorded on the oscilloscope with the scope sensitivities that were used. The absence of any recorded pulse during Operation Redwing tests could be explained if there had been an additional loading. A possible source for the additional loading might have been an unusual accumulation of moisture in the dielectric supporting the antenna. Another possible source of leakage current, which has not been studied in detail, might be the exchange of charge between the aircraft projections and the air through which they move. If the exchange of charge, due to air friction and the interception of ionized air particles by the whip antenna, were influenced by the electric fields induced on the antenna, then the result could be the loading of the antenna and the reduction of the voltage it could deliver to the cathode follower and to the oscilloscope.

2.2.5 Photohead Systems. Each photohead system contained a photocell detector with a lens system and an ambient-light-correcting circuit. The photoheads were cubic enclosures about six inches on each side, with the object lens mounted in one side and all controls mounted on the opposite side.

The lens system was designed to restrict the photohead field of view to 20 degrees; that is, to the region within a cone with a half-angle of 10 degrees. For light which reached the photohead from a source within its field of view, the lens system had an effective area of about one square inch, focusing onto the photocell the portion of the incident radiation intercepted by this area.

Two different phototubes were used, the 1P39 and the 6570. Their spectral response curves are shown in Figures 1.10 and 1.11 and are discussed in "Spectral Distributions", Chapter 1. The 1P39, with an S-4 response, has a sensitivity of 0.042 μa of output current per μw of incident radiant flux at 4,000 Å. Its greatest sensitivity is at this wave length, which lies at the violet end of the visible spectrum. For other wave lengths the sensitivity of the 1P39 falls off in accordance with its response curve, Figure 1.10. The 6570, with an S-1 response, has a sensitivity of 0.0027

$\mu a/\mu w$ at its peak in the near infrared at 8,000 Å, falling off on either side in proportion to its response curve, Figure 1.11, and rising again to a narrow peak in the ultraviolet.

Each photohead included a circuit designed to correct for the ambient light at the time of burst and to compress the large dynamic range of visible light from the burst, manifesting itself as a large variation of phototube current, into a relatively small range of output voltage and current to the recorder. The compression was needed in order to record the whole of the wide range of light variation within the narrower range covered by available recording instruments.

Photohead Circuit Operation. Figure 2.17 is a photohead schematic. As may be seen, the photohead contained, besides its phototube, a 6136 pentode (or its equivalent, 6AU6), a CK6111 subminiature dual triode a thyrite resistor (8386118G1), a 50-μa meter, a relay, and various resistors and condensers.

Ideally, the photohead circu   uld be adjusted so that with the relay closed all the current from the phototube due to ambient light would pass through the pentode and register on the meter. The thyrite, with no current through it, would have its highest impedance value, about 50 megohms. The degenerative loop in the circuit served to readjust the grid voltage on the pentode each time there was a change in ambient light. This occurred in such a way that the changed phototube current was balanced by an equal change in the pentode current, preventing the increment of current from flowing through the thyrite and changing its impedance.

When the relay was activated, the degenerative loop opened, and the pentode grid bias was held fixed by the charge on the 1-μf capacitor. The pentode then served as a constant current device. Any added current from the photocell necessarily passed through the thyrite. The voltage developed across the thyrite was impressed on the cathode follower, and nearly all of the cathode follower output was carried directly to one of the channels of the Heiland recorder through the 1.5-megohm resistor. When the Heiland recorder was operating, the current change was recorded as a deflection on the Heiland paper tape.

In the operation of the photohead during the test shot, the pentode plate current, held fixed when the relay was activated, was equal to the phototube current from the ambient light. The added current, passing through the thyrite and appearing as an output voltage and as a Heiland deflection, was the added phototube current from the thermal radiation produced by the nuclear detonation. The weak radiation from a small or distant burst or from a burst obscured by clouds gave a phototube current which was small but which could nevertheless develop a significant voltage across the thyrite when the latter was in its state of highest impedance. The stronger light from a large, near, unobscured burst gave a much larger phototube current. However, the thyrite's distinctive property is that its impedance drops quickly as the current through it rises, so that the much larger phototube current gave a voltage drop and Heiland deflection which were only moderately large, well within the range of the Heiland.

Photohead Circuit Adjustment. In practice, the adjustment of the photohead circuit was by means of the 25-kilohm potentiometer in the cathode of the cathode follower, which effectively controlled the voltage difference between the grid and plate of the pentode. During Operation Redwing tests, the potentiometer was adjusted to give about 1 μa through the meter in the cathode circuit of the pentode when the phototube was dark. One conclusion from Operation Redwing tests was that the above adjustment was not the best possible, that a more satisfactory potentiometer adjustment gave a current of about 0.25 μa.

Figure 2.18 is a typical thyrite characteristic showing the thyrite's resistance as a function of the current passing through it. The production tolerance for the thyrite used is about ± 50 percent in the impedance at a given current. The thyrite characteristic is temperature-dependent with a change in resistance at constant voltage of between −0.4 and −0.73 percent per degree C over the temperature range from 0 to 100 degrees C. Furthermore, under the high-humidity conditions that prevailed during Operation Redwing tests, it is probable that the maximum thyrite resistance of 50 megohms, shown in Figure 2.18, was shunted by a leakage path over a thin film
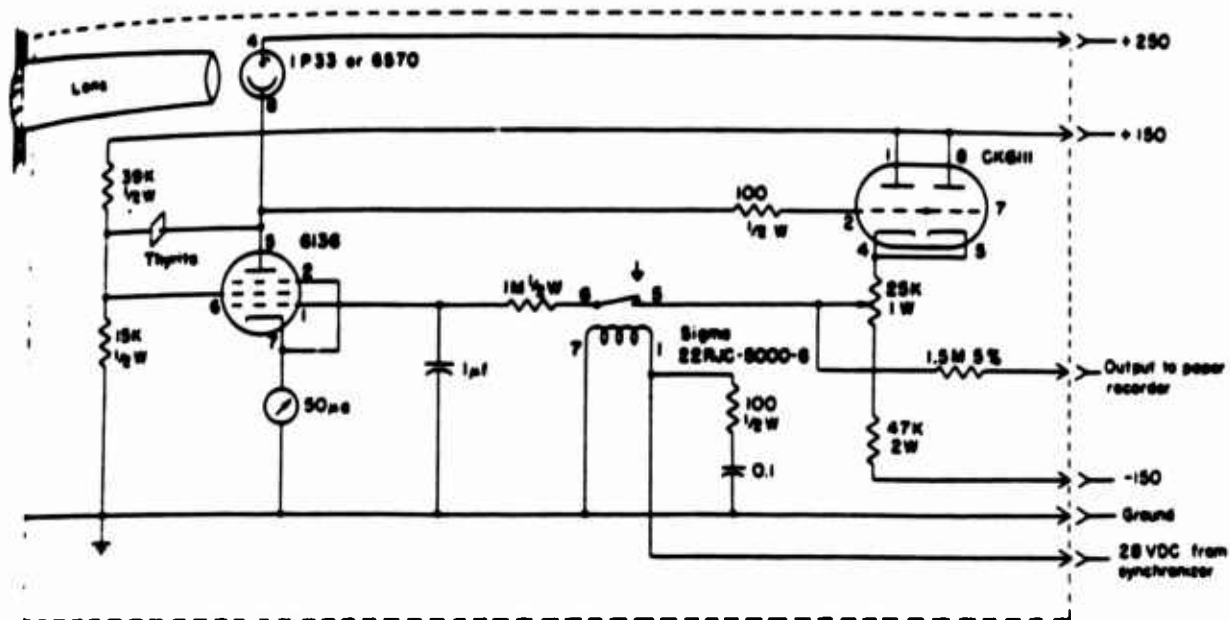
Figure 2.17 Schematic diagram of photohead.
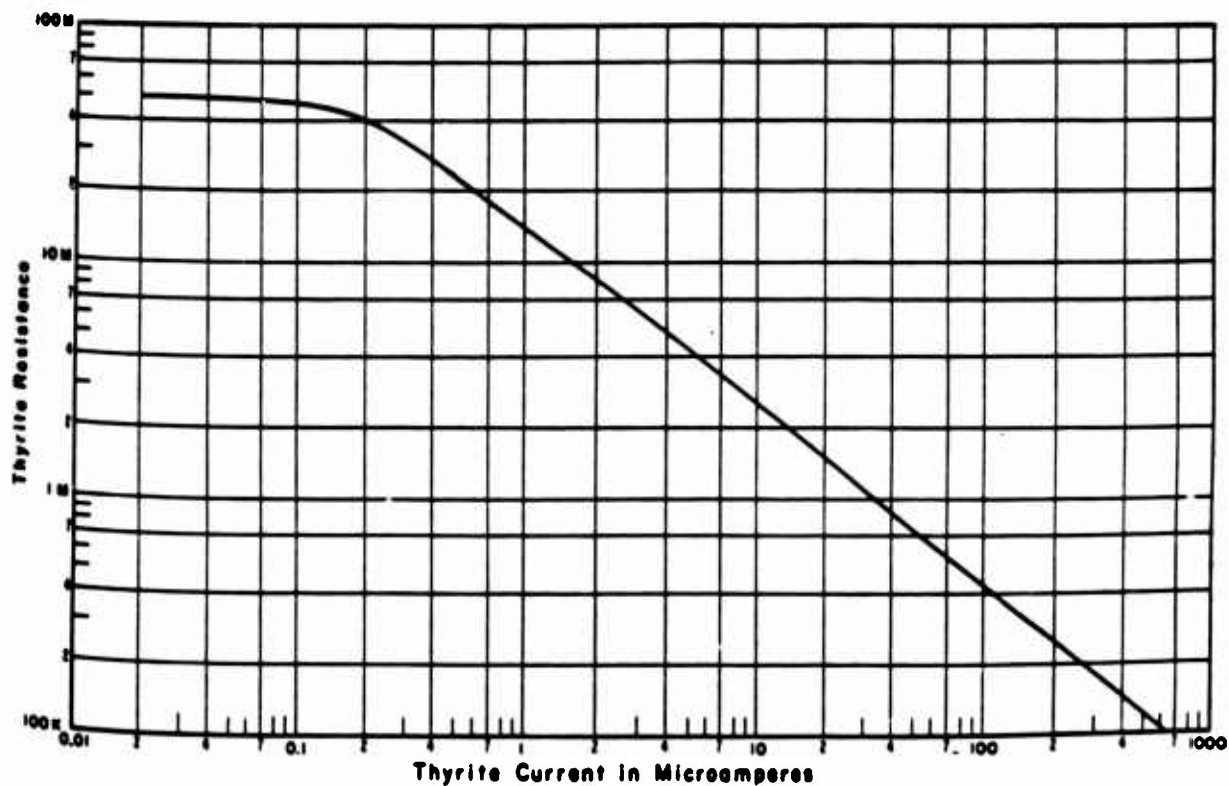
Figure 2.18 Thyrite resistance as a function of thyrite current.

71

of moisture, even though there was a coating on the thyrite to prevent any substantial accumulation of moisture on the thyrite itself.

As a result of the above considerations, a photohead analysis which is based on the thyrite curve of Figure 2.18 should not be expected to represent the exact behavior of the photoheads used in Operation Redwing tests. Nevertheless, the qualitative behavior of Operation Redwing photoheads can best be understood through a quantitative photohead analysis. In the following analysis, it is assumed that Figure 2.18 gives an exact thyrite characteristic for the thyrite in the photohead.

The current flowing out of the pentode cathode is equal to the sum of the currents flowing in at the plate and grids. Grid No. 3 is tied to the cathode, and the current through grid No. 1 (the control grid) is negligible here. Screen grid current is one third to one half as large as the plate current when the screen and plate both have voltages of about +42 volts. Thus, for a cathode current of 1 μa, the plate current is about 0.7 μa. Since the phototube dark current is of the order of 0.01 μa, nearly all the plate current must flow through the thyrite when the phototube is dark. A current of 0.7 μa, through the thyrite of Figure 2.18, gives a resistance of about 18.5 megohms, and therefore, a voltage drop of 13 volts across the thyrite. The direction of current is such that the voltage at the plate of the pentode is negative with respect to the screen voltage. That is, if the pentode screen is at +42 volts, the pentode plate will be at +29 volts. The cathode of the cathode follower then will be about 5 volts higher, or +34 volts, since 5 volts bias is needed on the cathode follower for the total current of 2.5 ma necessary for the 184-volt drop across the 72-kilohm cathode resistance. The tap on the potentiometer will be about −3 volts, the pentode grid voltage needed to cut the pentode current down to about 1 μa. To give these voltages, the 25-kilohm potentiometer should be divided with 14.5 kilohms on the cathode side and 10.5 kilohms on the side of the 47-kilohm resistor and the −150 volt supply.

For a pentode cathode current of 0.25 μa the plate current is about 0.17 μa, the thyrite impedance is 42 megohms, and the voltage drop across the thyrite is 7 volts. For a pentode screen voltage of +42 volts, the pentode plate will be at +35 volts and the cathode of the cathode follower will be at about +40 volts. The pentode grid voltage is again about −3 volts, and the 25-kilohm potentiometer is divided with 16 kilohms on the cathode side and 9 kilohms on the supply side.

The potentiometer setting may be specified indirectly by a specification of the current I_{kd}, which is defined as the current flowing through the pentode cathode when the feedback loop is closed and the phototube is dark. The two potentiometer adjustments described above can thus be specified by I_{kd} = 1 μa, and I_{kd} = 0.25 μa, respectively.

Once the potentiometer setting has been fixed, the behavior of the photohead circuit is determined. If the feedback loop is opened (by activation of the relay) while there is no light on the phototube, and if light is then admitted to the phototube, the output of the photohead will follow an S-shaped curve as a function of phototube current. For the potentiometer adjustment giving I_{kd} = 0.25 μa, the curve followed is the first curve at the left of Figure 2.19.

The curves of Figure 2.19 were measured in the laboratory after the conclusion of Operation Redwing tests. The photohead used was the 1P39 photohead from Operation Redwing equipment, but the conditions were somewhat different from those at Operation Redwing. In particular, the humidity was much lower in the later laboratory measurements than at the Pacific Proving Grounds.

As the light striking the phototube is increased, the increasing phototube current flows through the thyrite in the opposite direction to the current that was passing through the thyrite when the phototube was dark. The phototube current first reduces the thyrite current to zero and then reverses it. While the current is reversing, the thyrite passes through its region of maximum sensitivity. This is shown in Figure 2.19 by the steepness of the first curve just after its first rise. As the phototube current continues to increase with increasing light input, the curve flat-
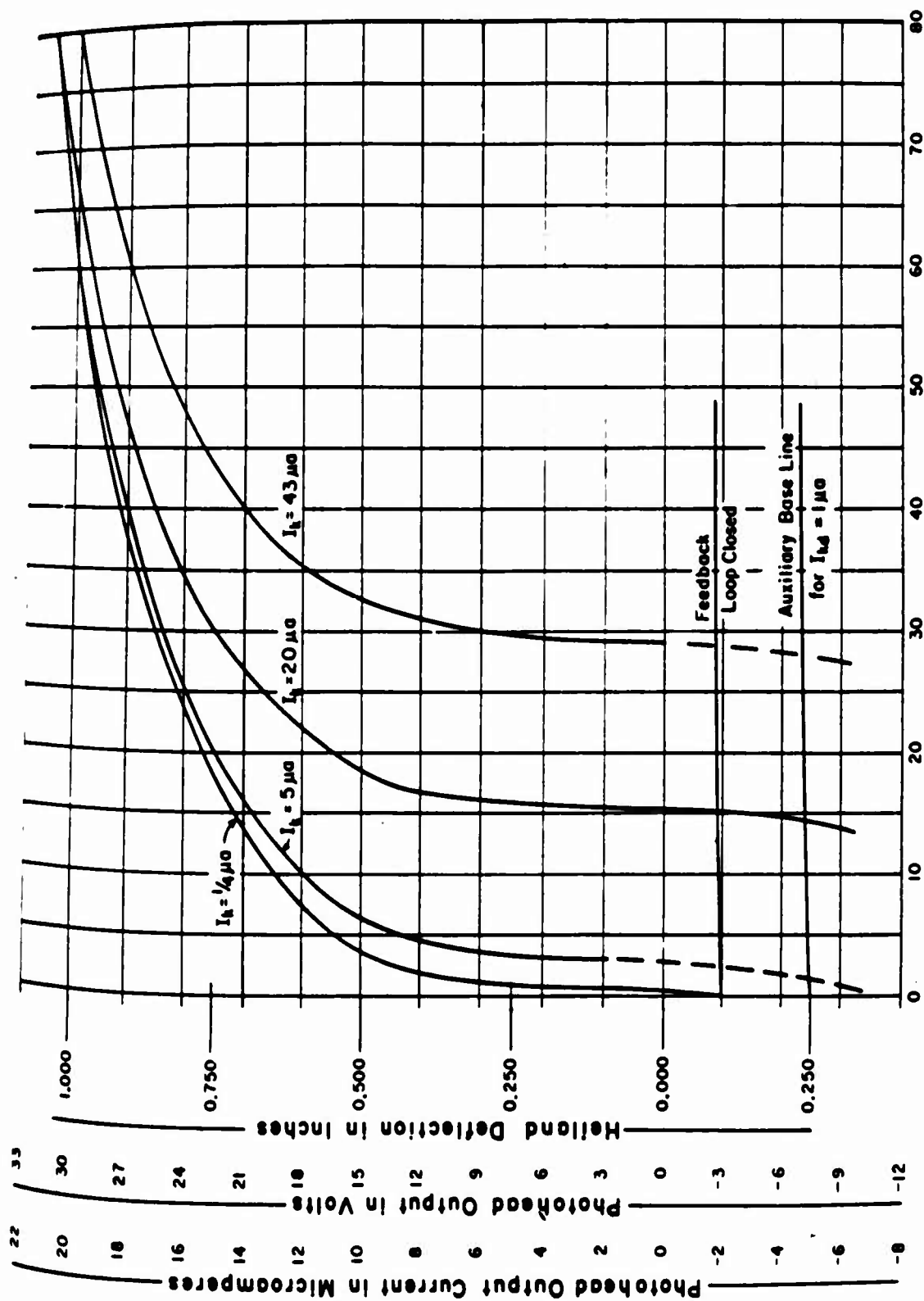
Photohead Current in Microamperes

Figure 2.19 Photohead characteristic curves. Potentiometer is adjusted for pentode cathode current, with phototube dark, of $I_{kd} = \frac{1}{4} \mu a$. The separate curves correspond to different levels of ambient light and are labeled by values of pentode cathode current I_k. The burst deflection starts from the line labeled "Feedback Loop Closed". An auxiliary base line is given for use when the circuit is adjusted for $I_{kd} = 1 \mu a$.

73

tens, showing the reduced sensitivity and output compression that result from the reduced impedance of the thyrite at higher current levels.

If the feedback loop is kept closed while the light input to the phototube is varying, the loop holds the photohead output very nearly fixed. The output voltage, which is the same as the voltage on the pentode control grid, varies just enough to make the plate current in the pentode follow the phototube current. The high gain of the feedback loop makes the change in the control grid voltage very small. The pentode cathode current, I_k, however, increases in close proportion to the phototube current, I_{ph}, approximately following the linear relationship in Equation 2.1

$$I_{ph} = (0.7) (I_k - I_{kd}) \qquad \text{(feedback loop closed)} \qquad (2.3)$$

By means of Equation 2.3, the pentode cathode current can be used as a measure of the phototube current resulting from ambient light.

The parallel curves in Figure 2.19 show the variation of the photohead output with phototube current for several values of ambient light, specified by the pentode cathode current, I_k, at the time the feedback loop was broken. The curves are all very similar, the characteristic S-shape being a result of the thyrite characteristic of Figure 2.18. The steepest part of each curve corresponds to the region of highest thyrite impedance, where the voltage across the thyrite is passing through zero. The curves appear to be symmetrical about the steepest region, which is centered at about +3 volts on the output voltage scale, 6 volts above the line near -3 volts representing the output voltage when the feedback loop is closed. The 6 volts can be compared with the previous estimate of 7 volts as the voltage across the thyrite when the feedback loop was closed, for the potentiometer adjustment giving $I_{kd} = 0.25$ μa.

That potentiometer adjustment divided the 25-kilohm potentiometer into 16 kilohms on the cathode side and 9 kilohms on the supply side. The total cathode resistance of 72 kilohms was thus divided into 16 kilohms between the cathode and the potentiometer tap, and 56 kilohms between the tap and the -150 volt supply. A voltage change at the cathode produced a somewhat smaller voltage change at the output, with the reduction factor equal to the resistance ratio 56/72.

A given voltage change across the thyrite is transmitted unchanged to the cathode of the cathode follower, but is reduced by the factor 56/72 at the photohead output. In particular, a 7-volt increase at the thyrite is reduced to 5.5 volts at the output. This voltage is in rough agreement with the estimate from Figure 2.19 of 6 volts as the voltage difference between the output with the loop closed and the output with the thyrite at its greatest sensitivity.

The curves of Figure 2.19 were all drawn for the potentiometer adjustment giving $I_{kd} = 0.25$ μa. In Operation Redwing tests, the potentiometer was usually adjusted to give a pentode cathode current nearer 1 μa, but the adjustment could not be held to any great precision on the 0 to 50 μa meter. The general effect of a different potentiometer adjustment is not to change the shape of the curves in Figure 2.19, since these depend primarily on the properties of the thyrite, but to displace the region of greatest sensitivity upward or downward with respect to the line representing the loop-closed condition. For certain limited purposes, the upward displacement of the curves can be replaced by a downward displacement of the loop-closed line.

The amount of displacement can be estimated for the circuit adjustment giving $I_{kd} = 1$ μa. With $I_{kd} = 1$ μa, an earlier calculation gave a thyrite voltage drop of 13 volts when the loop was closed. With the loop opened, a voltage rise of 13 volts at the pentode plate, or 10.5 volts at the potentiometer tap, would be needed to bring the thyrite to its most sensitive position. An auxiliary base line has been drawn on Figure 2.19, 10.5 volts below the position of greatest steepness of the curves.

With the potentiometer adjusted for $I_{kd} = 1$ μa, a steadily increasing illumination of the photocell will not cause a steadily increasing deflection of the Heiland trace. Instead, Figure 2.19

74

shows that the trace will move slowly at first, starting from the auxiliary base line; will move more rapidly as the phototube current reaches the value which reverses the current in the thyrite; and will move more slowly again as the reversed thyrite current increases and the thyrite impedance is reduced. The effect is to give the Heiland trace the appearance of a "step" each time the deflection passes through the region of highest sensitivity.

On most of the Heiland traces obtained during Operation Redwing tests, the step could readily be distinguished. Measurements could be made of the difference between the deflection corresponding to ambient light and the deflection corresponding to the center of the step. This difference could then be interpreted as the amount of displacement needed in Figure 2.19 for positioning of the auxiliary base line.

In practice, however, it was found that other adjustments were needed to make the curves of Figure 2.19 fit Operation Redwing photohead data. Photohead calibration measurements during Operation Redwing tests showed that the two photoheads used there contained thyrites whose resistances differed by about a factor of 2. This ratio is well within the manufacturing tolerances mentioned earlier. The difference between thyrites could, to some extent, be considered equivalent to a change in the vertical scale for the curves of Figure 2.19. (See the discussion in Section 3.3.9 of the photohead calibration measurements.)

Heiland Recorder. The output currents from the two photoheads were fed to separate channels of the Heiland recorder. The recorder used was a six-element, bifilar-type oscillograph employing light-sensitive paper film traveling at a rated speed of about 12 in/sec. Each element responded to frequencies from 0 to 30 cps, and had a sensitivity of approximately 20 μa/in of deflection.

There was an internally generated 100-cycle signal which was used for marker lines that were recorded photographically at the edge of the paper strip. These 10 m-sec markers provided a calibrated time base for the signals recorded on the tape. The timing of the markers was much more accurate than the tape movement, which was found to be as slow as 10 in/sec. However, the time marker mechanism was loose and subject to vibration. Time readings were sometimes difficult but could always be made, either directly from the time markers or indirectly from the paper movement. The speed of the paper movement could then be checked against the marker separation at a nearby position where the time markers were clear enough to measure. The mechanism was later repaired, but not until it had been brought back from the Pacific after the conclusion of Operation Redwing.

Photohead Test Box. A specially constructed test box was used in the photohead calibration measurements described in Section 2.1.5. Two open-ended boxes, about 8 inches on a side and 12 inches apart, were connected by a cylindrical tube 1.5 inches in diameter. The tube protruded one inch into each box. The interior of the boxes and the inside of the tube were painted dull black. In one of the boxes, at one end of the tube, a photoflood bulb could be mounted. At the other end of the tube, in the other box, the photohead could be set and aligned to receive the light transmitted through the tube.

The white bulb used was a reflector-type photospot, Type RSP2, with a color temperature of 3,400 K at full voltage (about 115 volts). An infrared bulb was also used. Its color temperature at full voltage was about 2,500 K. The light intensity was controlled by a Variac which unfortunately changed not only the intensity but also the color temperature of the light, as pointed out in Section 2.1.5.

2.2.6 **Synchronizer.** According to the original plan, the equipment would be fully automatic from 30 seconds before burst until several minutes later. The photoheads, the Heiland recorder, the sequence camera, and the two scope cameras would all be timed and operated by the synchronous motor and the various relays and circuits in the synchronizer. The synchronizer was consequently a rather elaborate instrument. It will not be described in detail because most of its auto-

matic features were not in use during the later tests in the series, when the more successful measurements were being made.

However, the synchronous motor in the synchronizer was always used when the sequence camera was operated. The 400-cycle motor was geared down to turn an output shaft at one rotation per second. On the shaft was a cam which closed a normally-open microswitch for an interval of about 50 msec once a second. The microswitch activated a relay which closed a heavier switch to give a 50-msec current pulse for the operation of the sequence camera. The camera consequently took pictures at one frame per second, but in order to keep the switching currents from interfering with other portions of the equipment, particularly the fiducial systems, the camera was not started until just after the burst.

Certain other parts of the synchronizer were also used in addition to the synchronous motor. For example, the switch for activating the relay in each photohead circuit was located on the synchronizer. Also, the +150 volt supply came from a circuit in the synchronizer which gave a separately regulated +150 volt output, using as input the voltage from the +250 volt power supply.

2.2.7 Cameras. The sequence camera, which was used to photograph the burst and the nuclear cloud and to make a photographic record of the ambient light conditions, was a Beattie Model D unit with a 50-mm focal length and an f/1.5 lens. The camera was modified for 400-cycle operation, had magazines capable of holding 100-foot rolls of 35-mm film, and was instrumented to operate at one frame per second. Tri-X film was used.

Photographed simultaneously with the main picture was a format which appeared at the corner of each frame. The format included a counter to identify each frame by number, and a clock to record the time at which the picture was taken. Usually the code name of the shot was also included in the format.

Each of the two cameras photographing the cathode-ray tubes of the oscilloscopes was a modified DuMont 302 scope camera with an f/1.9 lens and with a modified Beattie 70-mm film magazine. Because the magazines gave considerable trouble, their use was discontinued after the fifth shot and Polaroid film holders were substituted. There was space on one end of each Polaroid frame for a small amount of written data identifying the picture.

2.2.8 Filters. Two kinds of filters were used. For the sequence camera, neutral density filters were provided to cut down the amount of light reaching the film. These filters cut down the light evenly over the visible wave length region to which the camera and film were responsive. The rendition of the scene on the film was not noticeably affected by the filters.

Neutral density filters were provided in three different values: 2.0, which transmits 1 percent of the available light, absorbs 99 percent; 1.0, which transmits 10 percent, absorbs 90 percent; and 0.50, which transmits 32 percent, absorbs 68 percent.

In addition to the neutral density filters for the sequence camera, other filters were provided for the photoheads, to cut down the amount of thermal radiation reaching the phototubes. These filters were simply metal screens with holes that let the light through. Two sizes were provided one transmitting 10 percent and the other transmitting 1 percent of the incident radiation.

2.2.9 Light Meter. A Weston Master II exposure meter was used in some of the photohead calibration measurements described in Section 2.1.5. The meter scale readings were in candles per square foot. However, the meter readings needed to be reinterpreted. In the photohead calibration measurements, the light meter was used to measure incident light from a small source, the photoflood bulb, whereas the meter scales were made to read correctly for light reflected from an extended field.

The exposure meter, when directed toward an illuminated surface, gives a reading for the brightness of the surface in candles per square foot. One candle is a source radiating a flux of

one lumen per steradian (unit solid angle). The lumen is a measure of radiant flux, as weighted by the spectral sensitivity curve of the eye. One watt of radiant flux at 5,500 Å is equivalent to 680 lumens; one watt of radiant flux at any other wave length, λ, is less than 680 lumens by the luminosity factor at the wave length λ, given in Figure 1.12.

It can be seen from a comparison of Figure 1.12 and Figure 1.13 that the exposure meter, unless used with a special filter, does not follow the same response curve as the eye. In particular, it is sensitive to ultraviolet (and to some infrared) wave lengths outside the eye's sensitivity. For example, the exposure meter will give a nonvanishing reading in candles per square foot when exposed to ultraviolet light of 3,500 Å, even though that wave length has no luminous power since it is outside the luminosity curve. The exposure meter readings needed to be corrected and interpreted on the basis of the sensitivity curve in Figure 1.13, with 5,500 Å used as the reference point for the correction.

For light of 5,500 Å, the exposure meter will give a reading which can be converted from photometric units to radiometric units, from lumens to watts. A surface of area S, in square feet, with a luminance (or brightness) of B, in candles per square foot, viewed from a distance D, in feet, will give an illuminance of SB/D^2 in lumens per square foot at the point of observation. The exposure meter is ordinarily used to view a surface which is larger than the solid angle of acceptance, Ω. The area, S, from which illumination is received, is then equal to $D^2\Omega$, and the illuminance reduces to $B\Omega$, in lumens per square foot, where B is brightness in candles per square foot and Ω is solid angle in steradians.

The Weston exposure meter has two scales. There is a baffle which can be closed to reduce the amount of light reaching the photosensitive surface. The baffle is a disk with 46 small holes, and acts partly by reducing the acceptance angle, Ω, and partly by blocking some of the light in the narrowed field of view. With the baffle open, the meter has a 60-degree field of view and an acceptance solid angle, Ω, of about one steradian; the lower scale is used, with its maximum scale reading of 50 candles/ft^2. With the baffle closed, the field of view is about 30 degrees and the solid angle, Ω, is about $\frac{1}{4}$ steradian; the upper scale is used, with 1,600 candles/ft^2 as its maximum reading.

Since Ω is equal to one for the lower scale (baffle open), the brightness reading, B, is also a reading of illumination in lumens per square foot at the position of the meter, because of sources contained within the 60-degree field of view. The exposure meter can then be used directly as an incident light meter to measure the illumination from any source, such as the photoflood bulb discussed in Section 2.1.6, provided that the bulb is contained within the 60-degree field of view and that no other important light source is in the same angular field. For the upper scale (baffle closed), Ω is equal to $\frac{1}{4}$, and therefore the illuminance is B/4, one fourth of the scale reading. When the exposure meter is used with its upper scale for incident light measurements, the scale readings should be divided by four, to give illuminance in lumens per square foot.

Measurements of illuminance in lumens per square foot, for a wave length of 5,500 Å, can be converted to irradiance in watts per square meter through multiplication by the factor 0.01583. If the measurement refers to a wave length other than 5,500 Å, a further factor is necessary. The additional factor is the reciprocal of the relative sensitivity of the instrument used for the measurement of illuminance. For example, at 3,500 Å the sensitivity of the exposure meter is shown in Figure 1.13 to be about 0.28, referred to a sensitivity of unity at 5,500 Å. The reciprocal of 0.28 is 3.6. Ultraviolet light of 3,500 Å which gave an illuminance measured by the meter as E lumens per square foot would have an irradiance in watts per square meter which was the product of E and 0.01583 and 3.6, or 0.057E watts/meter^2.

As used with the photohead test box, the light meter readings on the two scales were found to match after a correction factor was applied to the readings on one of the scales. However, the correction factor was found to be two rather than four, indicating that the bulb in the test

box was not acting as a true point source. Most probably this could be attributed to incomplete light absorption by the black paint on the inside of the cylindrical tube. This caused a portion of the light striking the inside tube surface to be reflected and to reach the exposure meter from directions outside the 30-degree field of view for the upper scale, but inside the 60-degree field of view for the lower scale. (See Section 3.3.9.)

2.3 DATA REQUIREMENTS

The required data can be considered from two standpoints. In form, the data consisted of scope photographs, Heiland records, and sequence camera pictures, in addition to the meter readings and general identification information written on the data sheets.

From a functional standpoint, the burst data, directly recorded on the equipment in response to the different forms of radiation from the nuclear detonation, was supplemented by auxiliary data needed for calibration and interpretation of the burst data and for evaluation of the performance of the equipment.

2.3.1 Electromagnetic Signal. Scope pictures of the electromagnetic pulse from the burst were bracketed by scope pictures used for calibration. The calibration signals were of three kinds.

1. There was an internally generated calibration signal in each oscilloscope. This was a square wave whose amplitude covered the full scale of the graduations on the scope face when the scope amplifier was correctly adjusted. The vertical sensitivity of the scope presentation was then equal to the indicated value set into the dials on the scope. When the amplitude of the square wave differed from full scale, the ratio of full scale to square wave amplitude was then a correction factor to be applied to the dial settings to give the actual vertical sensitivity of the scope.

2. A sine wave from the Heathkit oscillator was fed directly to the oscilloscope, to give an independent calibration measurement of the vertical sensitivity of the scope and to give an oscillatory signal for the calibrated measurement of the oscilloscope sweep length.

3. A sine wave from the Heathkit, set at a much lower amplitude, was fed to the input of the fiducial amplifier, whose output led to the oscilloscope. Together with Item 2 above, this gave a measurement of the gain of the fiducial amplifier at the frequency of the Heathkit signal, which was usually set at 12 kc or 15 kc. It also gave a second scope picture for use in determining the sweep length, which sometimes was significantly different from the dial setting on the oscilloscope.

Both slow and fast sweeps were used, to show both the succession of sky waves and the detailed structure of the ground wave and the separate sky waves. In many of the fast-sweep pictures, however, the detailed structure was distorted by saturation in the fiducial amplifier, a result of the strong signals from the burst and the relatively short ranges between burst and aircraft.

For reduction and interpretation of the electromagnetic data, certain general information was needed concerning the shots, such as the time of burst, from which an estimate of ionosphere height could be made, and the range from burst to aircraft, which was provided by the central radar net controlling all participating aircraft during Operation Redwing.

The method of reduction used for the electromagnetic data is illustrated in detail in Chapter 3, in the sections dealing with the signal received from Shot Tewa.

2.3.2 Thermal Radiation. The Heiland records of the photohead outputs were the direct data from the burst. Calibration of the time scale was provided internally by the 0.01-sec markers recorded at the edge of the paper tape, to one side of the traces for the two photoheads.

For calibration of the Heiland deflection sensitivity, a measured current of about 69 μa was

fed into the five Heiland channels, connected in parallel so that 13.8 μa passed through each channel. A strip of the Heiland paper tape was run, before or after the shot, to record the deflection produced by the calibration current.

However, the Heiland calibration checked only how close the Heiland was to its rated sensitivity of 20 μa/in. It was a calibration required for determining the photohead output current from the Heiland deflection. A different kind of calibration was needed to permit the translation of photohead output current values into values of phototube current or values of incident radiation. Photohead calibration measurements were made on the ground with the use of the photohead test box and the Weston exposure meter. Later measurements of the response of the photohead circuit were made in the laboratory after the conclusion of Operation Redwing.

General information needed for interpretation of the Heiland data included such meteorological details as the description of the altitudes and densities of any layers of clouds located in the region between the detonation and the aircraft. For daylight shots, a measurement of ambient light, by means of the microammeter in each photohead, aided in data reduction. It was also important that the two Heiland channels used for the photohead outputs be clearly distinguished by a displacement in their zero settings so that no question could arise as to which trace referred to the 1P39 phototube and which to the 6570. The usual practice was to place the 1P39 trace above, and to place the 6570 trace below, nearer the edge of the Heiland paper strip. When a filter was used with either photohead, its value was noted on the data sheet.

As an aid in evaluating the performance of the equipment in the presence of ambient light, Heiland records were taken of the light from sunlit clouds. The same kind of direct and calibration data was needed for cloud measurements as for burst measurements.

2.3.3 Sequence Photographs. The sequence camera was used to photograph the burst and the nuclear cloud. It was also used for a photographic record of the intervening cloud layers between the burst and the aircraft and of the cloud formations studied during the measurements of ambient light variations resulting from sunlit clouds.

In all these applications, it was important that some means of synchronization be established between the groups of frames on the sequence film and the corresponding portions of the Heiland recorder tape. The sequence camera included a format with a counter, so that the counter number was photographed on each frame and changed by one unit from each frame to the next. On the data sheet a notation was made of the hour at which each group of frames, identified by counter number, was run off, and the same identification by counter number was written on the back of the Heiland paper tape after each interval of synchronized operation of sequence camera and Heiland recorder. This identification procedure was especially important for the cloud measurements.

The lens openings used with the sequence camera, in different applications, were included in the data recorded on the data sheets. Whenever a filter was used, the filter value was also recorded.

Chapter 3
RESULTS and DISCUSSION

The results obtained during Operation Redwing have been grouped under three headings: electromagnetic results, photohead results, and sequence camera results. For convenience, the discussion of these results has been included with their presentation. As preface, an operational synopsis has been prepared in tabular form.

3.1 OPERATIONAL SYNOPSIS

The operational procedure used in Operation Redwing was discussed at the beginning of Chapter 2. A description was given there of the changes which were made in the method of operation as experience was gained on the first few test shots.

Table 3.1 summarizes the tests in which Project 6.4 participated and shows that increasingly valuable data was obtained on the later tests as the equipment and the operating procedures were improved.

3.2 ELECTROMAGNETIC RESULTS

Because of the amplifier saturation discussed in "Fiducial Amplifiers", Chapter 2, many of the recorded electromagnetic pulses were badly distorted in wave shape, making it difficult to draw quantitative conclusions from them. However, during Shot Tewa a very slow sweep was used on the oscilloscope, and a number of sky waves appeared, most of which had amplitudes small enough to avoid saturation in the fiducial amplifier. From the detailed analysis of these sky waves, a considerable amount of information was obtained, making it easier to understand and interpret the electromagnetic signals from the other shots.

3.2.1 Shot Tewa. During Shot Tewa, the sixteenth of the seventeen Redwing test shots, the aircraft was 96 naut mi (178 km) south of the detonation, at the 18,000-foot altitude which was usual for the flights. The signals received on the two fiducial antennas were both shown in the dual-beam oscilloscope, Type 333. The amplified signal from the smaller fiducial antenna, mounted inside the aircraft on the window rack, was displayed on Channel A, while Channel B displayed the signal from the larger antenna, mounted outside the aircraft skin.

Figure 3.1 (left portion) is a photograph showing the signals received on the two fiducial antennas and displayed on the dual-beam oscilloscope; Figure 3.1 (right portion) is a tracing made from the photograph. Before the shot, Channel A was positioned about two small divisions above the center line, and Channel B was positioned below the center. The sweep was so slow that about six sky waves, in addition to the ground wave, can be identified on the sweep. The first part of the sweep, containing ground wave and first sky wave, shows very strongly the effects of amplifier saturation. The saturation is gone by the second sky wave, whose pulse shape can therefore be studied in detail and compared directly with the form of pulse expected from a loop antenna. The periods, the separations, and the amplitudes of the sky waves and ground wave can all be used as sources of information, as will be demonstrated in the following sections.

Oscilloscope Calibration. The oscilloscope was adjusted to a nominal vertical sensitivity of 100 volts full scale, or 25 volts per large division, on both channels. However, cali-
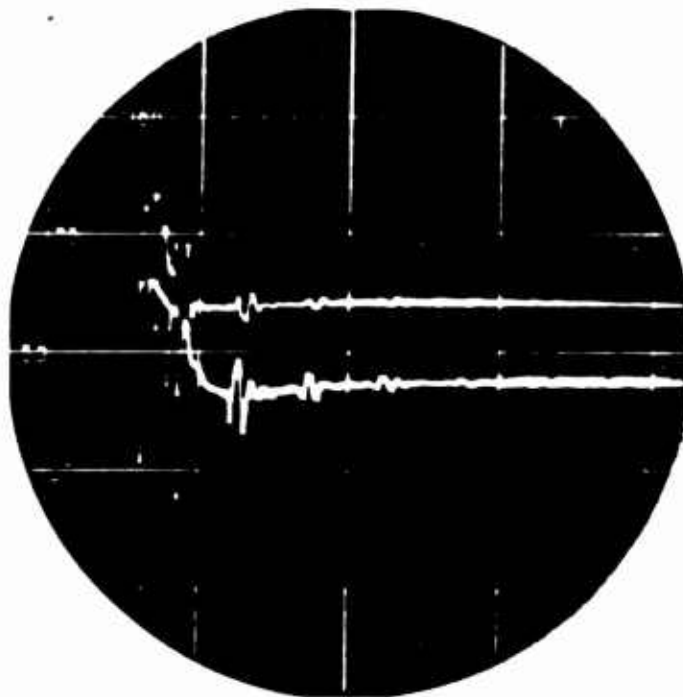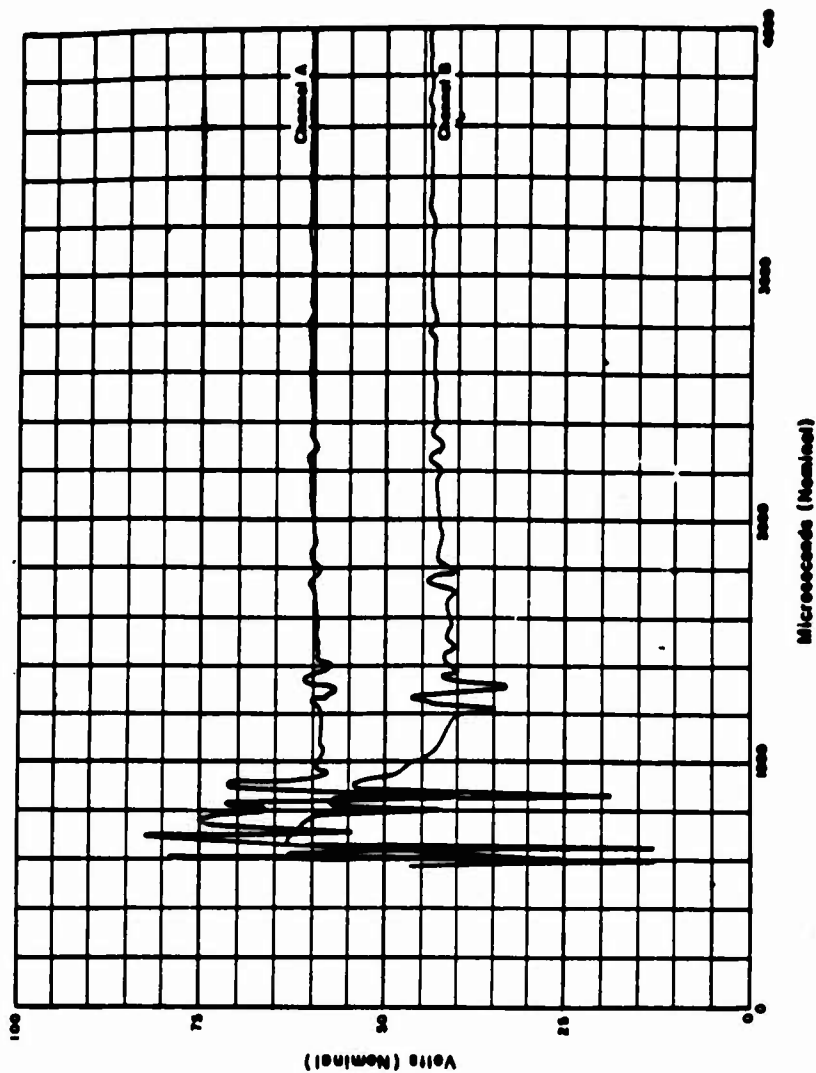
Page 81
Deleted

Figure 3.1 Electromagnetic signal from Shot Tewa. Photograph of oscilloscope display shown at left. Tracing from photograph shown at right.

bration pictures taken of the oscilloscope display before and after the shot showed that the deflection voltages were low. The calibration pictures showed that the sensitivity was actually about 140 volts full scale, or 35 volts per large division.

The sweep length was set at a nominal value of 4,000 μsec full scale, 1,000 μsec per large division. Calibration measurements, discussed in "Oscilloscopes", "Audio Generator", and Section 2.3.1, Chapter 2, showed the sweep circuits to be slow, so that the sweep time per large division was 1,100 μsec for Channel A and somewhat less for Channel B.

There was some distortion in the presentation on Channel B. This particular dual-beam oscilloscope was one of the first of its model and was not entirely free of distortion in its electron optics. In the calibration picture for Channel B, the calibration trace was not in the part of the oscilloscope face that was used for the Channel B signal trace in Figure 3.1. Consequently, the precision of the Channel B sweep calibration is open to question. From the calibration picture a sweep time of 1,090 μsec/div was inferred. However, certain internal evidence in the Shot Tewa photograph suggested that the sweep time was nearer to 1,070 μsec/div. A still closer examination of the Shot Tewa data suggested that the Channel B sweep time was between 1,070 and 1,080 μsec/div in the center of the oscilloscope with an added distortion near the corners of the presentation.

For the reduction of the Channel B data, the value 1,090 μsec/div has been used in tables and figures, but the consequences of a different calibration value for the Channel B sweep have been mentioned at several points in the text.

Pulse Shape, Period, and Yield. The second sky wave on Channel B in Figure 3.1 is relatively small in amplitude and is not affected by saturation in the fiducial amplifier. At the same time, it is large enough on the oscilloscope to permit a fairly detailed study of its pulse shape. The Polaroid print from which Figure 3.1 was made contains somewhat more detail than is shown in the reproduction. An area including the second sky wave on Channel B was enlarged photographically. Figure 3.2 (left portion) is a drawing made from the enlargement, with the help of the original print.

Figure 3.2 (left portion) is thus the pulse shape of the second sky wave as received on a loop antenna. It resembles very closely the pulse shape at the right of Curve B of Figure 1.2, the time derivative of the first sky wave as received by a vertical whip antenna from a shot in an earlier series of tests. Figure 3.2 (right portion) has been computed from Figure 3.2 (left portion) by numerical integration, and can be compared directly with the pulse shape received on a vertical whip antenna. It resembles the right-hand part of Curve A of Figure 1.2.

From the (corrected) time scale shown in Figure 3.2 (left portion), it can be seen that the period of the oscillation is about 94 μsec. The pulse shape is not a simple sinusoidal curve, so that a precise period cannot be defined, but a measurement of the time interval between the first and third peaks gives about 94 μsec, and a measurement of the time interval between the second and fourth peaks also gives about 94 μsec. Figure 1.3 associates a yield of about 4.0 Mt with a pulse period of about 94 μsec.

The time scale in Figure 3.2 is based on the sweep calibration value of 1,090 μsec/div. If the value of 1,070 μsec/div had been used, the measured period of the oscillation would have been a little more than 91 μsec, and the yield inferred from Figure 1.3 would have been about 3.7 Mt.

The official yield for Shot Tewa was 5.0 Mt. The two yield estimates given above are low by 20 percent and 26 percent, respectively.

A period of 94 μsec corresponds to a frequency of 10.6 kc, which is within the frequency band for which the fiducial antenna and amplifier are considered to act as a differentiating system, as shown in Figure 2.15 (right portion) and discussed in "Fiducial Amplifiers", Chapter 2. The close resemblance between the pulse shapes of Figure 3.2 and the pulse shapes on the right-hand side of Figure 1.2 is verification that the ferrite-core magnetic loop antenna, with its amplifier, does give a pulse shape which is approximately the first derivative of the pulse shape received
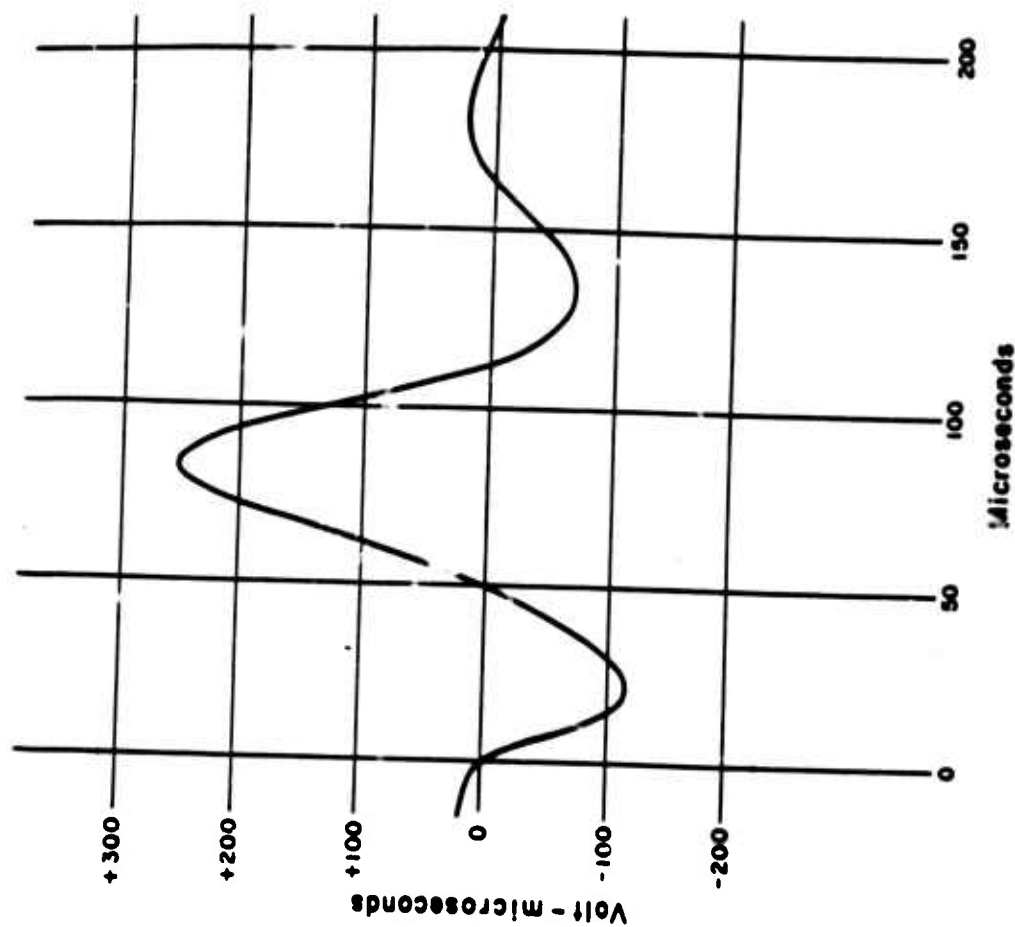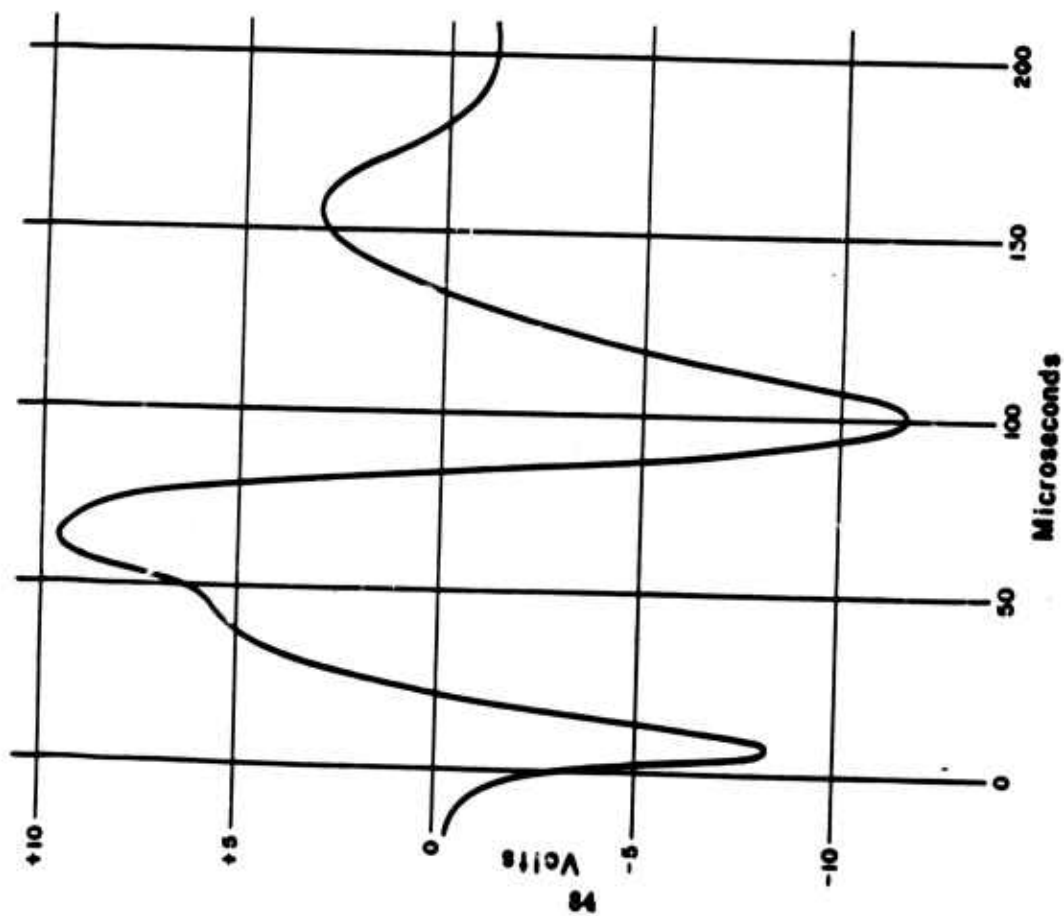
Figure 3.2 Shot Tewa: Second sky wave on Channel B. Tracing from photograph of oscilloscope display shown at left. Numerical integration of tracing shown at right.

84

by a vertical whip antenna responding to the electric field of the electromagnetic wave from the burst.

Polarity. On Channel B the characteristic pulse shape is a pair of negative deflections separated by a positive deflection and followed by a small positive overshoot and sometimes by further oscillations of small amplitude. On Channel A the same characteristic pulse shape appears, but the polarity is reversed and the initial deflection is positive rather than negative. The polarities as shown in Figures 3.1 and 3.2 agree with the polarities described in "Polarity and Wave Form", Chapter 2, and establish that the phase shift for ionospheric reflection was not far from zero for the Shot Tewa measurements, whereas the phase shift was closer to 180 degrees for the first sky wave in the Operation Teapot measurements mentioned in "Electromagnetic Wave Form", Chapter 1.

Ground Reflection. In the wave form of Figure 3.2 (left portion) there is an indentation on the left side of the second peak, roughly 30 to 40 μsec after the first peak. The indentation can be interpreted as the result of reflection by the ground beneath the aircraft.

With the aircraft at 18,000 feet, the second sky wave received directly from the ionosphere is followed after a brief time interval by the ground reflection of the same sky wave. For the conditions of Shot Tewa measurements, the time interval was computed to be 32.4 μsec for the second sky wave. Table 3.4, which is given later, includes the computed time intervals between direct and ground-reflected paths for the first six Shot Tewa sky waves. Indentations similar to those of Figure 3.2 can be found on other sky waves on both channels in the Shot Tewa photograph.

It is the narrow first peak of the ground-reflected wave which is added to the broader second peak of the direct sky wave to produce the indentation. The broader second and third peaks of the ground-reflected wave are also added, but they are not so easily distinguished since they combine with equally broad peaks of the direct sky wave and produce only a resultant change of phase and amplitude.

The wave form of Figure 3.2 (left portion) would have been more complex if the ground-reflected wave had been equal in amplitude to the direct sky wave, as it should have been if the aircraft were flying over the open ocean. However, the aircraft was actually over Wotho Atoll, and the land areas may have reduced the amplitude of the ground-reflected wave. In addition, the angle of incidence was about 28 degrees from the vertical direction, so that the path of the direct sky wave was 62 degrees above the horizontal, while the path of the ground-reflected wave was 62 degrees below the horizontal. There might have been a difference in the antenna reception from those two directions, caused perhaps by field distortions around the aircraft. A difference in antenna reception would have had the same effect as a difference in signal amplitude and could have contributed to the observed amplitude difference between the direct sky wave and the ground-reflected wave that accompanied it.

There can be reflection from the ground below the aircraft, as described above, but there can also be reflection from the ground in the neighborhood of the source of the electromagnetic radiation, the nuclear detonation. The character of the wave form emitted upward from the detonation should then depend on the altitude of the burst and the resulting time interval between the pulse from the burst and the pulse reflected from the ground below the burst.

The Shot Tewa detonation was on a barge, but there have been other detonations that were positioned at various altitudes. The examination of wave forms from these higher-altitude detonations reaching a receiver over sky-wave paths should show whether the direct sky wave can be distinguished from the wave reflected from the ground beneath the burst. If it were possible to measure the time delay between these two waves, that measurement could be used to determine the altitude of the burst. In case the burst and the receiver were both at a high altitude, there would be four alternate paths for each sky wave and the resulting wave forms might be difficult to analyze.

In principle, with a broad-band receiving system, it should be possible to use as reference points the spikes which are often included in the radiated pulse from a high-yield detonation. (See Reference 1.) The duration of a spike is of the order of a few μsec or less, and the frequencies involved are accordingly relatively high, most of the energy being concentrated in

frequencies above 100 kc. The fiducial system used in Project 6.4 was strongly attenuating for such frequencies, as shown in Figure 2.15 (right portion). Consequently, any spikes which may have been present in the electromagnetic wave were eliminated from the signal which reached the oscilloscope.

Saturation. In Section 2.2.3, the saturation in the fiducial amplifier was discussed. The effects described there are illustrated in the left-hand portions of the two traces in Figure 3.1. The trace on Channel B shows clearly the effect of grid current at the second stage of amplification.

The grid current drawn by the first large pulse charged the grid condenser and established a displaced grid bias on the tube and a displaced zero point on the output of the tube. Succeeding pulses produced deflections away from the displaced zero, but the tube was then nearly cut off and its amplification characteristic was, therefore, very unsymmetrical. The deflections were quite one-sided during the several hundred μsec needed for the grid condenser to discharge.

In Figure 3.3 the first portions of the two Shot Tewa traces have been drawn in detail. A partial reconstruction of the peaks clipped off by saturation has been made, to show that the characteristic loop antenna pulse shape (a triple peak plus overshoot) was applicable to the ground wave and first sky wave as well as to the later sky waves. The amplitudes of the deflections, especially the ground wave amplitudes, may have been considerably different from those indicated in the figure. A rough estimate of the ground wave amplitude is made under "Amplitude Comparison", a later section of this chapter.

The later sky waves appeared to be largely unaffected by saturation, but there may have been certain residual effects. Figure 3.1 shows that the two traces were slightly lower for times between 1,000 and 2,000 μsec than they were for times between 2,000 and 4,000 μsec. This displacement could perhaps have been associated with the charging of the third 1,000-$\mu\mu$f condenser in the fiducial amplifier (Figure 2.14) by grid current in the cathode follower, drawn during the high-voltage peaks of the ground wave and first sky wave.

An additional possibility is that the grid current drawn during the high signal peaks might have affected the performance of the tubes themselves, perhaps changing the gain of the circuit. For a precise quantitative interpretation of the amplitudes of the various sky waves in Figure 3.1, a thorough study of the performance of the fiducial amplifier under overload conditions would be desirable. Without such a study the analysis of comparative amplitudes, as carried out under "Amplitude Comparison", should be considered very tentative. On the other hand, amplifier saturation could have little effect on the time interval measurements discussed immediately below.

Timing of Sky Waves. The time intervals between the sky waves were determined from the traces shown in Figure 3.1. They are listed in Table 3.2. A careful measurement of the intervals was made. Because of scope distortions and doubts concerning the calibrations, some of these measurements do not really carry the precision that is implied in the tables and graphs. However, the tables and graphs illustrate the procedure that could be used with data from more elaborate instrumentation. Time measurements can, in principle, be made with very high precision.

As a reference point on each sky wave, for measuring its separation from the ground wave, the first peak of the characteristic three-peak pattern was used. A small error may have arisen here because the later sky waves did not rise as sharply to the first peak as did the ground wave, but an attempt to measure from the initial rise would also have given errors for the later sky waves, because the initial rise was often partially submerged in noise. The distances between the various waves and the second heavy scale marker on the scope face were measured on the original Polaroid print with the aid of a microscope. The direct measurements in inches were listed in the second column of Table 3.2. In the third column of the table the distances were referred to the ground wave as the zero point.

Measurements on the original photograph showed the heavy vertical lines on the oscilloscope grid to be separated by 0.410 inch, which is thus the length of one large time division in inches. The separations in the third column were converted to the time intervals in the fourth column
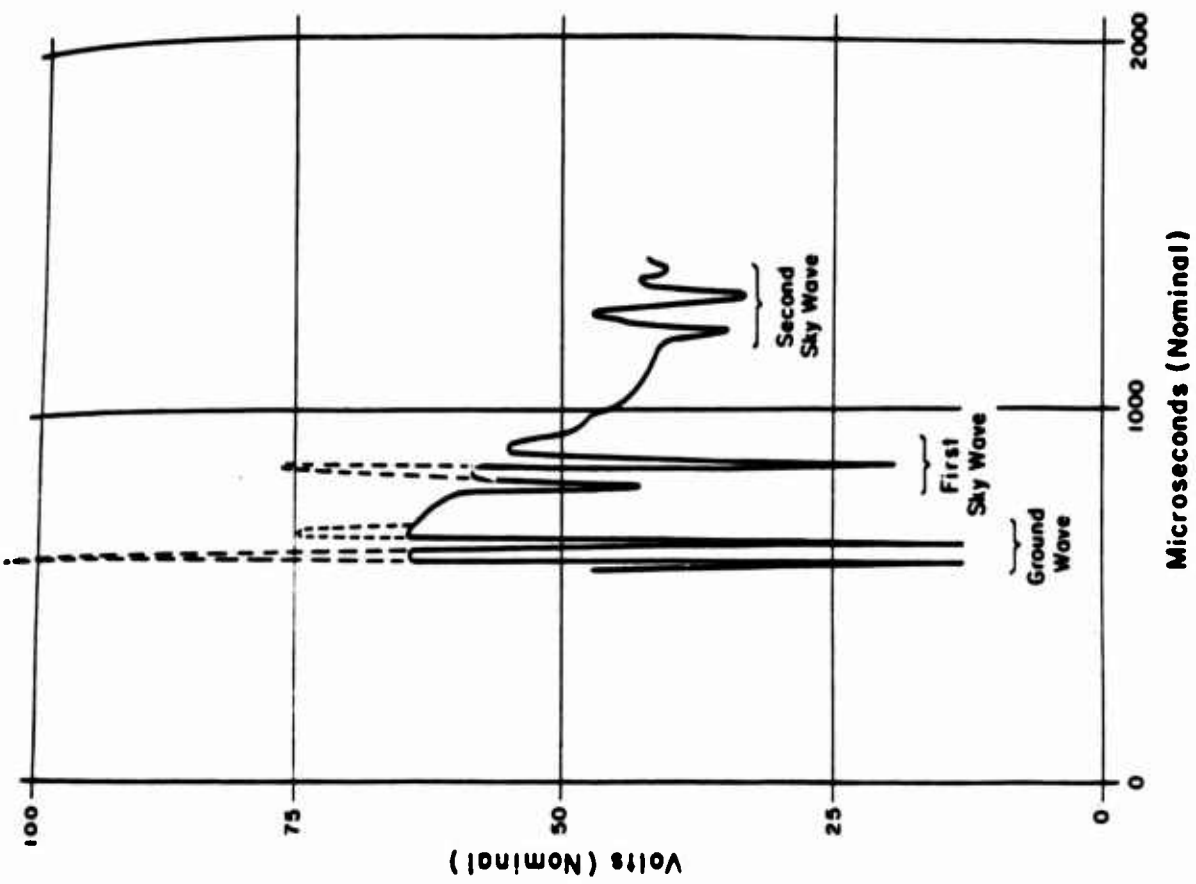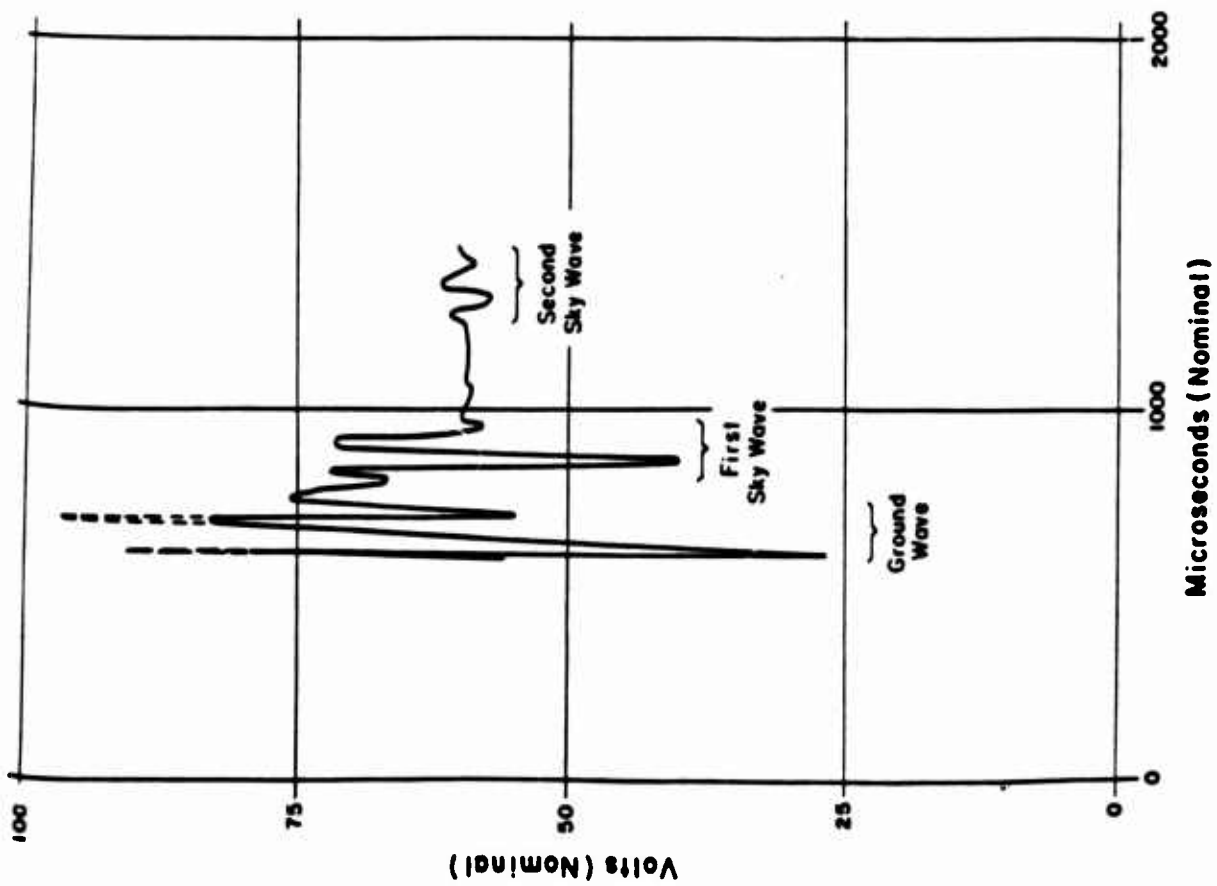
Figure 3.3 Shot Tewa: partial reconstruction of first part of trace on Channel A shown at left. Partial reconstruction of first part of trace on Channel B shown at right.

through division by 0.410 inch and multiplication by the calibration factor, in μsec per division, that has been discussed above; that is, 1,100 μsec/div for Channel A, and 1,090 μsec/div for Channel B.

From each time interval in the fourth column of Table 3.2 it is possible to calculate a value of the range from burst to receiver if the height of the ionosphere is known. If the height, H, is not known but is assumed to have a given value, H_1, then the calculated range will depend on H_1 and on the number, n, characterizing the sky wave used for the calculation. A plot of calculated range against time interval will be a horizontal straight line at the actual range, D_0, if the assumed ionosphere height H_1 happens to equal the actual height, H_0. If not, the plot will still be a straight line (unless the assumed altitude is very wrong and the range is very great), but the line will have a nonvanishing slope.

The last three columns of Table 3.2 show calculated ranges, for assumed ionosphere heights of 90, 80, and 70 km, as read from the dashed curves of Figure 1.5. As pointed out in " Timing

TABLE 3.2   REDUCTION OF TIME INTERVAL DATA FROM SHOT TEWA OSCILLOSCOPE
PHOTOGRAPH

	Distance from Second Scale Marker	Distance from Ground Wave	Time	Range		
				H = 90 km	H = 80 km	H = 70 km
	in	in	μ sec	naut mi	naut mi	naut mi
Channel A						
Ground Wave	−0.153	0.000	0	—	—	—
First Sky Wave	−0.069	0.084	225	107	79.5	54.5
Second Sky Wave	+0.104	0.257	690	108.5	73.5	42
Third Sky Wave	+0.297	0.450	1,207	116	72	30.5
Fourth Sky Wave	+0.500	0.653	1,750	121.5	65	16
Fifth Sky Wave	+0.716	0.869	2,330	120	54	−3
Channel B						
Ground Wave	−0.180	0.000	0	—	—	—
First Sky Wave	−0.088	0.092	245	95	70	46
Second Sky Wave	+0.087	0.267	710	102.5	68	38
Third Sky Wave	+0.285	0.465	1,236	108	64	25
Fourth Sky Wave	+0.498	0.678	1,800	110	55.5	7
Fifth Sky Wave	+0.711	0.891	2,370	112	47.5	−9
Sixth Sky Wave	+0.915	1.095	2,910	—	—	—

of Sky Waves", Chapter 1, the use of the dashed curves implies that the time measurement refers to the sky wave which was traveling downward toward the aircraft, not to the companion sky wave traveling upward after one additional reflection from the earth. The ground-reflected wave did not arrive at the aircraft until after the first peak of the direct sky wave had been received. Since the time measurements were based on the location of the first peak of each sky wave, the ground-reflected wave could have had no effect on the time measurements.

In Figure 3.4 (left portion) the calculated ranges for Channel A are plotted, with the time interval as abscissa and the range as ordinate. For each of the three assumed ionosphere heights there are five points lying roughly along a straight line. Three straight lines have been drawn intersecting at a point with the ordinate value of 96 naut mi, which was the range measured by the radar control center at the time of Shot Tewa. If the time intervals had been measured with an instrument of greater precision in time, such as a scope presentation with time markers and a raster scan or a gradually spiraling circular sweep, then the points themselves could have been used to determine the positions of the three straight lines, and the range could have been obtained from the point of their intersection.

For ranges that are short enough, so that the curvature of the earth does not play an important role, the point of intersection of the straight lines lies along the focus line shown in the figure. This is a line whose slope equals minus one half the velocity of light. In the units of Figure 3.4,
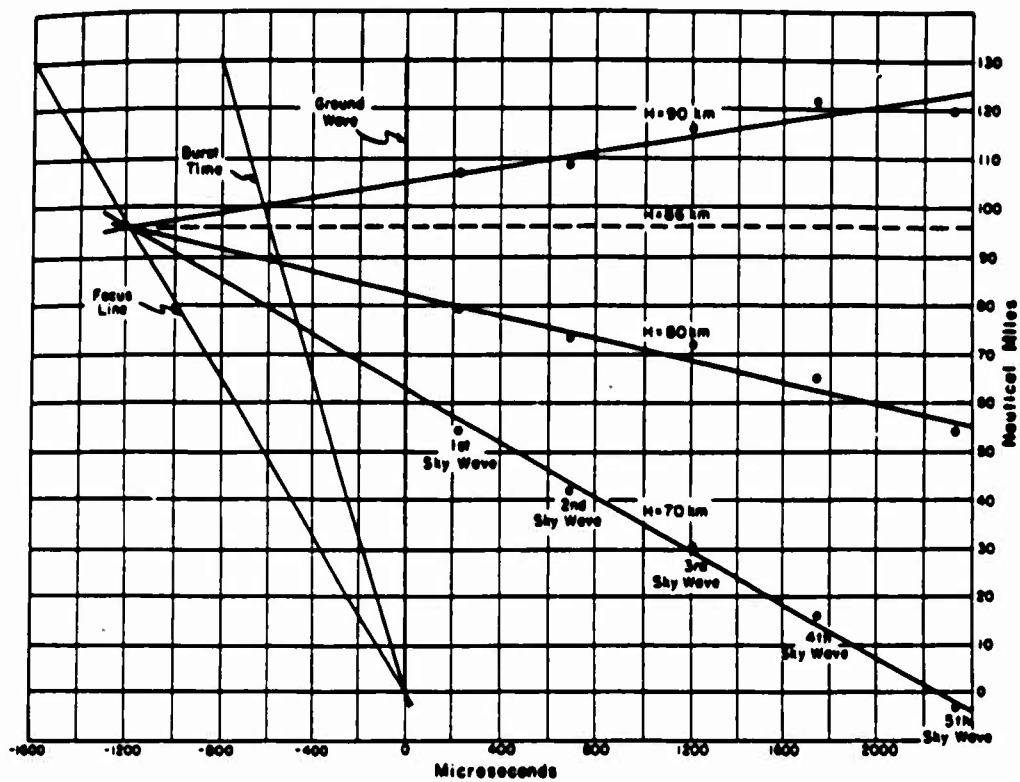
Channel A (Left Portion)
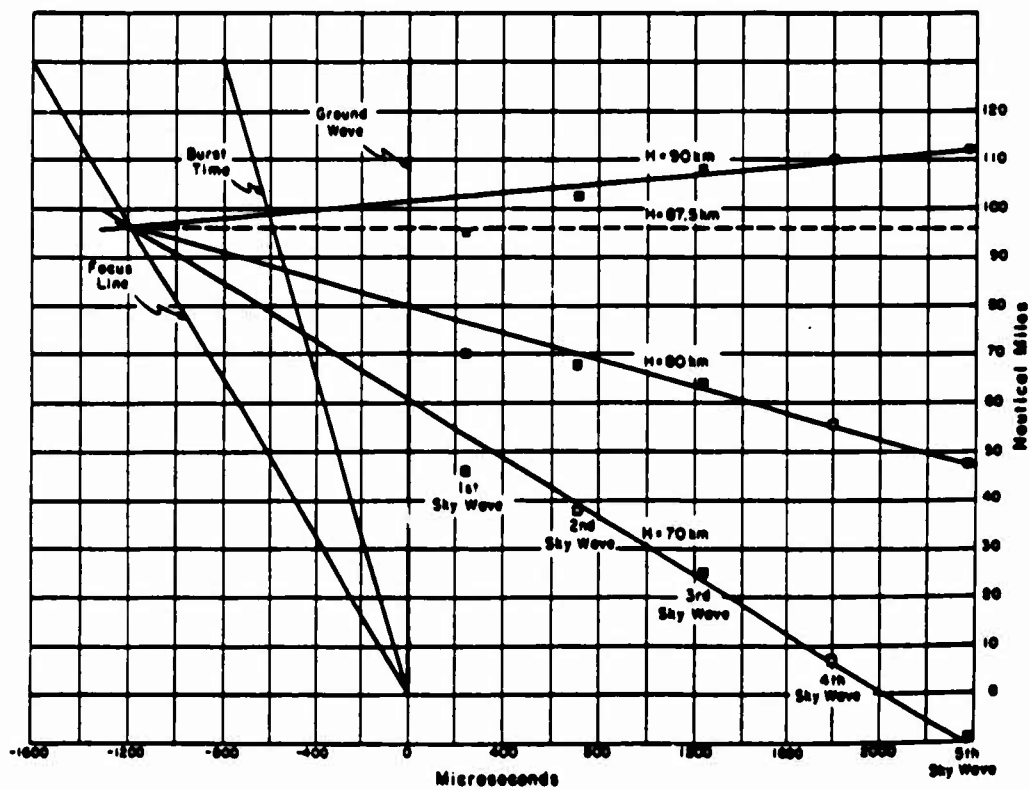
Channel B (Right Portion)

Figure 3.4 Reduction of time interval data of Shot Tewa oscilloscope photograph.

89

the velocity of light equals 0.162 naut mi/μsec, and the slope of the focus line is therefore equal to −0.081 naut mi/μsec.

The focus line can be located mathematically by the condition in Equation 3.1.

$$\left(\frac{\partial Y}{\partial H}\right)_{X=constant} = 0 \tag{3.1}$$

Where: X and Y = abscissa and ordinate in Figure 3.4
         H = assumed height of the ionosphere

The equation locating the specific points on the intersecting lines is:

$$cX = \sqrt{Y^2 + (2nH)^2} - Y \tag{3.2}$$

provided that the curvature of the earth can be neglected. The velocity of light is written as c, and n is the number labeling the particular sky wave associated with each point along the line. If the actual ionosphere height, $H = H_0$, is used, then the line is horizontal and Y equals the actual range, D_0. In that case,

$$cX = \sqrt{D_0^2 + (2nH_0)^2} - D_0 \tag{3.3}$$

Equations 3.2 and 3.3 can be combined to eliminate n:

$$Y = \frac{cX}{2}\left(\frac{H^2}{H_0^2} - 1\right) + D_0\,\frac{H^2}{H_0^2} \tag{3.4}$$

This is the equation of a family of straight lines whose intersection, defined by Equation 3.1, is located by:

$$cX = -2D_0 \tag{3.5}$$

If D_0 is now considered the ordinate and allowed to vary, then Equation 3.5 becomes the equation of the focus line, as described above, with slope equal to −c/2.

There is an additional line shown in Figure 3.4 (left portion) with twice the slope of the focus line. Along the dashed horizontal line representing the actual ionosphere height this additional line, which locates the burst time, is displaced from the vertical line locating the ground wave by an interval in μsec equal to the time between the burst and the arrival of the ground wave at the receiver.

The three lines in Figure 3.4 (left portion) corresponding to the three selected ionosphere heights belong to the family of lines contained in Equation 3.4, as does the horizontal line that would have been obtained if the actual height, H_0, had been used. Equation 3.4 shows the slope to be a linear function of H^2. Plotting H^2 against the slope should give a straight line from which the ionosphere height for zero slope can be found by interpolation. In Figure 3.5 the circles represent the slopes obtained from Figure 3.4 (left portion), and the point of zero slope comes at $H^2 = 7,400$ km², or H = 86 km. That is, 86 km is the ionosphere height which can be inferred from the Shot Tewa data on Channel A and the corresponding calibration data.

In Table 3.2 there is a second set of ranges, which was calculated from the data on Channel B, by the same procedure used with Channel A. The ranges for Channel B have been plotted as small squares on Figure 3.4 (right portion), and three straight lines have been drawn through the points, as they were on Figure 3.4 (left portion), intersecting on the focus line at the 96 naut mi range. The slopes of the three lines are plotted as small squares on Figure 3.4, and the interpolated value of the ionosphere height is found to be 87.5 km.

In Table 3.2 the sweep calibration used for Channel B was 1,090 μsec/div. If 1,070 μsec/div

had been used instead, the points on Figure 3.4 (right portion) would have been displaced upward, changing the slopes of the three lines and bringing them very close to the positions of the lines in Figure 3.4 (left portion). In Figure 3.5 the small squares would have been displaced toward the small circles, and the interpolated value for the ionosphere height would have been 86.2 km.

It should be noted that the points in Figure 3.4 (right portion) do not fall as closely to the straight lines as they did in Figure 3.4 (left portion). The first few sky waves give points that are too low, and no improvement is found when 1,070 μsec/div is used as the sweep calibration instead of 1,090 μsec/div. The points are displaced but they do not move any closer to a straight
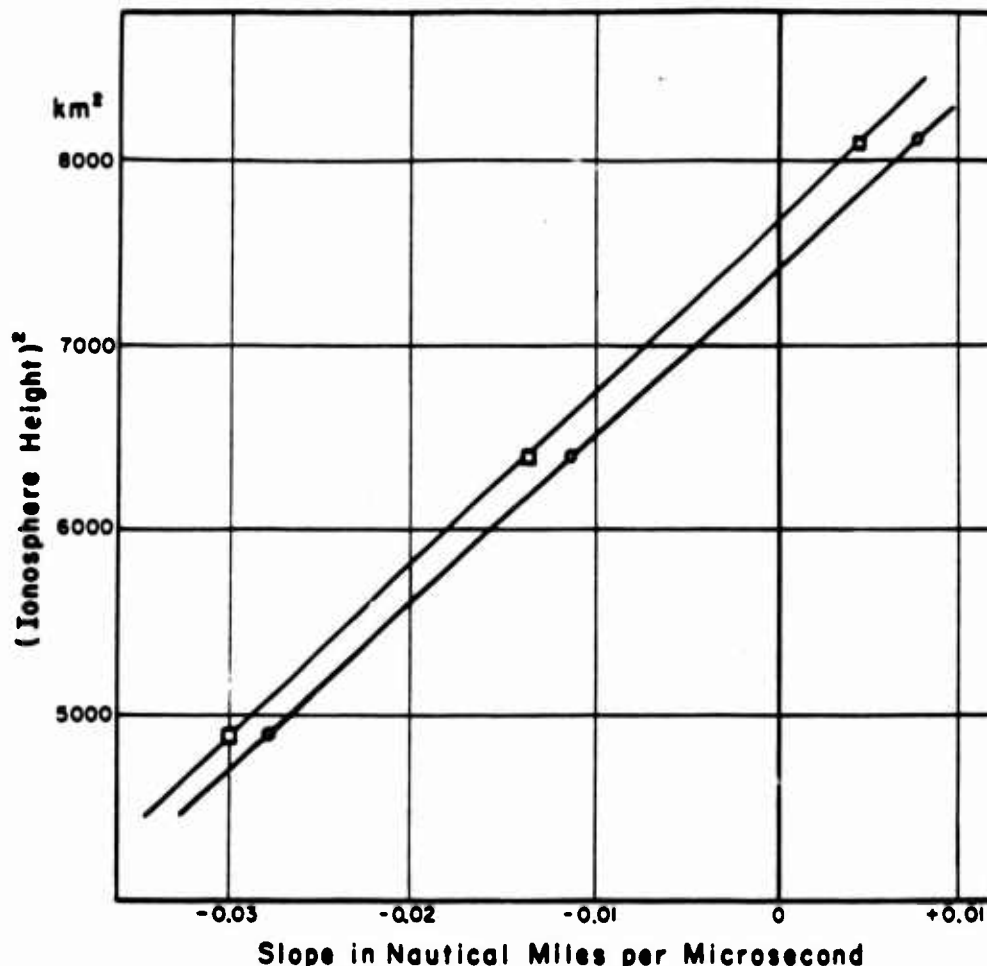
Figure 3.5 The square of the assumed ionosphere height plotted against the slopes of the straight lines in Figure 3.4.

line. It seems necessary to attribute the curvature of their positions to a distortion in the electron optics of Channel B, particularly at the edges of the scope face. A change, for instance, of 0.005 inch in the position of the ground wave on the scope face would mean a substantial straightening of the rows of points.

Amplitude Comparison. In the Shot Tewa photograph, Figure 3.1, it can be seen that the characteristic wave form was changing somewhat from one sky wave to the next. The sharp initial peak tended to lose its sharpness and to be attenuated more rapidly by successive reflections than the second and third peaks of the wave form. An explanation can be found in Figures 1.6 and 1.7.

The curves of Figure 1.6, considered together with Table 1.1, show that reflection from the ionosphere is accompanied by absorption that is greatest for the high-frequency portions of the

spectrum of the pulse. That is, the absorption is greatest for the spectral regions responsible for the relatively sharp initial peak of the wave form. The phase shift given by the curves of Figure 1.7 also has its effect on the wave form of successive sky waves, tending to reduce the initial peak and to add small oscillations at the end of the pulse.

In addition, it should be noted that successive sky waves were radiated upward from the source at angles increasingly closer to the vertical, and that the original radiated wave form may have depended somewhat on the direction from which the radiating electrical currents were viewed. Also, the steeper angles for the later sky waves meant that the delay time between the direct sky wave and the ground-reflected wave was a little different from one sky wave to the next, affecting the resultant wave form.

The changing wave form made it difficult to compare amplitudes of the different sky waves. As a reference voltage which seemed least affected by the wave form changes, the average of

TABLE 3.3   REDUCTION OF AMPLITUDE DATA FROM SHOT TEWA PHOTOGRAPH

	Deflection Second Peak to Third Peak	Average Deflection Center to Peak	Voltage Center to Peak, Transformed into an Equivalent Ground Wave at 100 km, for Various Ionosphere Reflection Curves					
			Curve a	Curve b	Curve c	Curve d	Curve e	Curve f
	inches	volts	volts	volts	volts	volts	volts	volts
Channel A								
Ground Wave	—	—	—	—	—	—	—	—
First Sky Wave	—	—	—	—	—	—	—	—
Second Sky Wave	0.069	3.86	41	46	56	70	116	205
Third Sky Wave	0.022	1.23	29	33	45	62	125	280
Fourth Sky Wave	0.010	0.56	25	30	44	68	169	473
Fifth Sky Wave	0.004	0.22	17	21	34	58	176	630
Channel B								
Ground Wave	—	—	—	—	—	—	—	—
First Sky Wave	—	—	—	—	—	—	—	—
Second Sky Wave	0.189	10.57	112	125	153	192	317	561
Third Sky Wave	0.066	3.69	86	100	135	186	376	840
Fourth Sky Wave	0.031	1.73	76	93	136	209	522	1,463
Fifth Sky Wave	0.011	0.62	47	59	95	163	497	1,775
Sixth Sky Wave	0.005	0.28	34	45	79	150	562	2,574

the second and third peaks was chosen. The vertical displacement of the trace from the second peak to the third peak was measured on the scope photograph and is recorded in the second column of Table 3.3, for each sky wave not badly distorted by amplifier saturation. The measured displacement was divided by two to give the average of the two peaks, was then divided by the height of one large vertical division, 0.313 inch, and was multiplied by the scope sensitivity, 35 volts/div. The resulting voltage values are given in the third column of Table 3.3. (The other columns of Table 3.3 will be explained below.)

A reconstruction of the ground wave amplitude from the measured sky wave amplitudes was considered desirable. In preparation for this reconstruction a number of quantities were calculated and included in Table 3.4. The calculations were based on a range of 96 naut mi and an ionosphere height of 86 km. (See "Timing of Sky Waves" in a previous section of this chapter.) The earth's radius was assumed to be 6,368 km.

There was uncertainty as to the directivity of the source, the directivity of the receiver, and the reflection coefficient of the ionosphere. In Table 3.4 six different curves from Figure 1.6 were used, to represent six alternative conditions of the ionosphere. Of these six, Curve D most nearly represented the ionosphere condition that would have been predicted from the data in Reference 4.

No directivity was assumed for the receiver in the vertical plane. That is, the receiver di-

TABLE 3.4 NUMERICAL QUANTITIES USED IN REDUCTION OF DATA FROM SHOT TEWA OSCILLOSCOPE PHOTOGRAPH

		Ground Wave	First Sky Wave	Second Sky Wave	Third Sky Wave	Fourth Sky Wave	Fifth Sky Wave	Sixth Sky Wave
Path	km	177.8	244.4	382.9	541.0	705.6	873.1	1,042.0
Path	μ sec	592.6	814.8	1,276.4	1,803.2	2,352.0	2,910.2	3,473.4
$\bar{\theta}$ at Ionosphere		(90 deg)	45 deg 44 min	27 deg 17 min	19 deg 0 min	14 deg 29 min	11 deg 41 min	9 deg 46 min
θ at Ground		90 deg	46 deg 32 min	27 deg 41 min	19 deg 16 min	14 deg 41 min	11 deg 50 min	9 deg 54 min
Ground Reflection Delay	μ sec	0	25.2	32.4	34.5	35.4	35.8	36.0
$R(\bar{\theta})$, Curve a		(1.000)	0.851	0.880	0.888	0.891	0.892	0.892
$R(\bar{\theta})$, Curve b		(1.000)	0.793	0.834	0.845	0.849	0.851	0.851
$R(\bar{\theta})$, Curve c		(1.000)	0.694	0.755	0.765	0.771	0.774	0.774
$R(\bar{\theta})$, Curve d		(1.000)	0.599	0.674	0.688	0.693	0.695	0.695
$R(\bar{\theta})$, Curve e		(1.000)	0.443	0.524	0.544	0.551	0.556	0.558
$R(\bar{\theta})$, Curve f		(1.000)	0.314	0.394	0.416	0.426	0.431	0.433
F_a		1.778	3.96	10.64	23.4	44.2	75.4	120.3
F_b		1.778	4.25	11.85	27.2	53.6	95.4	159.5
F_c		1.778	4.85	14.46	36.6	78.8	153.2	282
F_d		1.778	5.62	18.14	50.3	120.7	262	537
F_e		1.778	7.60	30.0	101.8	302	801	2,006
F_f		1.778	10.73	53.1	227	845	2,862	9,192

rectivity was assumed to be that of the fiducial antenna itself, a simple magnetic dipole. Induced currents on the aircraft surface could distort the radiation pattern to some extent, but the whole structure is so small in comparison with the average wave length of the radiation that the induced currents could hardly introduce any significant radiation that was of higher order than magnetic-dipole or electric-dipole. The resulting directivity pattern could only be a very simple one, varying gradually with angle.

The source, however, had in each case a dimension that was a significant fraction of a wave length. (See Reference 1.) Furthermore, the Compton electrons believed responsible for the radiation moved at velocities which were close to the velocity of light. The radiation from such a rapidly moving electron tends to be concentrated in the forward direction. Whether such a relativistic narrowing can affect the directivity of the source as a whole must depend on such factors as the detailed distribution of the Compton currents in the air above and around the detonation. The quality of the data from the Shot Tewa photograph did not appear to justify such a detailed theoretical discussion for inclusion in this report. Instead, the source was considered to have the directivity of a simple electric dipole.

A factor F can be defined by the following equation:

$$F = \frac{L}{100} \; \frac{1}{\sin\theta} \; \frac{1}{|R(\bar{\theta})|^n} \tag{3.6}$$

Where: L = path length, km

This factor was used to reconstruct from the amplitude of the nth sky wave the amplitude which a ground wave at a range of 100 km should have had, provided that the assumptions described above, concerning the source and receiver directivities, were valid. It was assumed that the reflections from the ground which alternated with the ionosphere reflections gave no loss of amplitude, and that the ionosphere reflection coefficient was given by $R(\bar{\theta})$. Since six alternate choices for the ionosphere reflection coefficient were included in Table 3.4, there were also six sets of F-factors, labeled F_a, F_b, ..., F_f.

The F-factors did not include the contribution of the ground-reflected wave following each direct sky wave. In "Ground Reflection", a previous section of this chapter, it was concluded that the amplitude of the ground-reflected wave was substantially less than the amplitude of the direct sky wave. Furthermore, comparison of the calculated time delay (Table 3.4) with the 94-μsec period of the oscillation in the section "Pulse Shape, Period and Yield" showed that for the second through the sixth sky waves the phase shift associated with the time delay ranged from about 120 degrees to about 140 degrees. A vector construction showed that the resultant amplitude of the two waves was very nearly equal to the amplitude of the direct wave alone, no matter how poor or how good a reflector the ground under the aircraft might have been. The effect of the ground reflection was to reduce the resultant amplitude, but in no case among the second through sixth sky waves was the resultant amplitude less than 70 percent of the amplitude of the direct sky wave alone. If the receiver had been located at ground level, over ground that was a good reflector, the two waves would have been in phase and the amplitude of each sky wave would have been doubled. The F-factor defined in Equation 3.6 should then have included an extra factor of $\frac{1}{2}$.

The application of the F-factors in Table 3.4 is illustrated in the last six columns of Table 3.3. The voltages in the third column of the latter table have simply been multiplied by the appropriate F-factors to give the transformed voltages in the last six columns. In Figure 3.6 the transformed voltages for Channel A from four of the six columns for Channel A in Table 3.3 have been plotted as functions of the sky wave label, n. In Figure 3.7 the corresponding quantities for Channel B have been plotted.

Straight lines have been drawn in each of the figures to project the sets of points back to a common point representing the ground wave itself. However, the straight line projection was based on the assumption that the F-factor defined in Equation 3.6 made adequate allowance for

Figure 3.7 Reduction of amplitude data from Channel B of Shot Tewa oscilloscope photograph.

Volts, Center to Peak

Figure 3.6 Reduction of amplitude data from Channel A of Shot Tewa oscilloscope photograph.

Volts, Center to Peak

all sources of amplitude variation among the sky waves. If that assumption were valid, then the correct choice of ionosphere reflection curve should correspond to a horizontal line in the family of lines.

The slopes of the four lines in Figure 3.6 are almost identical to the slopes of the corresponding lines in Figure 3.7. The slopes have been averaged and plotted in Figure 3.8, against the
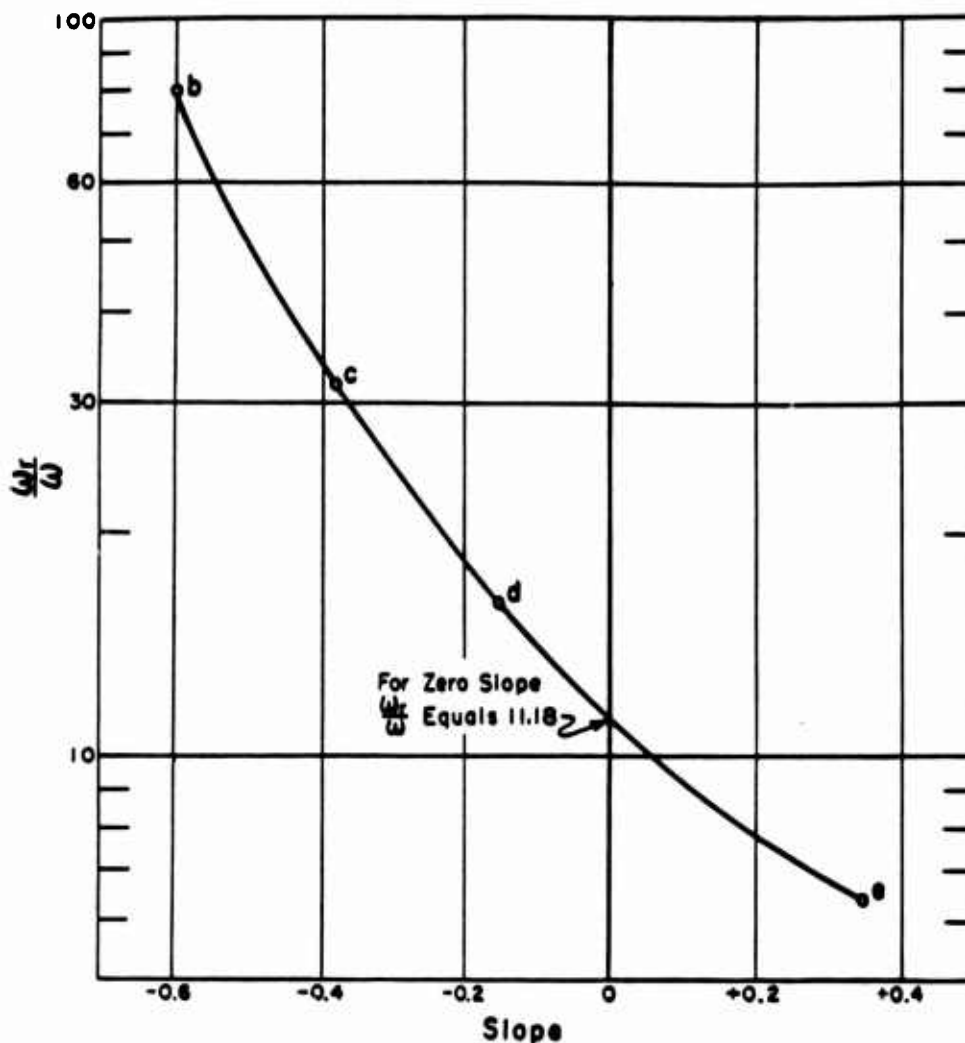
Figure 3.8 Values of ω_r/ω plotted against average slopes of corresponding curves in Figures 3.6 and 3.7.

values of ω_r/ω obtained from Table 1.1. Interpolation to the point of zero slope gives a value of 11.18 for ω_r/ω.

In a previous section of this chapter, "Pulse Shape, Period and Yield", the period of the oscillation in the Shot Tewa electromagnetic signal was estimated as 94 μsec, and the corresponding frequency as 10.6 kilocycles. From this frequency and the above value of ω_r/ω, the quantity ω_r can be determined to be 7.4×10^5 radians/sec. This value can be associated with the ionosphere height of 86 km (see "Timing of Sky Waves", this chapter) and compared with the values of ω_r given in Equation 1.4. These were 10^6 for night (H = 90 km) and 2×10^5 for day (H = 70 km). Figure 3.9 is a semilogarithmic plot of ω_r against H, the ionosphere height. It can be seen that the three points lie along a straight line, suggesting an exponential relationship between ω_r and H during the interval near dawn when the ionosphere is moving down from its night position to its day position.

In Figures 3.6 and 3.7 the straight lines intersect at points representing the ground wave as extrapolated from the higher sky waves. The voltage values are 82 volts for Channel A and 230 volts for Channel B. These values, which are tabulated in the first row of Table 3.5, refer to a ground wave at a range of 100 km (54 naut mi). Division by the F-factor for the ground wave (see Table 3.4) converts these voltages into those in the second row of Table 3.5, which are thus referred to the actual range, 96 naut mi. The voltages in the third row are obtained from those
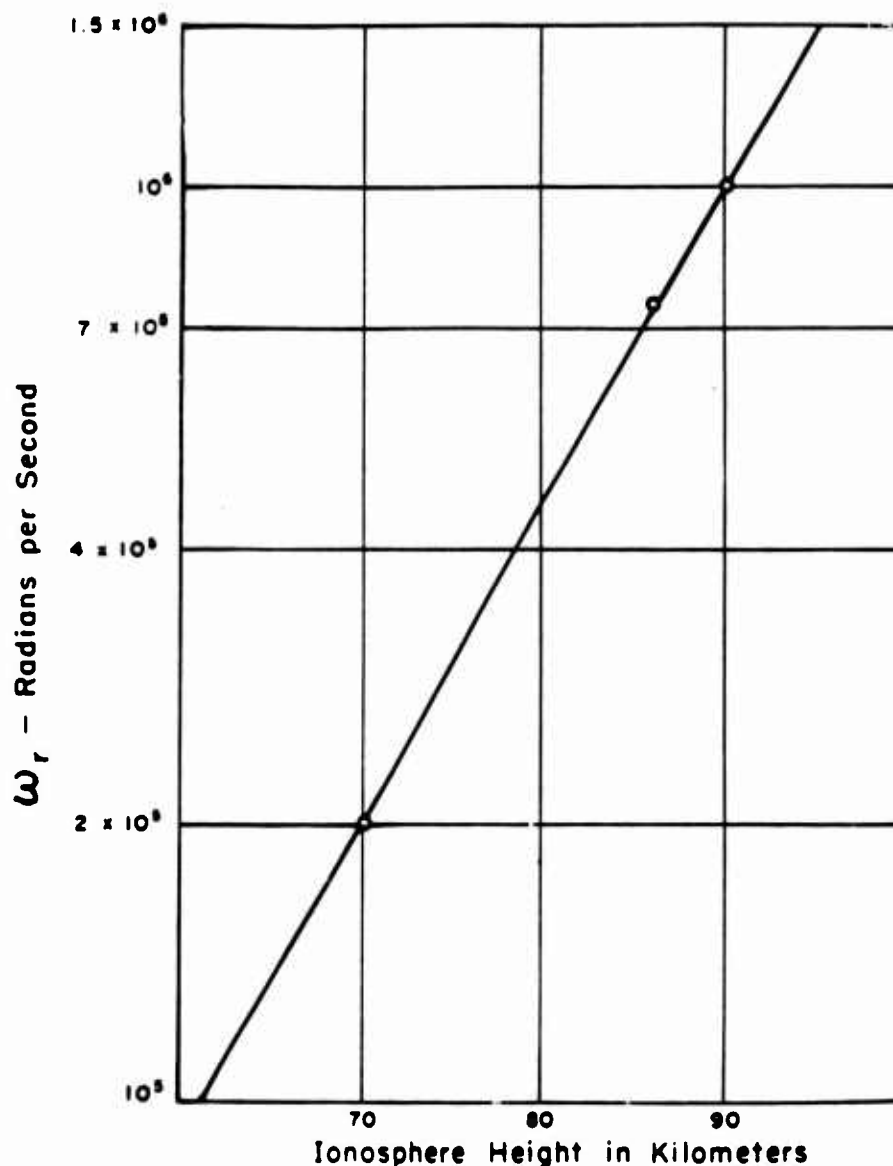
Figure 3.9 Values of ω_r plotted against ionosphere height.

in the second row through multiplication by the factor 25/35, which is the factor needed to convert from the corrected voltage scale to the nominal scale used in Figures 3.1 and 3.3.

The amplitude of the first sky wave, at the actual range of 96 naut mi, can be calculated from the ground wave amplitude in the first row of Table 3.5 through division by the appropriate F-factor. To obtain the latter, it is necessary to interpolate between F_d and F_e, or else to com-

pute the new F from the interpolated value of ω_r/ω, which was given above as 11.18. By interpolation, the value 6.22 was obtained as the F-factor corresponding to the first sky wave. The voltages in the fourth row of Table 3.5 are obtained from those in the first row through division by 6.22. Multiplication of the fourth-row voltages by 25/35 gives the voltages in the fifth row.

The nominal voltages in the third and fifth rows of Table 3.5 were used as rough guides in the preparation of Figure 3.3. However, the ground wave on Channel B, in Figure 3.3 (right portion), is shown for convenience as being considerably smaller in amplitude than indicated in Table 3.5.

It was concluded from Figures 3.6 and 3.7 that the extrapolated ground wave amplitudes, referred to a range of 100 km, were 82 volts for Channel A and 230 volts for Channel B. A rough conversion into an incident field strength in volts per meter can be made with the help of Figure 2.15 (right portion), which gives about seven volts as the output of the fiducial amplifier when an incident field of 1 volt/meter reaches the fiducial antenna at a frequency of 10.6 kc. Outputs of 82 and 230 volts would then correspond to input field strengths of 12 and 33 volts/meter.

Figure 1.2 shows 37 volts/meter as the field strength expected from a detonation the size of Shot Tewa (5.0 Mt), but the data used in drawing the high-yield portions of Figure 1.2 were from

TABLE 3.5 AMPLITUDES OF GROUND WAVE AND FIRST SKY
WAVE FOR SHOT TEWA ELECTROMAGNETIC SIGNAL,
EXTRAPOLATED FROM AMPLITUDES OF HIGHER
SKY WAVES

	Channel A	Channel B
	Volts, Center to Peak	
Extrapolated Ground Wave Amplitude Referred to Range of 100 km	82	230
Ground Wave Amplitude Referred to Actual Range (96 naut mi)	46	129
Ground Wave Amplitude Referred to Nominal Voltage Scale on Oscilloscope	33	92
First Sky Wave Amplitude Computed with Use of F-Factor	13	37
First Sky Wave Amplitude Referred to Nominal Voltage Scale on Oscilloscope	9.5	26.5

an earlier series of tests (Operation Castle) and might not be representative of the type of detonations that took place during the Operation Redwing series of tests. It would be desirable to have a comparison with an independent measurement of the Shot Tewa field strength from a ground-based calibrated antenna responding to the electric field of the incident wave. Without such a comparison any conclusions drawn concerning the efficiency of the airborne fiducial antenna must remain rather tentative.

It can be noted, nevertheless, that the signal on Channel B was nearly three times as strong as the signal on Channel A. That is, the antenna on the outside of the aircraft gave an output nearly three times as large as the output of the antenna inside the aircraft window. The difference in reception may not have been due entirely to the favored location of the outside antenna, since the outside antenna was also the wider antenna shown in Figure 2.9, while the inside antenna was the narrower one.

Although the size itself was not expected to make much difference in the performance, since there was no difference in the number of turns or the cross sectional area, still there was a difference in coil inductance (see Section 2.2.3) and therefore a difference in impedance match. The fiducial amplifier was designed for the narrower antenna and no change was made in capacitance or resistance values when the amplifier was used with the wider antenna. Further study in the laboratory would be desirable to determine how much of the difference in performance can

be attributed to the difference in antennas and how much remains to be attributed to the difference in location on the aircraft.

3.2.2 Shot Navajo.

For Shot Navajo the aircraft was 55 naut mi south of the detonation point, at an altitude of 18,000 feet. The narrower fiducial antenna was mounted outside the aircraft and its amplified output was presented on the single-beam Type 324 oscilloscope. The pulse received from the detonation was recorded by the oscilloscope camera. A tracing of the photograph is included as Figure 3.10.

The wider fiducial antenna was installed just inside the aircraft window, and its output was presented on Channel B of the dual-beam Type 333 oscilloscope. For Shot Navajo there was no input connection to Channel A. The Type 333 oscilloscope presentation was photographed at the time of burst. A tracing of the photograph is shown as Figure 3.11.

In the figures there is evidence of strong saturation in both fiducial amplifiers. There is also a curious irregularity present on Channel A in Figure 3.11 and an apparently parallel irregularity on Channel B. Since there was no signal input to Channel A, the irregularity must have been caused by some kind of interference, but the source of the interference could not be identified.

Both oscilloscopes were set for a nominal sweep time of 400 μsec, or 100 μsec per large division, and for a nominal vertical deflection sensitivity of 100 volts full scale, or 25 volts per large division. Calibration pictures were taken shortly after the detonation. They showed that the Type 324 oscilloscope sweep speed and deflection sensitivity were within about 1 percent of the nominal values.

For Channel B of the Type 333 oscilloscope, the calibration pictures showed that the deflection sensitivity and sweep speed were not quite so close to the nominal values as in the case of the Type 324 oscilloscope. The deflection sensitivity was off by only a few percent, but the sweep was slow by about eight percent. This error in sweep speed has already been discussed under "Oscilloscope Calibration", this Chapter, in connection with the oscilloscope photograph for Shot Tewa, and also under "Oscilloscopes", Chapter 2.

Because of severe saturation, the period of the wave forms from Shot Navajo could not be measured with sufficient accuracy to be used for determining the detonation yield.

Both the Type 324 and the Type 333 oscilloscopes were designed to trigger on a signal of a preselected polarity. For Shot Navajo the Type 324 oscilloscope was set to trigger on a positive signal, while the Type 333 oscilloscope was set to trigger on a negative signal. Both choices were unfortunate, because the first lobe of the received wave form was lost in each case. (See "Polarity and Wave Form", Chapter 2, for a discussion of the polarity of the initial deflection.)

In Figures 3.12 and 3.13 an attempt was made to reconstruct the wave forms of Figures 3.10 and 3.11 as they might have been had there been no amplifier saturation and no loss of the first lobe of the oscillation. The wave forms actually received are shown as solid curves, and the reconstructions are shown dashed.

In each case, the first sky wave could be identified on the original oscilloscope trace, and has been included in the reconstruction. The time interval between ground wave and first sky wave, as indicated in the reconstructed curves, can be used, together with the known range (55 naut mi) and the curves of Figure 1.5, to give a rough estimate of 80 to 90 km as the height of the ionosphere at the time of the detonation (0556 hours).

3.2.3 Shot Kickapoo.

For Shot Kickapoo the equipment was set up at the ground station, 14

Pages 100 - 103
Deleted

naut mi south of the detonation. The amplified outputs of the two fiducial antennas were fed to the two channels of the dual-beam Type 333 oscilloscope. The output of the narrow antenna was fed to Channel A, with a nominal sensitivity of 100 volts full scale or 25 volts per large division. The output of the wide antenna was fed to Channel B, with a sensitivity that was much greater, four volts full scale or 1 volt/div. The sweep time for both channels was a nominal 80 μsec full scale, 20 μsec/div. Calibration pictures showed the actual sweep time to have been about 22 μsec/div.

It is interesting to note that the oscilloscope was set to be triggered on a negative deflection on Channel B, according to a notation on the Shot Kickapoo data sheet, yet the first part of the trace on Channel A is positive. The two antennas were installed parallel to each other without any such reversal as gave the 180-degree phase difference in the Shot Tewa signals (Figure 3.1). Accordingly, the signal on Channel B should have been just an amplified version of that on Channel A, and it is not clear how the oscilloscope was triggered, unless the pulse actually started with a short negative spike before the longer positive deflection.

It is also interesting to note the shape of the Shot Kickapoo pulse as distorted by saturation. It has the appearance of a series of exponentials, which can be explained as a result of saturation in the second stage of amplification, which limits the output of that stage, combined with the integrating action of the 100-$\mu\mu$f condenser in the circuit between the second stage and the final cathode follower (Figure 2.14). For frequencies as high as 30 kc, the fiducial amplifier has some of the characteristics of an integrating circuit as pointed out in "Polarity and Wave Form", Chapter 2.

3.2.4 Other Shots. Oscilloscope photographs were obtained during a number of other shots, including Shots Dakota, Ince, Apache, Mohawk, and Huron. These photographs were, for the most part, of doubtful value. Most of them contained more than one trace. The oscilloscope amplification was set rather high for these shots, and the triggering level rather low, so that individual sky waves were able to trigger the oscilloscope and register as separate traces on the picture. In some instances it was difficult to determine whether the traces on the picture were sky waves from the burst or interference from other sources.

104

Page 105 Deleted

The ground wave amplitude to be expected, according to Figure 1.4, was about 12.7 volts/ meter. The expected output signal from the fiducial amplifier was about 100 volts, which was far off scale for the oscilloscope sensitivity in use.

The oscillations in Figure 3.16 are about $1/100$ as large as the expected ground wave amplitude.

If they are sky waves, then they probably begin with the third, fourth, or fifth sky wave, as can be inferred from the discussion of Table 3.4 in "Amplitude Comparison", this Chapter.

3.2.5 Whip Antenna. No photographs were obtained showing any signal received on the whip antenna. It was known that the whip antenna and its cathode follower were in operating condition, since they easily received the interference from various radio transmitters, but during the radio silence immediately preceding and following the burst, the whip antenna did not function as it had been expected to.

Since the whip antenna was approximately one meter long, it was expected that its output might be roughly equal in volts to the incident field strength in volts per meter.

Based on information obtained since the Operation Redwing tests, it is believed likely that

106

there is a substantial reduction in the effectiveness of such a whip antenna mounted in a moving aircraft and used at very low frequencies. It is believed that an increase of the order of 10 or 20 in the sensitivity of the oscilloscope might have been enough to result in triggering of the oscilloscope by the whip antenna output and in a satisfactory photographic record of the whip antenna wave form and the amplitude of its signal output for a given incident electromagnet wave.

3.3 PHOTOHEAD RESULTS

Although most of the valuable electromagnetic results came from a single shot (Tewa), there were useful photohead results from seven separate shots: Osage, Dakota, Mohawk, Apache, Navajo, Tewa, and Huron. Yield estimates, made from time measurements on most of the seven Heiland recorder traces, were found to agree closely with the official yields. Estimates of light intensity were also made from measurements on the Heiland recordings, but these were less precise because of uncertainties in the calibration of the equipment. The equipment was originally intended to be used for precision time measurements but not for precision intensity measurements.

Figure 3.17 shows the Heiland records obtained from six of the seven shots mentioned above. The time scale runs from left to right. For four of the shots, both the narrow first peak and the broad second peak are clearly resolved in the figure. These seven Heiland records are discussed individually in the following seven sections, after which the quantitative results are tabulated and summarized.

3.3.1 Shot Osage.
Shot Osage, the tenth of the Redwing series, was the first shot for which the photoheads and the Heiland recorder performed satisfactorily. On earlier shots there had been interference from the equipment of Project 6.3, but for Shot Osage and succeeding shots the Project 6.3 equipment was turned off two minutes before detonation time and remained off until two minutes after the detonation.

While most of the other tests occurred just before dawn, Shot Osage took place in the middle of the day, in bright sunlight with scattered clouds. There was considerable ambient light, as indicated by the compensating feedback current, I_k, which was 28 μa for the 1P39 photohead and 3.5 μa for the infrared (6570) photohead.

During the three seconds between the breaking of the feedback loop and the moment of burst, there was a slight rise in both Heiland traces. (See the Shot Osage strip in Figure 3.17.) The rise was attributed to an increase of three or four percent in the ambient light intensity, probably caused by the movement of clouds or cloud shadows across the photohead field of view.

At the time of the Shot Osage burst, the time markers in the Heiland recorder were not registering clearly because of the vibration discussed under "Heiland Recorder", Chapter 2. It was necessary to determine the speed of tape motion from measurements of the marker separation at neighboring portions of the tape. The tape speed was found to have been 8.1 in/sec, which was rather slow in comparison with the nominal value of 12 in/sec, and slow even in comparison with the values, between 9 and 11 in/sec, found for the Heiland tapes from other tests.

The quantitative results obtained from the Heiland record of the Osage burst have been included in the tabulations in Sections 3.3.8 and 3.3.10.

3.3.2 Shot Dakota.
The Heiland recorder had barely been turned on before the time of burst for Shot Dakota. The spacing of the time markers on the Shot Dakota strip in Figure 3.17 shows

Page 108 Deleted

that the tape started slowly but reached nearly its final speed in less than one half second. The markers are clearly resolved, indicating that the vibration which mars the other Heiland records in Figure 3.17 had not started at the time of the Shot Dakota burst. As a result, the time interval between first and second peaks could be obtained directly from the time markers.

On the upper Shot Dakota trace (6570), both the first peak and the step on the side of the second peak are very clearly seen. On the lower trace (1P39), the first peak is very low and there is no clearly defined step. Both traces show a small amount of 400-cycle interference.

3.3.3 Shot Mohawk.

Only the 6570 trace was recorded on the Heiland strip for Shot Mohawk. The 1P39 trace had been adjusted by mistake to a position well off the edge of the paper tape. The deflection of the 6570 trace was small. The first peak was so small that it cannot be seen in Figure 3.17 and could be located only with great difficulty on the original paper strip. The second peak can be seen on the figure but it is very broad and the location of its summit point was difficult to establish, partly because of the slight ripple caused by 400-cycle interference.

The weak intensity of the signal can be attributed to the fact that the aircraft was buried in solid overcast which began at a height of 15,000 feet and continued on up to a height well above the aircraft's altitude of 18,000 feet.

3.3.4 Shot Apache.

Both the first peak and the second peak appeared clearly on each of the two traces for Shot Apache. The second peak was broad and flat, both for the upper trace (1P39) and the lower trace (6570). The steps were easily located, for use in the amplitude calibration (see Section 3.3.9). The time markers were subject to vibration, but pairs of markers appeared as solid marks and these were easily distinguished and counted for use in the timing calibration.

However, because of the layered nature of the condensation cloud, it is difficult to tell from the photographs the time at which the evaporation of some of the dryer layers might have permitted the infrared light to be transmitted.

3.3.5 Shot Navajo.

The maximum deflection of the 1P39 trace on the Shot Navajo tape was only one sixteenth of an inch, or three percent of the two-inch width of the strip. The 6570 deflection was even smaller, only one twentieth as large as the 1P39 deflection. The first peak could not be found at all on either trace. The weakness of the deflections could be attributed to the use of filters with one percent transmission to cut down the light reaching the photoheads, and to the fact that there were thick clouds between the fireball and the aircraft.

Because the first peak did not appear on the Heiland record, the time interval between peaks

could not be measured. Only a lower limit to the computed yield could be determined for inclusion in the tabulation in Section 3.3.8.

3.3.6 Shot Tewa. The first peaks on the two traces for Shot Tewa were small but identifiable. The second peaks were broad and flat. The steps were easily distinguished.

The time markers on the Heiland record were badly smeared by vibration but could be used if care was taken in counting them. The measured time interval and computed yield are given in Section 3.3.8.

A ten percent filter was used with each photohead, and the light reaching the photoheads was further reduced by the clouds which can be seen in the Shot Tewa sequence photographs in Figure 3.25.

3.3.7 Shot Huron. The pairs of time markers were much clearer for Shot Huron than for Shot Tewa. The first peak, second peak, and step are all easily identified on each of the two traces.

3.3.8 Timing and Yield. The quantities relating to the use of the Heiland records for yield computations have been computed in Table 3.6. The time interval, T, from the beginning of the first peak to the top of the second peak has been given in the third column of the table for each of the seven shots listed in the first column. The official yield, Y_0, in the second column can be compared with the computed yield, Y_1, in the fourth column, where Equation 1.6 has been used for the yield computation. The errors in percent are listed with the computed yields. However, there is a somewhat closer correlation between the official yield, Y_0, and another computed yield, Y_2, which is obtained from Equation 1.6 as modified by the insertion of an empirical constant, 0.92. The yields computed from the modified equation are shown in the sixth column and the corresponding errors are included in the seventh column.

For either set of computations, the table shows that three of the six computed yields were within ten percent of the official yields.

These results can be compared with the limit of 20 percent specified for the IBDA system in which the bhangmeter equipment was designed to be used.

For Shot Navajo, in Table 3.6, only a lower limit was given for T, since the first peak could not be distinguished from noise on the Heiland trace.

3.3.9 Photohead Calibration. Measurements of thermal radiation intensities were included among the objectives of Project 6.4 (see Section 1.1). It had been planned to use the Heiland de-

flections as the directly measured quantities. These deflections would be converted to absolute measurements of thermal irradiance by means of photohead calibration data obtained on the ground with the use of the photohead test box and the Weston exposure meter (see Section 2.2.9, and "Photohead Test Box", Chapter 2).

Two series of extensive calibration measurements were made, one on July 11, after Shot Navajo, and the other on July 22, after Shot Huron. In both sets of measurements the intensity of the light source at one end of the test box was adjusted to different levels by means of the Variac, and the photohead and exposure meter were placed in turn at the other end of the test box.

There were two methods by which the exposure meter readings could be utilized. The first method was as an absolute measure of light intensity. For this, the spectral distribution of the light source and the different spectral sensitivities of the phototubes and the exposure meter had to be taken into account.

The second way to use the exposure meter was as a monitor of light intensity. Its readings could then be converted to absolute values of irradiance through the use of empirical curves correlating exposure meter reading and phototube current. For this procedure it was necessary to

TABLE 3.6 DETONATION YIELD COMPUTED FROM TIMING OF SECOND THERMAL RADIATION PEAK

make use of the rated sensitivity of the phototube to convert phototube current into irradiance.

For each of the two photoheads the two calibration methods gave about the same result. The second method was the one used for the reduction of the thermal intensity data obtained during Operation Redwing.

The July 11 calibration measurements were more elaborate than the July 22 measurements. From the earlier series it was possible to establish a correlation between the exposure meter readings and the photohead current (actually the cathode current, I_k, as described below). The correlation thus established was then used in the reduction of both series of calibration measurements.

For the July 11 measurements the Variac was first adjusted until the photohead, with its feedback loop closed, gave a predetermined value for the pentode cathode current, I_k. The Variac adjustment was then kept fixed while the photohead was replaced by the exposure meter. The reading of the exposure meter was recorded. With the photohead back in position, the Variac was switched off and the feedback loop was opened while the phototube was dark. The Heiland recorder was then started and the Variac was switched on and off so that the light intensity rose quickly to the level previously measured with the exposure meter and then dropped back again to zero. After the Heiland record was developed, the deflection could be measured directly on the paper strip.

From the July 11 calibration measurements it was possible to establish correlations among the Variac setting, the current I_k, the exposure meter reading, and the Heiland deflection. The

111

July 22 photohead calibration measurements were similar, but more limited in scope. The Variac setting was not recorded and the cathode current, I_k, was not measured. The only correlation obtained was between exposure meter reading and Heiland deflection.

In the July 11 measurements, with the white bulb as light source, the exposure meter was used in three different ways to measure the light intensity for each Variac setting. The three ways were: (1) directly, with no filter; (2) with a 0.5 neutral density filter covering the exposure meter aperture; and (3) with a 1.0 neutral density filter. These filters are described in Section 2.2.8. Readings 2 and 3, for a given Variac setting, will be more directly comparable to Reading 1 if Reading 3 is divided by 0.10 and Reading 2 is divided by 0.32. This compensates for the filters.

However, there is an additional compensation factor needed to make the readings on one of the exposure meter scales comparable to the readings on the other scale. In Section 2.2.9 it was explained that the exposure meter has a narrower field of view on its 0 to 1,600 scale than on its 0 to 50 scale. The two scales have been made comparable for evenly distributed light sources, but for point sources the two scales differ by a factor of four. The calibration measurements showed that the light bulb at one end of the photohead test box was neither a point source nor a distributed source, but instead was a source intermediate between the two. It was found that the two exposure meter scales could be made to correspond if readings made with the lower scale (0 to 50) were multiplied by two.

The photohead calibration measurements made on July 11 have been given in Tables 3.7 and 3.8. The relationship between exposure meter reading and cathode current, I_k, are shown graphically in Figures 3.18 and 3.19.

The pentode cathode current, I_k, can be converted to the phototube current, I_{ph}, by the use of Equation 2.3. Computed values of I_{ph} corresponding to the measured values of I_k have been included in Tables 3.7 and 3.8. Also included in the tables are values of irradiance computed from the phototube current values. For this computation, certain characteristics of the phototube and the lens system needed to be specified.

The lens system for each phototube consisted of three lenses arranged to focus onto the photosensitive surface, the incident radiation striking an area of one square inch. The field of view included the directions contained within a cone with a half angle of ten degrees as described in Section 2.2.5. The six air-glass surfaces in the lens system were estimated to reflect a total of 22 percent of the incident radiation. The glass itself was estimated to absorb an additional eight percent of the radiation within the S-4 band but to transmit all of the radiation in the S-1 band, except, perhaps, for a part of the ultraviolet peak shown dashed in Figure 1.11.

For the average 1P39 phototube, the rated sensitivity is 0.042 $\mu a/\mu w$ of incident radiation at 4,000 Å. If the incident intensity is 1 watt/meter^2, then the amount striking one square inch will be 645 μw. The amount passing through the lens system will be 70 percent of this, or 451 μw, and the phototube current, I_{ph}, will be 19 μa. For the average 6570 phototube, the sensitivity is 0.0027 $\mu a/\mu w$ at 8,000 Å. With 78 percent of the incident radiation penetrating the lens system, an incident intensity of 1 watt/meter^2 will mean that 503 μw reaches the phototube and the resulting current, I_{ph}, is 1.36 μa.

In the bottom rows of Tables 3.7 and 3.8 the phototube current values have been converted into values of irradiance in watts per square meter, through the use of the two conversion factors derived above, 19 $\mu a/watt/meter^2$ for the 1P39 phototube and 1.36 $\mu a/watt/meter^2$ for the 6570 phototube.

Specific phototubes may differ considerably from the average. The sensitivity may deviate by 30 to 50 percent from the rated sensitivity in some cases. There was no detailed measurement made of the sensitivity and the spectral response curve of either of the actual phototubes used. The use of average sensitivity data thus introduced a possible source of error in the thermal intensity measurements. However, any such error could not have been very great for either phototube, since an independent use of the exposure meter as an absolute measure of light intensity gave about the same result, as described below.

For the use of the exposure meter as an absolute measure of irradiance reaching the photohead, a number of conversion factors must be applied. First of all, the 0 to 1,600 scale should

TABLE 3.7   PHOTOHEAD CALIBRATION MEASUREMENTS OF JULY 11, WITH 1P39 PHOTOHEAD AND WHITE BULB

Variac Setting		44	48	57	60
I_k	μa	14	20	40	50
Exposure meter readings					
(a) no filter on meter		375	450	825	1,175
(b) filter: N. D. 0.5		80	125	275	350
(c) filter: N. D. 1.0		13*	25*	45*	85
Meter readings	(a)	375	450	825	1,175
corrected for	(b)	250	390	860	1,093
filter factor	(c)	130*	250*	450*	850
Readings referred to 0-1600 scale	(c)	260	500	900	850
Heiland reflection	Inches	0.602	0.640	0.728	0.755
Approximate deflection to center of step		0.237	0.226	0.237	0.234
I_{ph}	μa	9.1	13.3	27.3	34.3
Irradiance	w/m²	0.48	0.70	1.44	1.80

* Indicates 0-50 scale.

TABLE 3.8   PHOTOHEAD CALIBRATION MEASUREMENTS OF JULY 11, WITH 6570 PHOTOHEAD AND INFRARED BULB

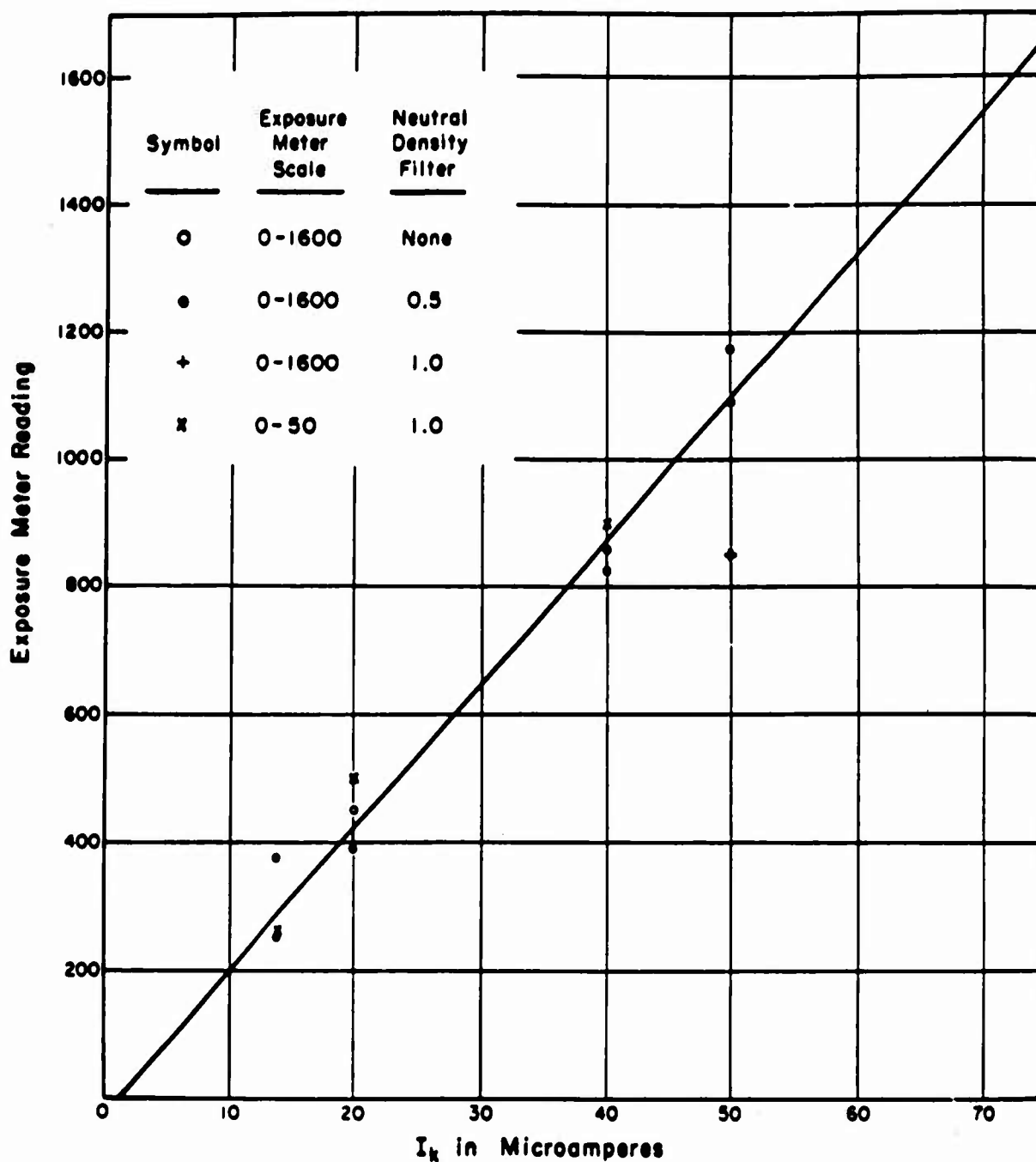| Variac Setting		67	79	104	116
I_k	μa	14	20	40	50
Exposure meter readings		13*	23*	75	100
Readings referred to 0-1600 scale		26	46	75	100
Heiland deflection	Inches	0.306	0.337	0.385	0.405
Approximate deflection to center of step		0.100	0.099	0.106	0.100
I_{ph}	μa	9.1	13.3	27.3	34.3
Irradiance	w/m²	6.7	9.8	20.1	25.2

* Indicates 0-50 scale.

Figure 3.18 Comparison of exposure meter scale readings and values of photohead current, I_k, in cathode of pentode, for 1P39 photohead with white bulb as light source.
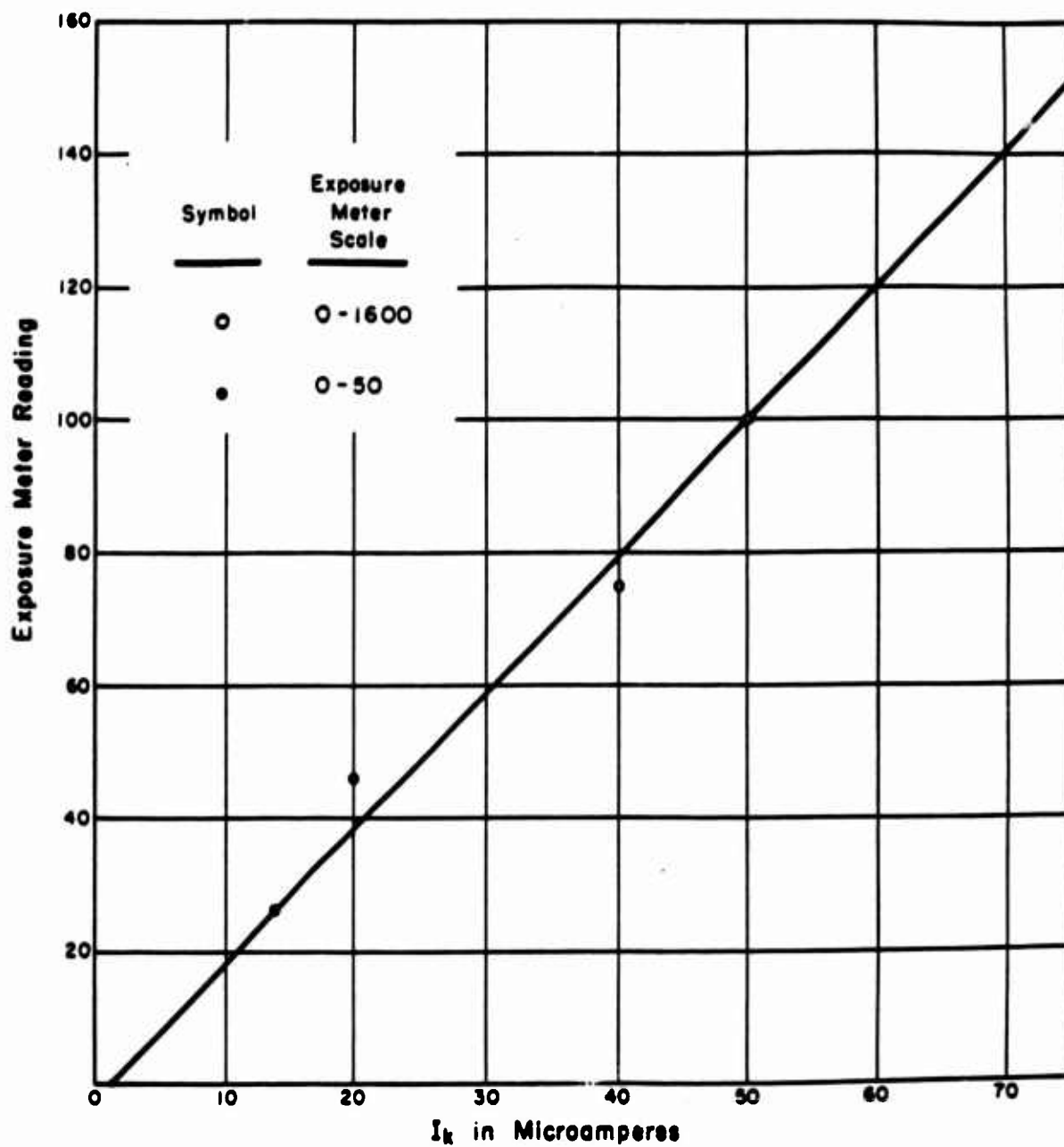
114

Figure 3.19 Comparison of exposure meter scale readings and values of photohead current, I_k, in cathode of pentode, for 6570 photohead with infrared bulb as light source.

be used as the basis for comparison, since the 30-degree field of view for the 0 to 1,600 scale is closer to the 20-degree field of view of the photohead than is the 60-degree field of view for the 0 to 50 scale on the exposure meter. Second, since the desired measurement is of incident light from a narrow source, the exposure meter reading should be divided by four, as explained in Section 2.2.9. Third, the exposure meter reading in lumens per square foot should be translated into watts per square meter, with the use of a special conversion factor.

The conversion factor which is applicable to light of 5,500 Å wave length is 0.01583, but an additional factor is needed to allow for the differing spectral distributions of (1) the light source, (2) the exposure meter, and (3) the phototube. Without allowing for these spectral distributions, an exposure meter reading of 1,000 lumens/ft^2 would become 250 lumens/ft^2 after the division by 4, and 3.96 watts/meter^2 after multiplication by 0.01583.

In the case of the 1P39 phototube, a comparison was made between (1) the spectral distribution of the photospot light source, at the low voltage indicated by the Variac setting; (2) the luminosity curve of Figure 1.12 and the exposure meter distribution curve shown in Figure 1.13; and (3) the S-4 phototube response curve shown in Figure 1.10. It was concluded that the irradiance within the S-4 band was about one third of the irradiance within the luminosity curve, for the given light source. The difference between the luminosity curve and the exposure meter distribution was not considered important for this source, since it was assumed that the exposure meter scale was designed to read correctly in lumens for a light source having approximately the same distribution as the source actually used in the 1P39 calibrations.

Division of 3.96 by 3 gives 1.32 watts/meter^2 as the irradiance within the band of the 1P39 phototube corresponding to an exposure meter reading of 1,000 in the calibration measurements. This should be compared with 1.65 watts/meter^2, which is the irradiance which would be obtained from the exposure meter reading of 1,000 and the straight line in Figure 3.18. The discrepancy is well within the uncertainty in the factor of three obtained by comparing distributions and could also be accounted for by the range in rated sensitivities for 1P39 phototubes.

For the 6570 phototube with the infrared bulb as light source, the problem of converting the exposure meter reading to watts per square meter in the S-1 band was a more difficult one. The infrared light source differed considerably from the light source for which the exposure meter was designed. Furthermore, the infrared bulb was a type with red-painted reflector, which tends to cut off the short-wave end of the bulb spectrum somewhat more sharply than would be expected if the bulb were acting as a blackbody with a color temperature between 2,400 K and 2,500 K.

With no allowance for the red-painted reflector, it was estimated from the several spectral distributions that the irradiance within the S-1 band of the 6570 phototube should be roughly ten times as great as the illuminance within the luminosity curve. Thus, an exposure meter reading of 100, which would give a value of 0.396 watts/meter^2 referred to the peak of the luminosity curve, would then give 3.96 watts/meter^2 in the S-1 band, for the assumed blackbody infrared source.

However, the infrared bulb was not operating as a simple blackbody source, as was proved by a separate measurement using the 6570 photohead but using the white bulb as the light source. With the two sources adjusted to give the same value of Heiland deflection, showing the same irradiance in the S-1 band from 7,000 to 9,000 Å, the irradiance within the visible band should have differed by a factor of two for the two sources if they were acting as blackbody radiators. Instead it was found that the exposure meter readings differed by a factor of 10. The extra factor of five could only be accounted for as a consequence of the red-painted reflector on the infrared bulb, which could have removed a large part of the visible light radiated from the filament.

When the extra correction factor of five was included, it was found that the exposure meter reading of 100 with the infrared bulb should correspond to an irradiance of 19.8 watts/meter^2, or roughly 20 watts/meter^2, in the spectral band of the 6570 phototube. This can be compared

with 25.2 watts/meter^2, which is the value given by Table 3.8 and Figure 3.19 as the irradiance corresponding to an exposure meter reading of 100, as determined by the second method of calculation, the method making use of the rated sensitivity of the phototube. The discrepancy between 20 and 25.2 is not significant in comparison with the uncertainties in the calculations using the spectral distributions, and in comparison with the acceptable variation in phototube sensitivity values.

For both photoheads, the two methods of reducing the calibration data gave about the same results. For convenience, the second method was chosen, the method making use of the rated phototube sensitivities and using the exposure meter readings only for relative measurements, not absolute measurements. With the use of this selected method of calibration data reduction, the calibration measurements of July 11 and July 22 have been plotted in Figures 3.20 and 3.21. The Heiland deflection has been plotted against the irradiance in watts per square meter. For each curve the position and approximate size of the step has been indicated. The curves for July 11 have been plotted from Tables 3.7 and 3.8, and the July 11 curve in Figure 3.20 has been extrapolated well beyond the measured points, with the extrapolated section shown dashed.

The July 22 measurements gave the Heiland deflection in terms of the exposure meter reading only. The meter readings were converted to irradiance in watts per square meter through the use of Figures 3.18 and 3.19, as explained above. Tables 3.9 and 3.10 show the July 22 data. Included are the exposure meter readings, the Heiland deflections, and the computed values of irradiance used for plotting in Figures 3.20 and 3.21.

It appears from the 1P39 calibration curves in Figure 3.21 that the 1P39 photohead may have changed its characteristics somewhat between July 11 and July 22. The discrepancy between the two curves could alternately be attributed to a change in the operating temperature of the photoflood bulb and a consequent change in the spectral distribution of its radiation. If the change was in the photohead itself, the cause might have been a difference in moisture accumulation or a difference in the properties of the thyrite resulting from a change in its temperature.

There was less shift in the 6570 calibration curve, as shown in Figure 3.21. Only at the low end does the July 22 curve appear significantly displaced from the July 11 data.

3.3.10 Burst Light Intensity. The photohead calibration curves in Figures 3.20 and 3.21 have been used for estimates of the intensity of the thermal radiation from the seven bursts for which Heiland records were obtained. One of these seven, Shot Osage, occurred in bright daylight. For the estimate of its thermal intensity, these calibration curves were used in conjunction with the photohead characteristic curves of Figure 2.18.

In Table 3.11 the Heiland deflection measurements and the thermal intensity calculations are tabulated. The results for both photoheads, the 1P39 (blue-green) and 6570 (infrared) are included in the same tabulation.

A comparison has been made in Table 3.11 between the incident intensity as computed from the Heiland deflection and the intensity expected from the burst in the absence of atmospheric attenuation. The expected intensity was calculated from Equations 1.7 to 1.9, Figure 1.8, and the official yields as given in Table 3.1. From the ratio of expected intensity to incident intensity a value for the attenuation per kilometer can be computed. The attenuation per kilometer is the factor B in the following equation:

$$\frac{\text{Expected intensity}}{\text{Incident intensity}} = \exp{(B\,D_{km})} \tag{3.7}$$

Where: D_{km} = Range, km
(Included in Table 3.11)

From the results shown in Table 3.11 it appears that there was a generally greater attenuation in the blue-green band of the 1P39 phototube than in the infrared band of the 6570 phototube. The nature of the attenuation is indicated by the sequence photographs in Section 3.4.1. These

117
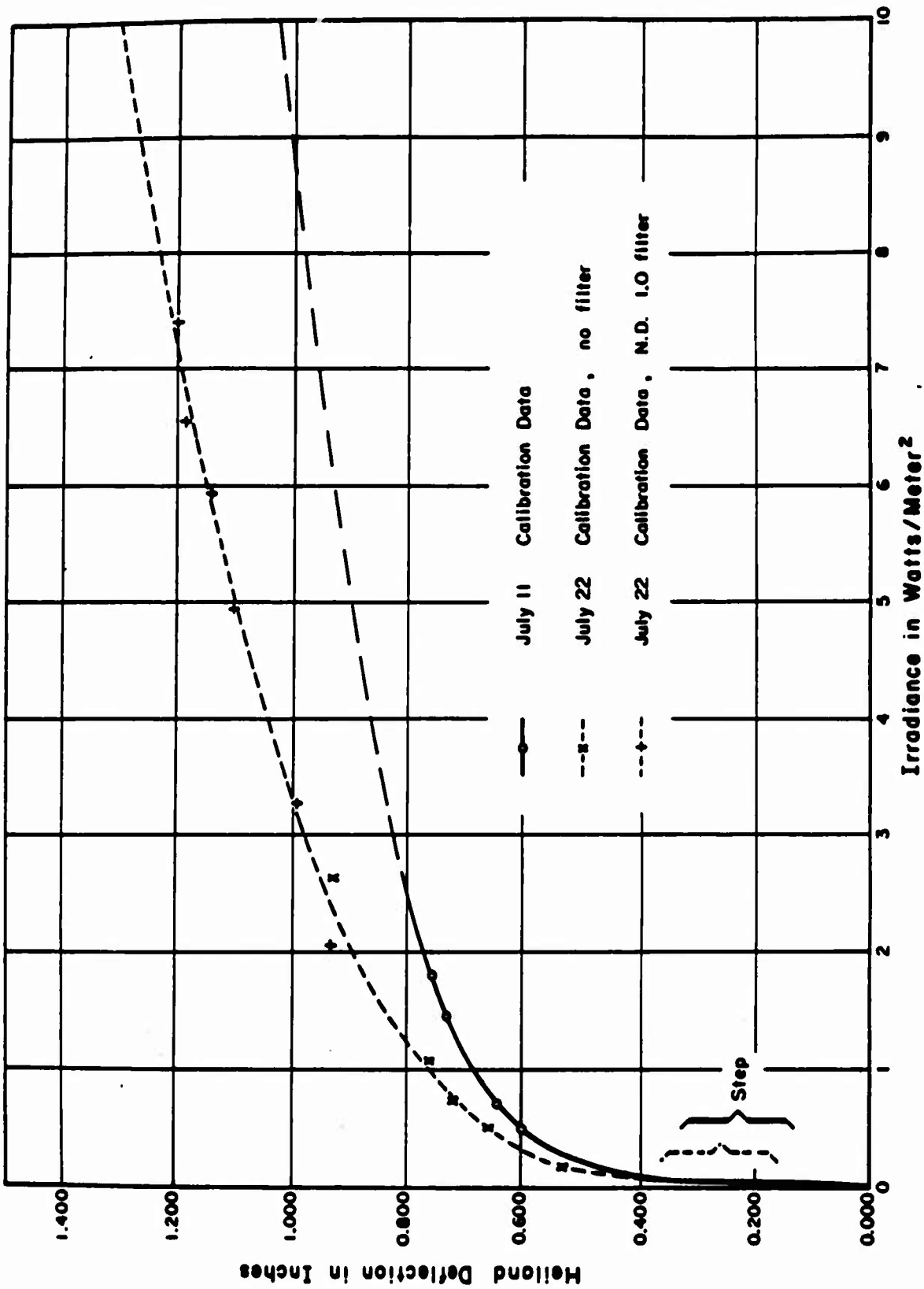
Figure 3.20 Calibration curves for 1P39 photohead.
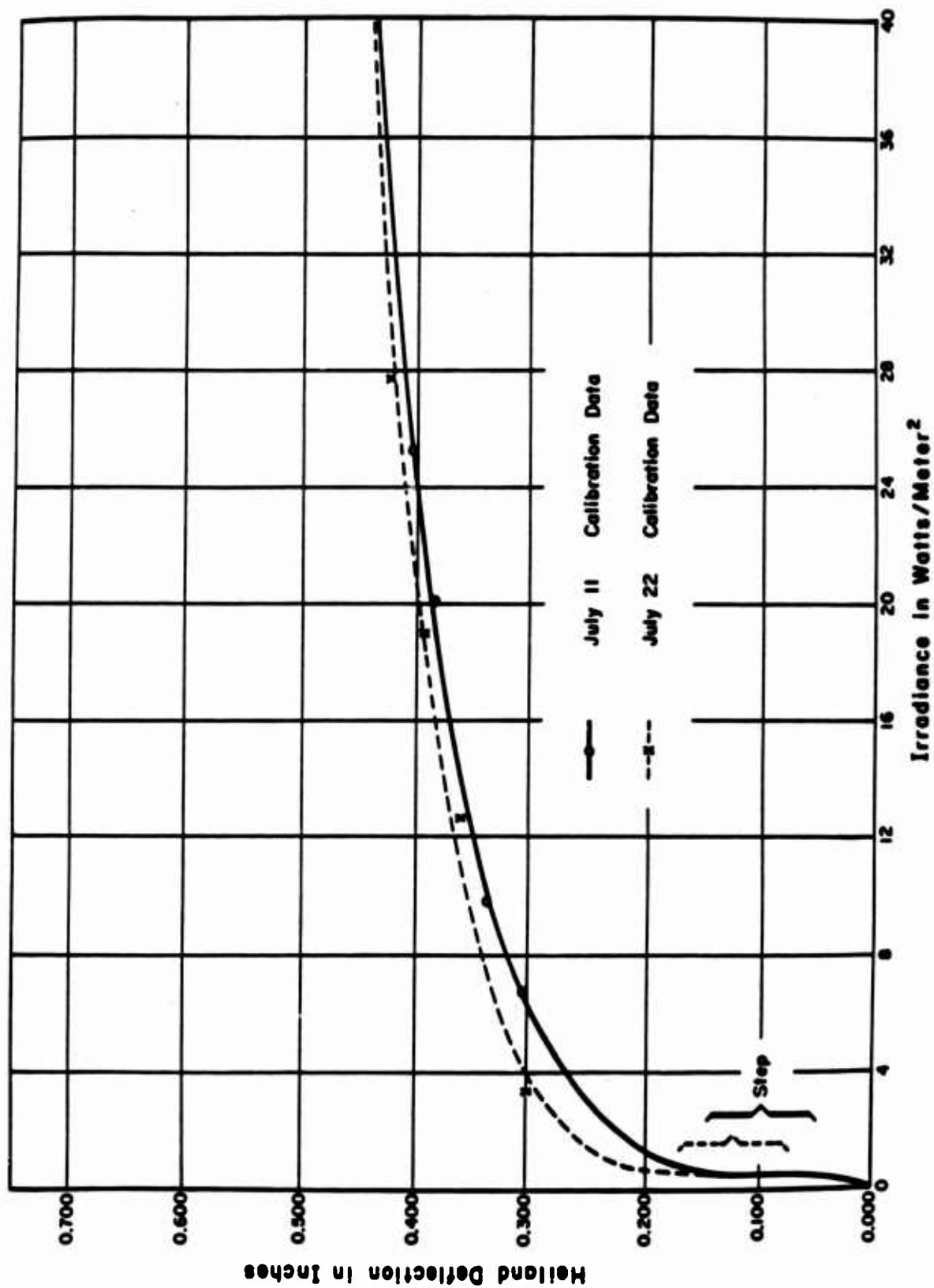
Figure 3.21 Calibration curves for 6570 photohead

TABLE 3.9   PHOTOHEAD CALIBRATION MEASUREMENTS OF JULY 22, WITH 1P39 PHOTOHEAD AND WHITE BULB

Exposure Meter Reading	Neutral Density Filter	Approximate Deflection to Step	Deflection to Maximum	Irradiance
		in	in	w/m²
100	—	0.265	0.531	0.17
300	—	0.263	0.655	0.50
450	—	0.260	0.716	0.74
650	—	0.252	0.761	1.07
775	—	0.272	0.798	1.27
1,600	—	0.271	0.931	2.64
125	1.0	0.271	0.931	2.05
200	1.0	0.265	0.994	3.28
300	1.0	0.255	1.104	4.94
360	1.0	0.277	1.144	5.94
400	1.0	0.261	1.184	6.56
450	1.0	—	1.199	7.40

TABLE 3.10   PHOTOHEAD CALIBRATION MEASUREMENTS OF JULY 22, WITH 6570 PHOTOHEAD AND INFRARED BULB

Exposure Meter Reading	Reading Referred to 1-1600 Scale	Approximate Deflection to Step	Deflection to Maximum	Irradiance
		in	in	w/m²
6.5 *	13	0.126	0.300	3.35
25 *	50	0.120	0.360	12.7
75	75	—	0.394	19.0
110	110	—	0.422	27.7
175	175	0.130	0.438	44.3

* 0-50 scale on exposure meter.

Page 121
Deleted

show that a substantial part of the attenuation could be attributed to obstruction of the path from burst to receiver by intervening cloud formations. The pictures also show evidence of considerable haze. This haze might account for the greater attenuation observed in the blue-green (S-4) band than in the infrared (S-1) band. (See "Attenuation of Thermal Radiation", Chapter 1.)

Ambient Light Measurements. The ambient light was measured in two ways, by means of the pentode current, I_k, with the feedback loop closed, and by means of the Heiland deflection caused by ambient light changes when the feedback loop was open. The first kind of

TABLE 3.12 AMBIENT LIGHT INTENSITY MEASUREMENTS

Date	Time	1P39 Photohead			6570 Photohead		
		I_k	I_{ph}	Irradiance	I_k	I_{ph}	Irradiance
		μa	μa	w/m^2	μa	μa	w/m^2
June 12	1315	28	19	1.0	3.5	1.8	1.3
June 22	0840	32	22	1.1	8	4.9	3.6
		39	27	1.4	5	2.8	2.1
		36	25	1.3	8	4.9	3.6
	0850	34	23	1.2	8	4.9	3.6
		46	32	1.7	12	7.7	5.7
July 11	0655	4	2.1	0.11	1	0	0
	0701	6	3.5	0.18	1	0	0
	0705	8	4.9	0.26	2	0.7	0.5
	0755	10	6.3	0.33	2	0.7	0.5
	0800	22	15	0.8	3	1.4	1.0
July 21	0920	25	17	0.9	4	2.1	1.5
	0922	22	15	0.8	3	1.4	1.0
		21	14	0.7	3	1.4	1.0
July 22	0728	14	9	0.5	2	0.7	0.5
	0729	16	11	0.6	2	0.7	0.5
	0730	18	12	0.6	2	0.7	0.5
	0755	25	17	0.9	3	1.4	1.0
		>50	>34	>1.8	8	4.9	3.6
		25	17	0.9	4	2.1	1.5
	0800	20	13	0.7	3	1.4	1.0
		28	19	1.0	4	2.1	1.5
		>50	>34	>1.8	8	4.9	3.6
		16	11	0.6	2	0.7	0.5

measurement was one of greater precision, but it could not show the dynamic variations of ambient light quite so well as the second kind of measurement.

A number of measurements of ambient light have been collected in Table 3.12. The date and the time of day have been included, as well as the measured currents and their interpretation in terms of incident intensity of thermal radiation within the wave length bands of the two phototubes and within the acceptance solid angle of the photohead lens system.

The June 12 measurements of ambient light were made at the time of Shot Osage in bright sunlight with scattered clouds. The four later sets of measurements were made while the aircraft was flying in and out of sunlit clouds.

A comparison could be made between the ambient light intensity values in Table 3.12, which

ranged generally around 1 or 2 watts/meter^2 for the 1P39 photohead and up to 5.7 watts/meter^2 for the 6570 photoheads, and the estimates given under "Ambient Light", Chapter 1. The maximum light from the horizon sky was estimated there at 1.6 watts/meter^2, while the maximum light from sunlit clouds was estimated at 6 watts/meter^2. These estimates were for the 1P39 phototube with its field of view narrowed by the photohead lens system to the solid angle within a cone with a half-angle of 10 degrees. For the 6570 phototube the estimate was roughly the same. The values listed in the table were found to be quite consistent with the above estimates of ambient light in the open sky and in or near sunlit clouds.

In a number of cases Table 3.12 shows a considerably higher level of ambient light for the 6570 photohead than for the 1P39 photohead. As pointed out later in Section 3.4.3, this difference might be attributed partly to the greater width of the S-1 response curve, as compared with the S-4 curve, and partly to the fact that most of the measurements referred to were obtained before the sun was very high in the sky.

An example of the dynamic variation of ambient light is included in Section 3.4.3. The Heiland record is there shown correlated with a sequence of three photographs taken as the aircraft moved from a clear region into a brightly lit bank of clouds.

3.4 SEQUENCE CAMERA RESULTS

The sequence camera was used to photograph the nuclear burst, the nuclear cloud, and the ambient conditions during measurements of ambient light intensity. Selected frames have been enlarged and are shown in Figures 3.22 to 3.28. They are discussed in Sections 3.4.1 to 3.4.3.

3.4.1 Burst Pictures. Useful sequence photographs of the nuclear burst were obtained for the following five shots: Dakota, Apache, Navajo, Tewa, and Huron. In each case the photographs were taken at one-second intervals, starting five to ten seconds after the moment of detonation.

The pictures have been examined from several points of view. The center of the burst was located on the pictures by means of: (1) radial rays of light from the fireball; (2) the condensation dome; and (3) the fireball, when it was visible. The growth of the condensation dome could be used for a rough measure of the range of the detonation and of the time interval between the burst and the first photograph. The fireball, where visible, could be used for a rough estimate of yield. The pictorial record of cloud formation obscuring the burst could be compared with the photoelectric measurements of thermal intensities and thermal attenuation discussed in Section 3.3.10.

Selected burst photographs have been reproduced in Figures 3.22 to 3.26. Discussions of the burst sequences are included in the following five sections.

Shot Dakota. Figure 3.22 contains six frames from the filming of Shot Dakota. The frames included are the second, fifth, eighth, ninth, tenth, and eleventh in the sequence. There was a time interval of nine or ten seconds between the burst itself and the first frame of the sequence.

The Shot Dakota sequence illustrates the several kinds of information to be obtained from the burst photographs. In particular, the three ways of locating the center of the burst are clearly shown.

In the fifth and eighth frames there appear radial rays of light which can be extended back to their intersection at the position of the fireball. The rays of light may be caused by irregular holes in the dense cloud of dust and fission products which form around the fireball. Through these irregularities the bright interior of the fireball could radiate, scattering along the path of the radiation by haze particles in the air, and could appear as bright rays of light on the picture. The rays do not appear on the second frame. This might be interpreted as showing that the obscuring cloud had not developed sufficiently to cause bright rays at the time of the second frame.

The condensation dome is visible in all six frames of Figure 3.22. The characteristic stria-

123

tions, caused by stratification in the moisture content of the air, can be seen very clearly. The diameter of the dome increases steadily as the shock wave moves out from the burst center. The center of the burst can be located from the picture by means of the condensation dome since the burst center is at the central point of the dome.

Because of the lower layer of clouds it is difficult to determine the exact position of the ground beneath the detonation. However, if the top of the bright strip below the burst is taken

as the ground line, then the height of the upper cloud layer is found to be about 36,500 feet. The thickness of the lower cloud layer is measured from the film to be about 4,200 feet. These measurements are in fairly close agreement with the cloud conditions reported from a reconnaissance aircraft which surveyed the detonation area one half hour before the time of burst: "3/8 cumulus, bases 2,000 feet, tops 6,000 feet. 8/8 cirrus, bases at 35,000 feet, tops at 36,000 feet (thin overcast)."

Shot Apache. Selected frames from the Shot Apache sequence are shown in Figure 3.23. The radial rays of light seen in the Shot Dakota sequence do not appear in the Shot Apache pictures. However, the condensation dome is very clearly shown and the fireball with the nuclear cloud around it and the stem below it can also be seen as the condensation dome evaporates.

The cloud formations which appear on the first frame have heights which are between 20,000 feet and 28,000 feet as determined from the measurements on the film. Official weather summaries from aircraft in the vicinity include references to a few scattered cumulus clouds with tops to 25,000 feet and 35,000 feet in agreement with the evidence of Figure 3.24.

Shot Tewa. The light from the Shot Tewa burst was very bright and persisted for a long time, as reported by the operator on the aircraft and as shown by the sequence photographs in Figure 3.25.

The location of the burst center on the photographs can best be done through the radial rays of light which can be seen in the first and sixth frames. The striated condensation dome is visible on some of the frames, but the obstructing cumulus cloud between the burst and the air-

Pages 127-128 Deleted

(a) First frame   (b) Sixth frame   (c) Eleventh frame

(d) Sixteenth frame   (e) Twenty-first frame   (f) Twenty-sixth frame

Figure 3.25 Sequence photographs: Shot Tewa, 5.0 Mt, at 96 naut mi.

craft makes it difficult to determine a central point for the dome. The edge of the fireball itself is visible in the twenty-sixth frame, and an estimated position for the center of the fireball could be obtained from the part of the fireball that shows in the picture.

The diameter of the condensation dome could not be determined accurately from the pictures, but from the rough measurements that were made it was estimated that 10 seconds or more elapsed between the time of burst and the time of the first frame in the sequence.

From the portion of the fireball visible in the twenty-sixth frame it was estimated that the fireball radius was between 1.2 km and 1.5 km. At the second thermal peak the corresponding radius would have been between 0.97 km and 1.21 km. From Figure 1.8 the yield was therefore estimated as between 2.9 Mt and 5.5 Mt. The official yield was 5.0 Mt, which is within the estimated range. If a larger section of the fireball had been visible, a more precise estimate of yield would have been possible.

The cloud formations shown in Figure 3.25 include a low layer of cumulus clouds, a few high cumulus including one cluster directly in the line of sight, and cirrostratus at a height of about 33,000 feet, as measured from the film. The official weather summary from an aircraft in the vicinity refers to scattered cumulus clouds with bases at 2,000 feet, and 4/8 to 5/8 cirrostratus, bases at 35,000 feet, tops at 36,000 feet. This is in rough agreement with the sequence photographs.

Shot Huron.

The height of the upper cloud layer, as measured from the sequence photographs, was about 34,000 feet. The lower cumulus clouds can be seen to include several high tops. The weather summary described the cloud formations as: "3/10 cumulus, bases at 1,800 feet, tops estimated at 10,000 to 15,000 feet, with isolated tops to 30,000 feet. 10/10 cirrostratus with bases estimated at 30,000 feet (4/10 transparent)."

3.4.2 Pictures of Nuclear Cloud. After one of the shot   ne aircraft was flown to within 25 naut mi of the nuclear cloud and a sequence of photographs was taken. Six of these photographs are reproduced in Figure 3.27.

The photographs of the nuclear cloud were taken at 0636 hours, one half hour after the time of detonation (0606). The nuclear cloud had by that time risen to a height greater than the height of the overcast. What appears in the pictures is a portion of the stem of the nuclear cloud, the portion lying between the top of the lower layer of cumulus clouds (about 6,000 feet) and the bottom of the upper cirrus layer (about 35,000 feet).

At the time of burst the wind velocity was 14 knots at the surface, 8 knots at 18,000 feet, and 39 knots at 34,000 feet. The pictures show that the stem of the nuclear cloud did not rise straight as in the simplified drawings of Figure 1.1 D, but was pulled strongly by the winds. From the slant of the stem it can be inferred that the nuclear cloud itself, hidden from view by the upper cirrus cloud layer, was no longer above the point of detonation but instead had been carried 10 or 15 miles by the winds.

3.4.3 Ambient Conditions. On several flights there were sequence photographs taken of the

130

sky and cloud conditions, in synchronization with simultaneous Heiland recordings of the ambient light intensity as measured by the two photoheads. Figure 3.28 illustrates the procedure and results obtained from such measurements.

Three successive frames from the photographic sequence are shown in the upper part of Figure 3.28, and the Heiland record taken at the same time is reproduced in the lower part of the figure. Arrows have been drawn to indicate on the Heiland record the approximate times at which the three frames were photographed.

The explicit procedure used for these measurements was the following. As the aircraft approached a cloud whose brightness was to be measured, the feedback loop was opened so that

Figure 3.26 Sequence photographs: Shot Huron, _____ at 135 naut mi.

the pentode current would be held at the value needed to correct for the light from the open sky and the more distant cloud formations. Frame 94, Figure 3.28, shows this initial situation. The pentode cathode currents were recorded as 28 μa and 4 μa for the 1P39 and 6570 photoheads, respectively. The time was shortly after 0800 hours on July 22. These current readings are included with other ambient light measurements in Table 3.12, Section 3.3.11, where the corresponding irradiance values, 1.0 watts/meter^2 and 1.5 watts/meter^2 respectively, are also given.

At about the same time that the switch was thrown to open the feedback loop, the switches starting the sequence camera and the Heiland recorder were also thrown. The increasing light intensity, as the aircraft entered the edge of the cloud bank, was registered as an increasing deflection of the two Heiland traces. Successive frames of the sequence film, taken at one-second intervals, recorded photographically the cloud structure in the direction the photoheads were pointed, as shown in Frames 95 and 96 of Figure 3.28. The Heiland deflections at the times corresponding to these frames, together with the photohead calibration data from Section 3.3.9, were used to determine the increase in irradiance. The resultant values of irradiance, the initial amounts plus the increments contributed by the cloud bank, are listed in Figure 3.28 with the corresponding cloud photographs.

From the listed values of measured irradiance, it can be inferred that in the light from sunlit clouds there was a greater irradiance within the infrared (6570) spectral band than within the blue-green (1P39) band. In part, this can be accounted for by the fact that the S-1 response curve of the 6570 phototube covers nearly twice as wide a range of wave lengths as does the S-4 band of the 1P39 phototube, as shown in Figures 1.10 and 1.11. However, another important contributing factor may have been the fact that at 0800 hours the sun was not yet very high in

131

Page 132
Deleted

(b) Frame 94
1P39: 1.0 w/m²
6570: 1.5 w/m²

(b) Frame 95
1P39: 1.1 w/m²
6570: 2.1 w/m²

(d) Frame 96
1P39: 1.2 w/m²
6570: 2.5 w/m²

(e) Heiland Record. Upper trace: 1P39 photohead. Lower trace: 6570 photohead. Interval between time markers: 0.01 second.
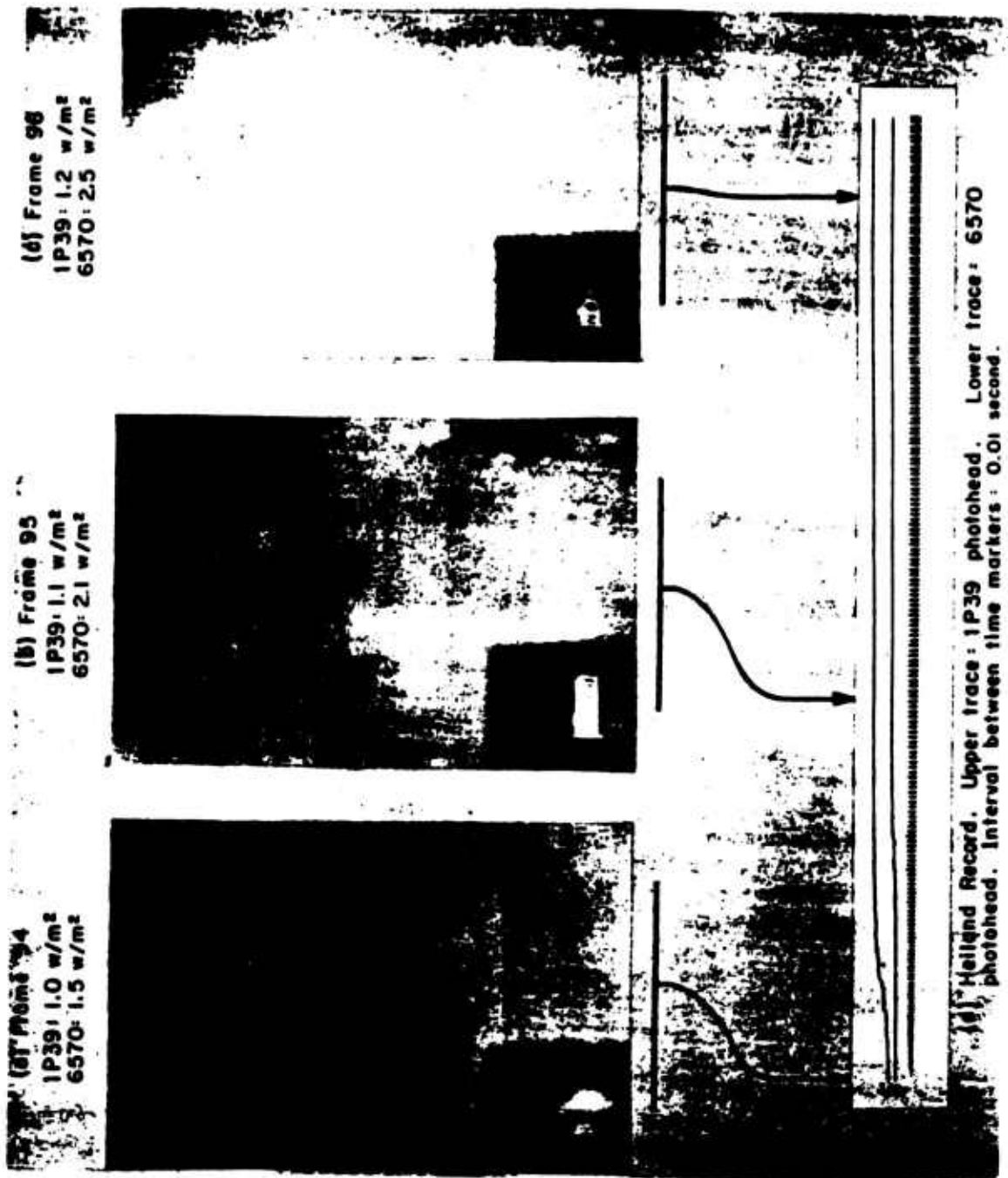
Figure 3.28 Ambient light measurements, July 22.

the sky, and the filtering action of the atmosphere could have left the light of the sun somewhat more red and less blue than it would have been with the sun more directly overhead.

The same considerations could apply to the other ambient light data in Table 3.12. Many of the measurements in that table show a greater irradiance for the 6570 photohead than for the 1P39 photohead, and the difference might be explained in the same way, as a consequence of the differing bandwidths and of the relatively low position of the sun for most of the measurements.

Chapter 4
CONCLUSIONS and RECOMMENDATIONS

4.1 CONCLUSIONS

The conclusions have been divided into four major sections. The first section contains general conclusions referring to the tests as a whole, while the other three sections refer more specifically to the three kinds of measurements that were made, those dealing with the electromagnetic signal, the thermal radiation, and the pictorial aspects of the nuclear detonations in the test series.

4.1.1 General Conclusions.

1. The data obtained during the Operation Redwing tests served to fulfill the objectives of Project 6.4 in a generally satisfactory way, and to substantiate the theoretical expectations, except in the case of the whip antenna.

2. Useful data of a broader nature was also collected. The data collected concerning reflection of the electromagnetic pulse from the ionosphere was of particular value for the design of future indirect-bomb-damage-assessment systems.

3. The time interval between the date when participation was authorized and the date when the tests began was too short. As a result of the inadequate time for preparation, it was necessary to use the first tests for the solution of equipment and procedural problems. Most of the useful data was obtained from the later tests in the series.

4.1.2 Conclusions: Electromagnetic Signal and Fiducial System.

1. It was concluded from the Operation Redwing tests that the ferrite-core magnetic loop antenna was suitable and satisfactory for use as a flush-mounted airborne antenna for the reception of very low frequency electromagnetic radiation. The wave form received by this magnetic antenna (the fiducial antenna) was observed to correspond to the theoretical prediction and to be closely similar in shape to the first derivative of the wave form received by a vertical whip antenna.

2. The output of the magnetic antenna was generally so strong that there was saturation in the fiducial amplifier. The amplified electromagnetic signal was usually distorted but the distortion did not interfere with the effectiveness of the electromagnetic pulse as a fiducial marker establishing the moment of the burst as a zero time from which the time interval to the second thermal maximum could be measured.

3. A comparison between the wide and narrow fiducial antennas had been planned as a part of the test program. Because of amplifier saturation there was only one test (Shot Tewa) which allowed a comparison between the output voltages from the two antennas. In this one case, the output voltage from the wider antenna was nearly three times that from the narrower antenna. However, the wide antenna was outside the aircraft, where the incident field was expected to be stronger than the field inside the aircraft window. At least a portion of the measured output difference could thus be attributed to a difference in location on the aircraft. A further portion could be associated with the difference in internal impedance of the two antennas. It was concluded that the data did not indicate any great difference in the effectiveness of the two geometrical antenna shapes for the reception of low frequency electromagnetic radiation.

4. The whip antenna did not, for any one of the test detonations, give an output signal strong

enough to trigger the oscilloscope and be photographed. It is believed that the oscilloscope amplification was set too low, that losses of unknown origin had left the output of the whip antenna much smaller than had been expected.

5. In one example for which the wave form was not distorted by saturation, the period of the oscillation was used to compute the detonation yield with an accuracy of about 20 percent. The wave form used was the wave form of a second sky wave, but other wave forms in the same wave train gave approximately the same measured period and computed yield.

6. It was found that the wave form of a sky wave could be used to give a rough measure of the altitude of the receiving equipment, and might perhaps be used to measure the altitude of the burst itself, particularly if the narrow-band receiving system used by Project 6.4 at Operation Redwing were replaced by a broad-band system capable of detecting the spikes which are characteristic of high yield detonations.

7. The direct sky wave was found to be stronger than the same sky wave after reflection from the ground beneath the aircraft. However, it was uncertain how much of the difference was caused by losses on reflection at the ground and how much was caused by the modification of the effective antenna pattern by the presence of the aircraft.

8. The measurement of the time intervals in a train of sky waves can give quantitative estimates for the distance between source and receiver and for the height of the reflecting ionosphere layer.

9. The measurement of the relative amplitudes in a train of sky waves can give a quantitative estimate for the effective ion density in the ionosphere, as specified by the characteristic angular frequency, ω_r. The measurements suggest that there is an exponential relationship between ω_r and the ionosphere height.

10. The measurement of the actual field strengths for a series of sky waves in an electromagnetic signal can be used to extrapolate to approximate field strengths for the ground wave and for other sky waves. From this procedure, as applied to Shot Tewa, it was found that the extrapolated ground wave amplitude was comparable with, though somewhat smaller than, the value that would have been predicted from the results of earlier nuclear weapons tests.

4.1.3 Conclusions: Thermal Radiation and Photohead System.

1. A modified formula, $Y = 0.92 \, T^2$, was found to be most satisfactory in giving the yield, Y, in megatons, as a function of the time interval, T, in seconds, between the beginning of the first thermal peak and the top of the second thermal peak. This modified formula gave yield estimates which were accurate to ± 16 percent for each of five bursts with yields in the range _____ to 5.0 Mt. For three of the five bursts the yield estimates were accurate to within 10 percent.

2. Of the two peaks in the thermal radiation intensity curve, the first peak was found to be considerably smaller in intensity than the second peak, by a factor which was usually of the order of ten for the blue-green (1P39) phototube and of the order of five for the infrared (6570) phototube. Although relatively small, the first thermal peak could easily be distinguished on four of the seven Helland records. The first thermal peak was strong enough to have been useful as a fiducial marker in these four cases, but not in the other three cases.

3. From the magnitude of the Helland deflection, rough estimates were made of the thermal intensity reaching the receiving equipment. Within the wave length band of the 1P39 phototube, the thermal intensities ranged from 0.04 watt/meter^2 to 19 watts/meter^2. In the 6570 band the range was from 0.9 watts/meter^2 to 54 watts/meter^2. The observed intensities were lower than

the expected intensities by factors generally between 2 and 100. The one percent and 10 percent filters which were used with three of the seven thermal radiation records were found to have been neither necessary nor desirable.

4. The reduction in thermal intensity was attributed to haze and clouds. In many cases both the clouds and the haze could be seen on the sequence photographs taken a few seconds after the burst. The attenuation could be expressed in terms of an average attenuation factor of the order of 0.01 to 0.05 per km. The data showed that there was substantially greater attenuation in the 1P39 band than in the 6570 band.

5. Ambient light measurements in the open sky and in sunlit clouds gave irradiance values of 1 or 2 watts/meter^2 for the 1P39 photohead and up to about 6 watts/meter^2 for the 6570 photohead. The somewhat larger readings for the 6570 photohead were attributed in part to the broader wave length band covered by the S-1 (6570) response curve in comparison to the S-4 (1P39) response curve.

4.1.4 Conclusions: Sequence Photographs.

1. The pictures of the nuclear burst suggest three principal methods by which the position of the burst can be located from the photographs: (a) the rays of light appearing on some of the pictures can be followed back to their point of intersection; (b) many of the pictures show the condensation dome, which has the point where the burst occurred as its center of symmetry; and (c) the fireball itself is visible in some of the pictures.

2. When the humidity is sufficiently high for the condensation dome to form, this dome gives a close indication of the position of the shock wave in the air around the burst. The measurement of the size of the condensation dome and its rate of growth can give a rough indication of the distance between burst and camera and can also give a check on the timing of the sequence frames relative to the time of burst.

3. When the fireball is visible on the film, the fireball radius can be used to give an estimate of yield, provided the timing of the photograph showing the fireball is roughly known with respect to the time of burst, and provided the distance between burst and camera is also known.

4.

4.2 RECOMMENDATIONS

As in the case of the conclusions, the recommendations have been separated into four sections. The more general recommendations are followed by recommendations concerned with the three categories of phenomena which were studied during the Operation Redwing tests.

4.2.1 General Recommendations.

1. Studies such as that carried out by Project 6.4 should be continued from the point of view of equipment development. Of particular value would be further development of ferrite-core magnetic loop antennas for other applications of the electromagnetic signal from a nuclear detonation.

2. Studies such as that carried out by Project 6.4 should be continued for added knowledge

concerning the phenomena accompanying a nuclear detonation. Further information would be desirable for use in the design of new indirect-bomb-damage-assessment (IBDA) systems. Of particular interest are the characteristics of the electromagnetic sky waves which can be received from the burst.

3. In future test series authorization should precede participation by six months or more to permit adequate preparation of equipment and procedures, and thereby avoid the loss of much valuable data during the earlier shots of the series.

4.2.2 Recommendations: Electromagnetic Signal and Fiducial System.

1. It is recommended that further study be made of ferrite-core magnetic loop antennas of designs similar to that of the fiducial antenna used in the Operation Redwing tests. A more detailed examination should be made of the response of this form of antenna to incident fields of various wave forms. The development of similar antennas with broader frequency bands would also be desirable to make possible the reception of the sharp spikes as well as the main oscillations contained in the electromagnetic signal from a nuclear detonation.

2. Methods of amplification and presentation should be selected or developed which will allow the extraction of all pertinent information from the electromagnetic signal. The strong ground wave and the weaker sky waves should both be presented without harmful saturation effects and with a minimum of electronic equipment.

3. A more detailed and extensive investigation should be made of the effect of antenna geometry and localized antenna shielding on the performance of the ferrite-core magnetic loop antenna.

4. The operation of airborne whip antennas at very low electromagnetic frequencies should be investigated in detail.

5. Further statistical information is needed concerning the correlation between the period of the electromagnetic pulse and the yield of the detonation. An examination should be made of the consistency in period for the ground wave and sky waves within a single wave train, as well as the correlation among the results from different detonations. Consideration should also be given to differences in construction of various types of nuclear devices, and the possible effect of these differences on the period of the electromagnetic pulse.

6. The wave forms of sky waves should be examined with broad-band receiving equipment to determine how closely the altitude of the receiver can be measured from such wave forms, and to determine whether the height of the burst itself can be measured from the timing of the spikes which are superimposed on the wave forms from high-yield detonations.

7. There should be an experimental and theoretical program to determine the effect of the aircraft structure on the directional radiation pattern of a flush-mounted magnetic loop antenna at very low frequencies.

8. In future weapons tests more precise and detailed measurements should be made of the timing of sky waves. The ranges and ionosphere heights calculated from these measurements should be compared with independent measurements of range and ionosphere height.

9. In future weapons tests the amplitudes of successive sky waves in a wave train should be measured carefully, and the values of ω_r calculated from these relative amplitudes should be checked against independent measurements of ω_r with the standard equipment used for ionosphere studies.

10. In future weapons tests the measured ground wave amplitude should be checked against the ground wave amplitude as extrapolated from the measured sky wave amplitudes. A statistical study should be made of the correlation between ground wave amplitude (as determined by direct measurement or by extrapolation) and the yield of the detonation. As in Item 5 above, consideration should be given to the possible effects of differences in type and construction of different nuclear devices.

4.2.3 Recommendations: Thermal Radiation and Photohead System.

1. A larger number of detonations should be studied to determine the best form of the math-

ematical relationship relating yield to the time interval between the burst and the second thermal intensity peak.

2. The first peak of the thermal radiation intensity curve should be used as an auxiliary fiducial mark in conjunction with the electromagnetic fiducial signal, but the latter signal should be considered the more reliable one at long ranges and in conditions of heavy clouds or dense haze.

3. The likelihood of thick clouds should be anticipated for the operational use of the IBDA system and allowance should be made for the possibility of heavy atmospheric attenuation before any reduction in the photohead sensitivity by filters or other means.

4. A comparative evaluation of the two phototubes showed that the 1P39 was more sensitive than the 6570, but that the radiation in the 1P39 wave-length band was more highly attenuated over long paths than the radiation in the 6570 band. These two considerations tend to counteract each other for long-range operation of IBDA equipment. The response of the two photoheads to ambient light does not differ sufficiently for a choice between them on that basis. It is recommended that the choice between 1P39 and 6570 be made freely on other grounds such as the probability that the infrared (6570) phototube is more sensitive than the blue-green (1P39) phototube to interfering thermal radiation from the jet exhaust of the aircraft carrying the IBDA system equipment.

4.2.4 Recommendations: Sequence Photographs.

1. Pictures of the nuclear burst were obtained for dawn shots only. It would be desirable to have comparable daytime burst photographs for evaluation of their usefulness in locating the point of burst.

2. The probability of the occurrence of a condensation dome should be determined as a function of humidity and detonation yield. Photographs for Nevada test shots should be examined for the possibility of other effects (dust clouds, etc.) which could make the position of the shock wave visible on the photograph. An estimate could then be made of the usefulness and reliability of the shock wave position and motion as a diagnostic aid for IBDA.

3. The choice of film and filters for the sequence camera should be made for giving maximum visibility to the fireball in the presence of clouds and haze.

4. In the operational use of the IBDA system the aircraft should avoid flying through irregular sunlit clouds at the time of burst and for five or ten seconds thereafter, to prevent the fluctuations of ambient light from giving an apparent displacement to the second peak in the thermal radiation intensity curve.

REFERENCES

1. R. E. Clapp; ⌐ ¬ (Title Classified); Report No. 264E002, 27 July 1956; Ultrasonic Corporation, Cambridge, Massachusetts; Secret Restricted Data.

2. R. A. Houghten, L. C. Humphrey, and R. B. Harvey; "Operation Teapot Measurements"; Air Force Cambridge Research Center, Laurence G. Hanscom Field, Bedford, Massachusetts; Secret, Restricted Data.

3. L. W. Yabroff; "Reflection at a Sharply-Bounded Ionosphere"; Proceedings of the IRE, Volume 45, June 1957, Pages 750 to 753; Institute of Radio Engineers, Inc., New York, New York; Unclassified.

4. J. R. Wait and A. Murphy; "The Geometrical Optics of VLF Sky Wave Propagation"; J. R. Wait; "The Mode Theory of VLF Ionospheric Propagation for Finite Ground Conductivity"; J. R. Wait; "The Attenuation vs. Frequency Characteristics of VLF Radio Waves"; Proceedings of the IRE, Volume 45, June 1957, Pages 754 to 771; Institute of Radio Engineers, Inc., New York, New York; Unclassified.

5. "Thermal Data Handbook"; 1954; AFSWP-700; Armed Forces Special Weapons Project; Washington, D. C.; Secret Restricted Data.

6. "The Effects of Atomic Weapons"; September 1950; Los Alamos Scientific Laboratory; U. S. Government Printing Office, Washington, D. C.; Unclassified.

7. "Measurements Supervised by Dr. Robert M. Chapman"; Geophysics Research Directorate; Air Force Cambridge Research Center, Bedford, Massachusetts.

8. "MX1964 IBDA Yield Measuring System; Final Technical Report"; Report No. 1158, 15 October 1954; Edgerton, Germeshausen and Grier, Inc., Boston, Massachusetts; Secret Restricted Data.

9. "Smithsonian Physical Tables"; Ninth Revised Edition, 1954; Smithsonian Institution, Washington, D. C.; Unclassified.

10. "RCA Tube Handbook"; Radio Corporation of America, Harrison, New Jersey; Unclassified.

11. "Weston Light Measuring Instruments"; Circular B-22-G, January 1957; Weston Electrical Instrument Corporation, Newark, New Jersey; Unclassified.

12. M. Miller and G. Cohen; "Missile Detonation Locator"; Project 6.3, Operation Teapot, ITR-1140, August 1957; Signal Corps Engineering Laboratories, Fort Monmouth, New Jersey; Secret Restricted Data.

13. J. E. Chrisinger; "Memo Report for Installation of Operation Ultrasonics"; 15 May 1956; Experimental Airborne Engineering Branch, Air Force Cambridge Research Center, Bedford, Massachusetts; Unclassified.

14. "Standards on Radio Receivers; Methods of Testing Amplitude-Modulation Broadcast Receivers"; 1948; "Methods of Testing Receivers Employing Ferrite Core Loop Antennas"; 1955; Institute of Radio Engineers, Inc., New York, New York; Unclassified.

15. R. W. P. King; "The Theory of Linear Antennas"; 1956; Harvard University Press, Cambridge, Massachusetts; Unclassified.

Pages 141-142 Deleted